



Curso intensivo de Cosmología Observacional

Claudia Scóccola

Profesora Asociada - Departamento de Física,
Facultad de Ciencias Físicas y Matemáticas
Universidad de Chile



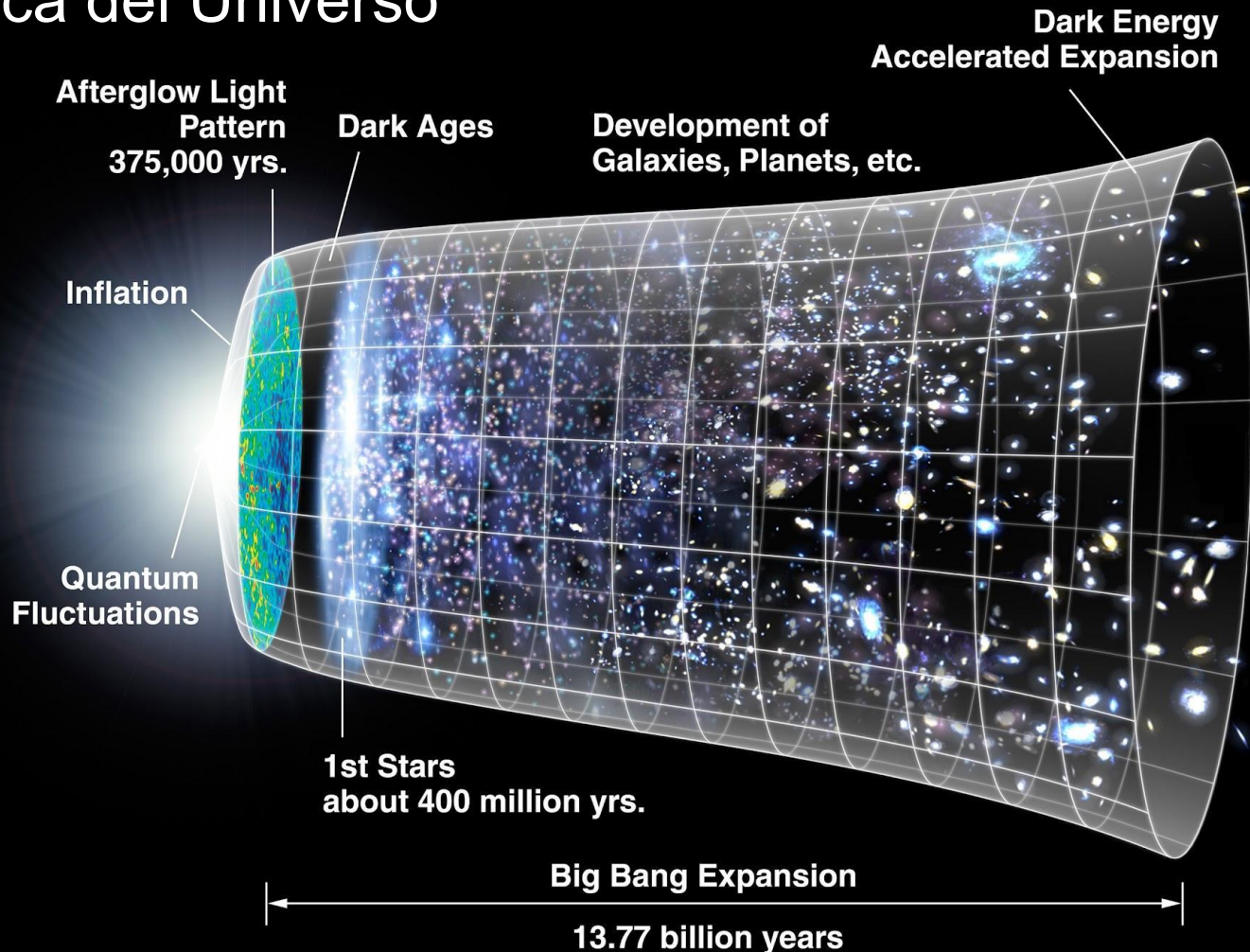
The background image is a reproduction of Vincent van Gogh's painting "Starry Night". It depicts a dark, cypress-tipped hill on the left against a vibrant, swirling night sky filled with stars and a crescent moon. In the foreground, a small town with a church steeple is nestled among rolling hills.

Fondo Cósmico de Radiación

Clase 1 & 2 (martes 25/03)

- Modelo cosmológico estándar
- Universo en expansión
- Ley de Hubble
- Origen del CMB: desacople y superficie de última dispersión
- Propiedades del CMB: temperatura e isotropía
- Fluctuaciones de temperatura: efecto Sachs-Wolfe, oscilaciones acústicas, amortiguación de Silk
- Polarización del CMB: E and B modes. Conexión con ondas gravitacionales primordiales.

Historia térmica del Universo



Clase 1: Expansión del Universo y CMB

Introducción al modelo cosmológico - Expansión - grilla comóvil

Principio Cosmológico - isotropía - homogeneidad.

Ecuación de Friedmann – Ley de Hubble – Distancias

Fondo Cósmico de Radiación - Recombinación y desacople

La Cosmología estudia el “origen” y la evolución del Universo

El modelo cosmológico estándar está basado en la **Relatividad General**

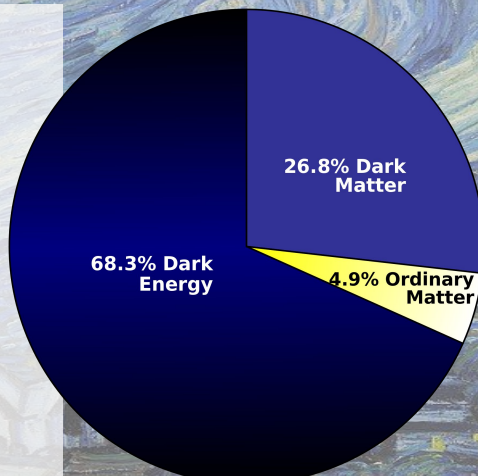
y la física de partículas, mediante las **ecuaciones de Boltzmann**

$$G_{\mu\nu} + \Lambda g_{\mu\nu} = 8\pi G T_{\mu\nu}$$

$$\frac{df}{dt} = C[f]$$

Pilares observacionales:

- ❖ Diagrama de Hubble (expansión)
- ❖ Abundancia de elementos químicos livianos (BBN)
- ❖ Radiación Cósmica de Fondo (CMB)
- ❖ Distribución de materia (LSS)



+

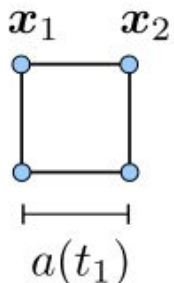
Mecanismo para producir las condiciones iniciales

Isotropía + Principio Copernicano → homogeneidad

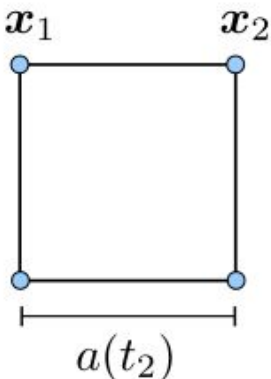
EXPANSIÓN

Imaginamos el espacio cubierto por una grilla, que se expande. Las coordenadas se mantienen constantes en la grilla son las **coordenadas comóviles**.

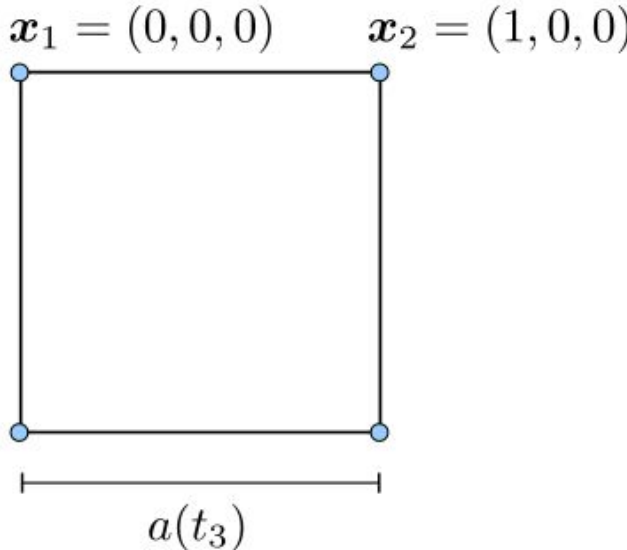
$t_1 :$



$t_2 > t_1 :$



$t_3 > t_2 :$



Expansión del Universo. La **distancia comóvil** entre puntos de una hipotética grilla se mantiene **constante** a medida que el Universo se expande. La **distancia física** es proporcional a la distancia comóvil, multiplicado por el **factor de escala α** : Crece a medida que pasa el tiempo.

EXPANSIÓN

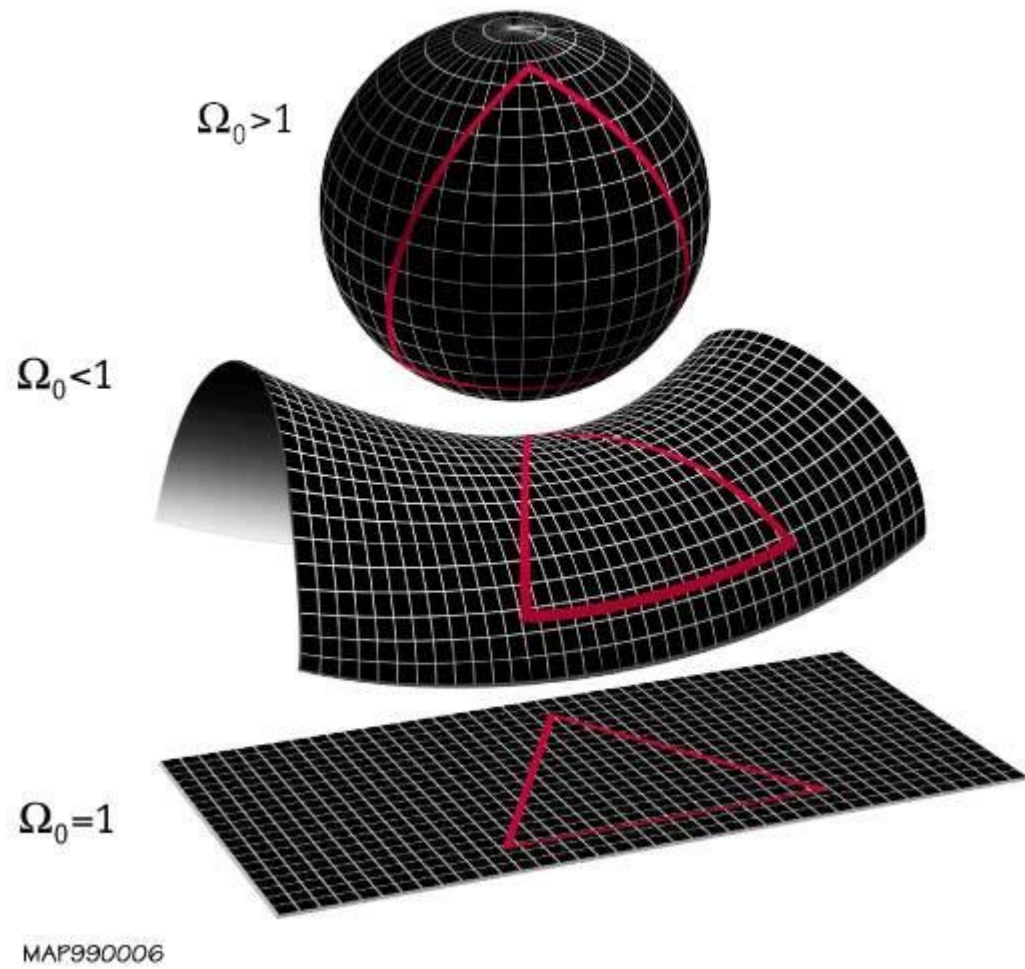
Efecto directamente relacionado: la **longitud de onda física** de la luz emitida por un objeto distante **se estira proporcionalmente al factor de escala**, de modo que la longitud de onda observada es mayor que la longitud de onda en la que se emitió la luz. Es conveniente definir este factor de estiramiento como el **corrimiento al rojo z**:

$$1 + z \equiv \frac{\lambda_{\text{obs}}}{\lambda_{\text{emit}}} = \frac{a_{\text{obs}}}{a_{\text{emit}}} = \frac{1}{a_{\text{emit}}}.$$

Además del factor de escala y su evolución, el Universo homogéneo está caracterizado por su **geometría**.

La RG conecta la geometría con la **energía**.

- Universo cerrado (curvatura positiva)
- Universo abierto (curvatura negativa)
- Universo plano (curvatura nula)



Ecuación de Friedmann (sale de las ecs. de Einstein)

Conecta la **evolución del factor de escala** con la **densidad de energía del Universo**.

Para cuantificar el cambio en el factor de escala, y su relación con la energía, definimos la tasa de expansión de Hubble (Hubble rate):

$$H(t) \equiv \frac{da/dt}{a}$$

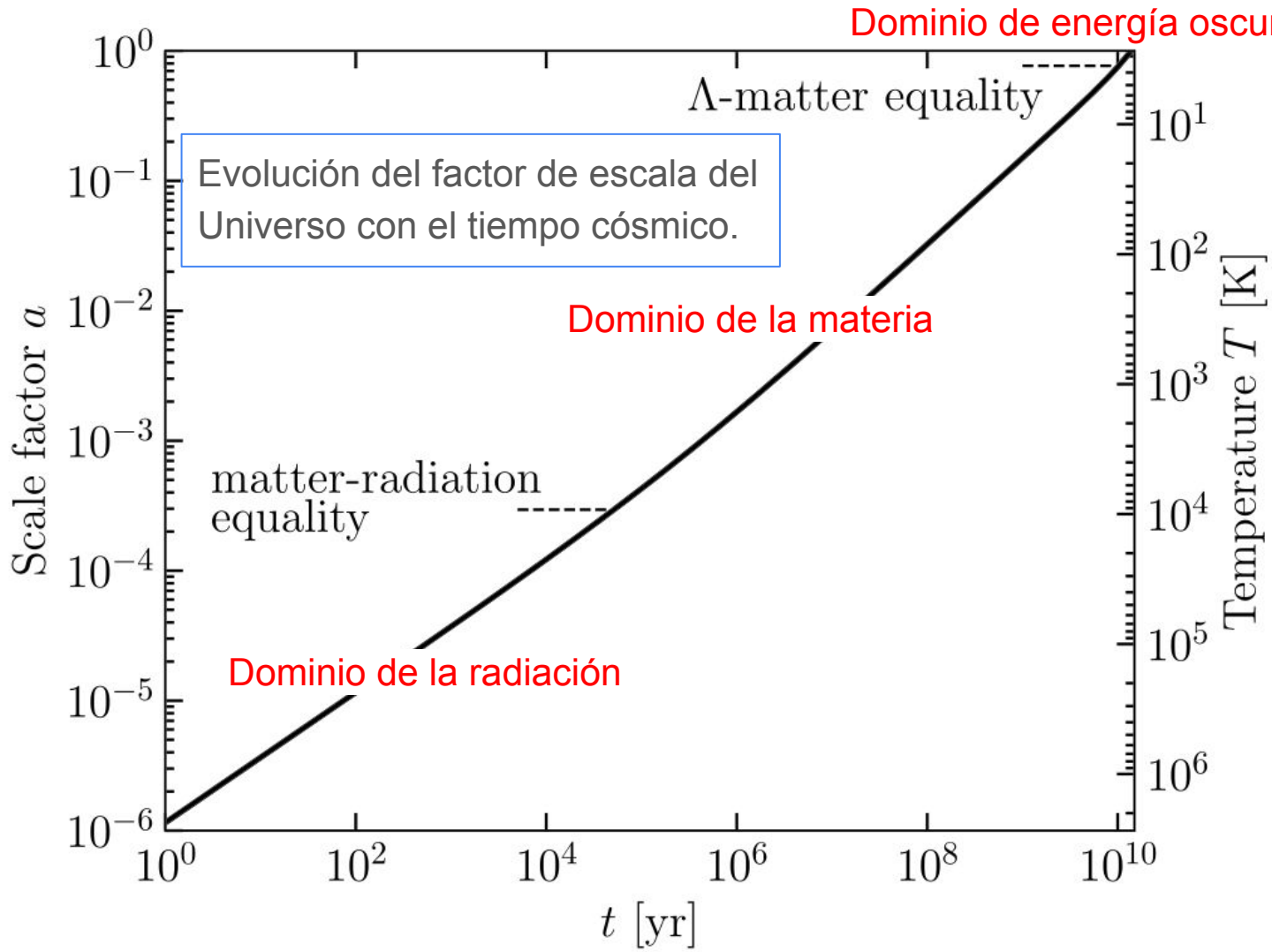
Mide qué tan rápido cambia el factor de escala.

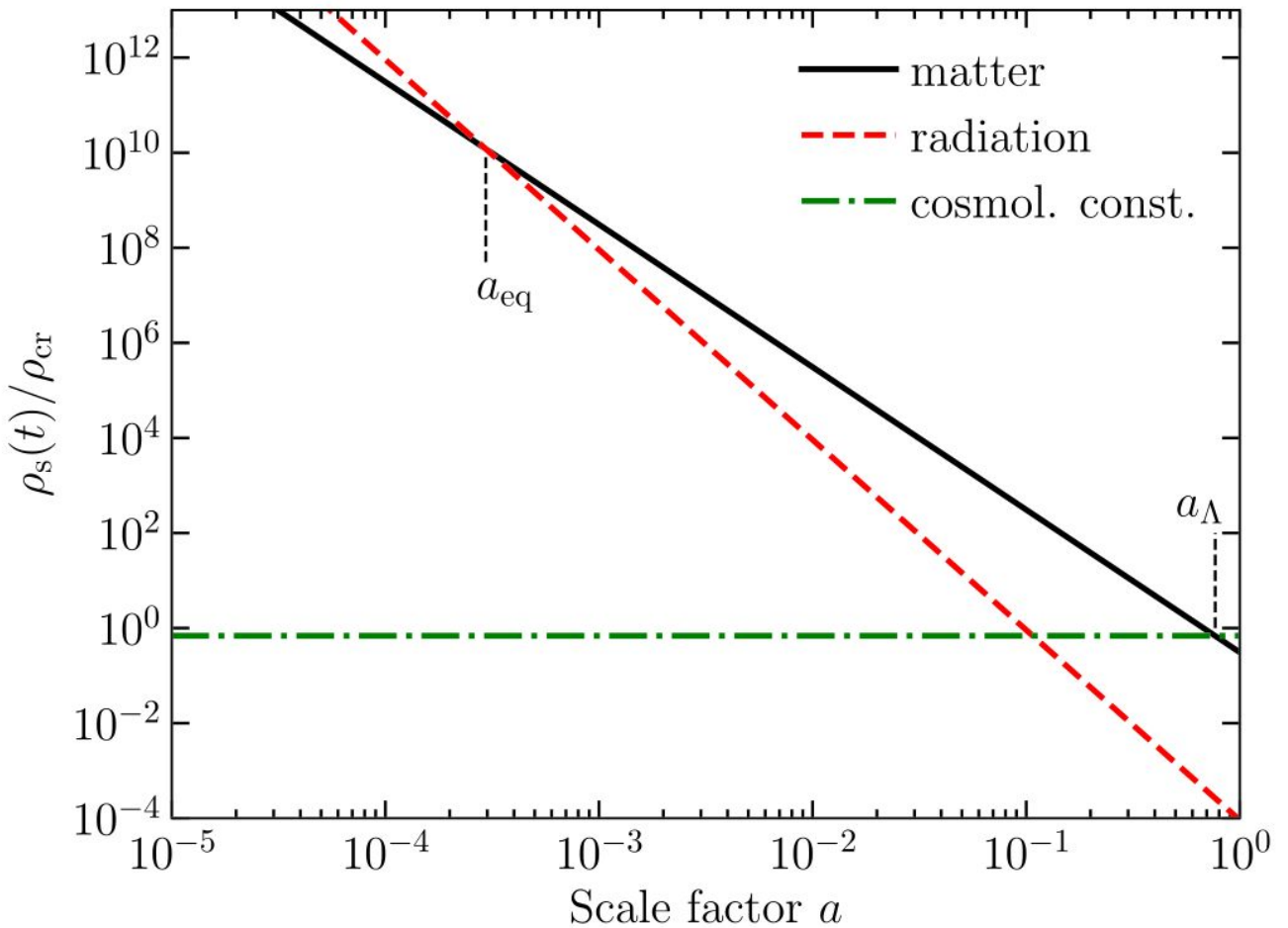
La evolución del factor de escala está determinada por la ecuación de Friedmann:

$$H^2(t) = \frac{8\pi G}{3} \left[\rho(t) + \frac{\rho_{\text{cr}} - \rho_0}{a^2(t)} \right]$$

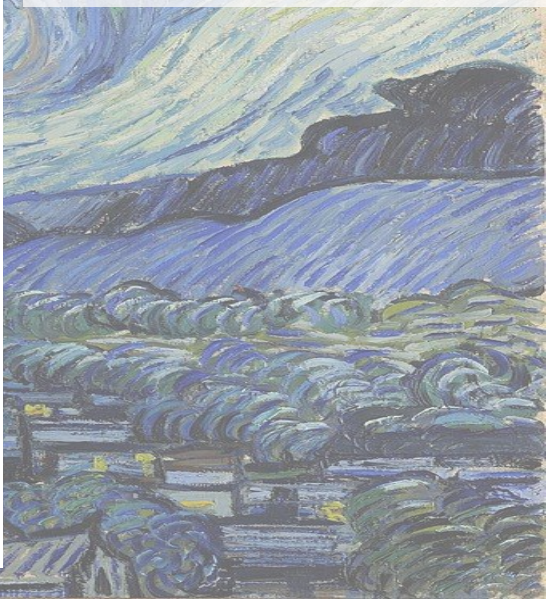
donde

$$\rho_{\text{cr}} \equiv \frac{3H_0^2}{8\pi G}$$





Densidad de energía como función del factor de escala para los diferentes componentes de la cosmología euclidiana fiducial.



Hubble Diagram for Cepheids (flow-corrected)

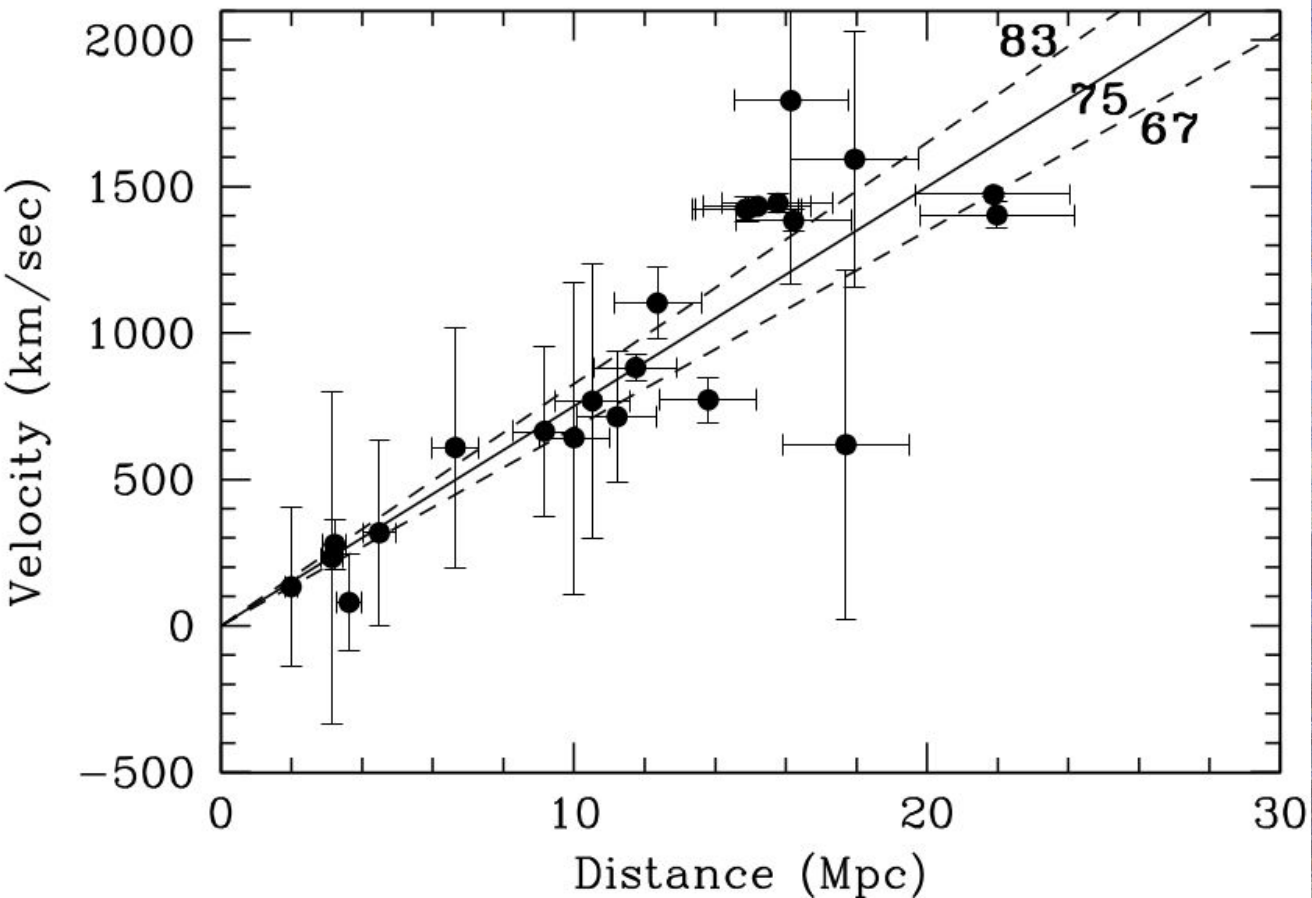


Diagrama de Hubble
(Hubble Space
Telescope Key project)

Cada punto: **galaxia** cuya distancia ha sido estimada utilizando **Cefeidas**.
Velocidad de recesión corregida con modelo para el campo de velocidad peculiar en el vecindario de la Vía Láctea.
Las líneas muestran la **predicción de la ley de Hubble-Lemaître** con diferentes valores de H_0 (en $\text{km s}^{-1} \text{ Mpc}^{-1}$), como se indica.

Distancias

- Distancia en la grilla comóvil
- Horizonte comóvil
- Distancia entre emisor y nosotros
(distancia comóvil)
- Distancia de diámetro angular
- Distancia de luminosidad

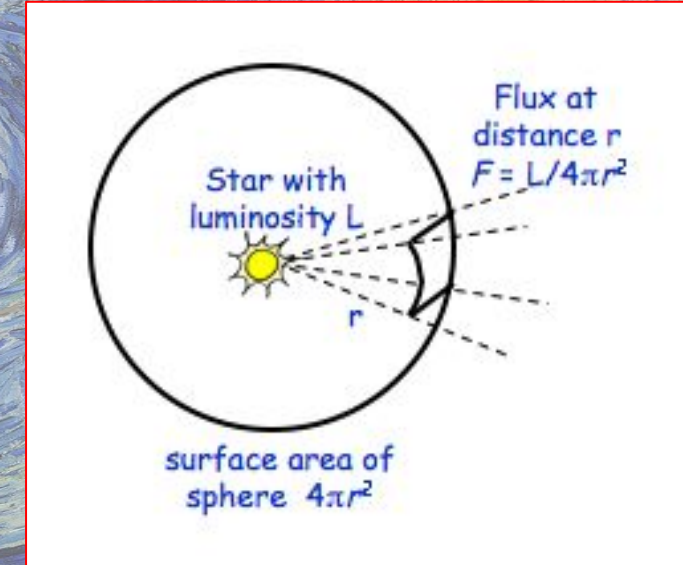
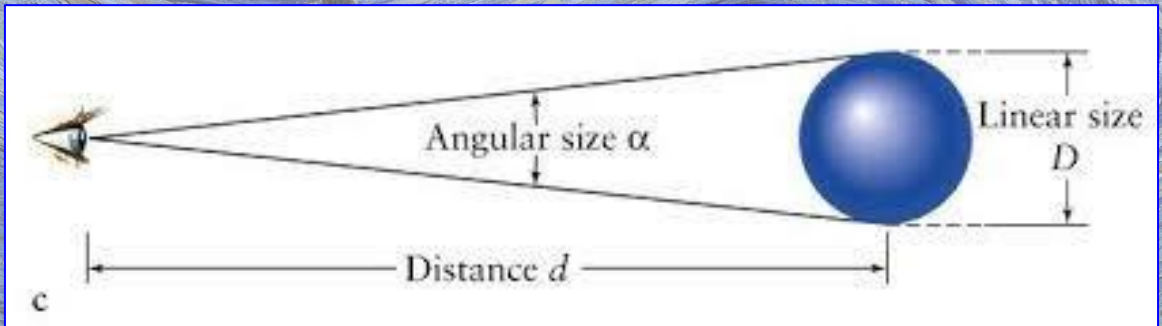
$$\eta \equiv \int_0^t \frac{dt'}{a(t')} \quad (\text{tiempo conforme})$$

$$\chi(a) = \int_{t(a)}^{t_0} \frac{dt'}{a(t')} = \int_a^1 \frac{da'}{a'^2 H(a')}$$

$$d_A^{\text{flat}} = a\chi = \frac{\chi}{1+z}$$

$$d_L \equiv \frac{\chi}{a}.$$

Conceptualmente: D_A y D_L



La **distancia de diámetro angular** se obtiene de comparar el tamaño físico de un objeto con su tamaño angular.

La **distancia de luminosidad** se obtiene de comparar la luminosidad de un objeto con su flujo observado.

La expansión del Universo introduce los **factores de $(1+z)$** que aparecen en las expresiones en la filmina anterior.

El Fondo Cómico de Radiación (CMB) (cuantitativamente)

Cuando la **temperatura** de la radiación era $\sim 10^4$ K (energías del orden de un eV), los electrones libres y los protones se combinaron para formar hidrógeno neutro. Antes de esa época, cualquier hidrógeno producido se ionizaba rápidamente por fotones energéticos. Después de ese momento, a $z \approx 1100$, los fotones del CMB dejaron de interactuar con partículas y viajaron libremente por el espacio.

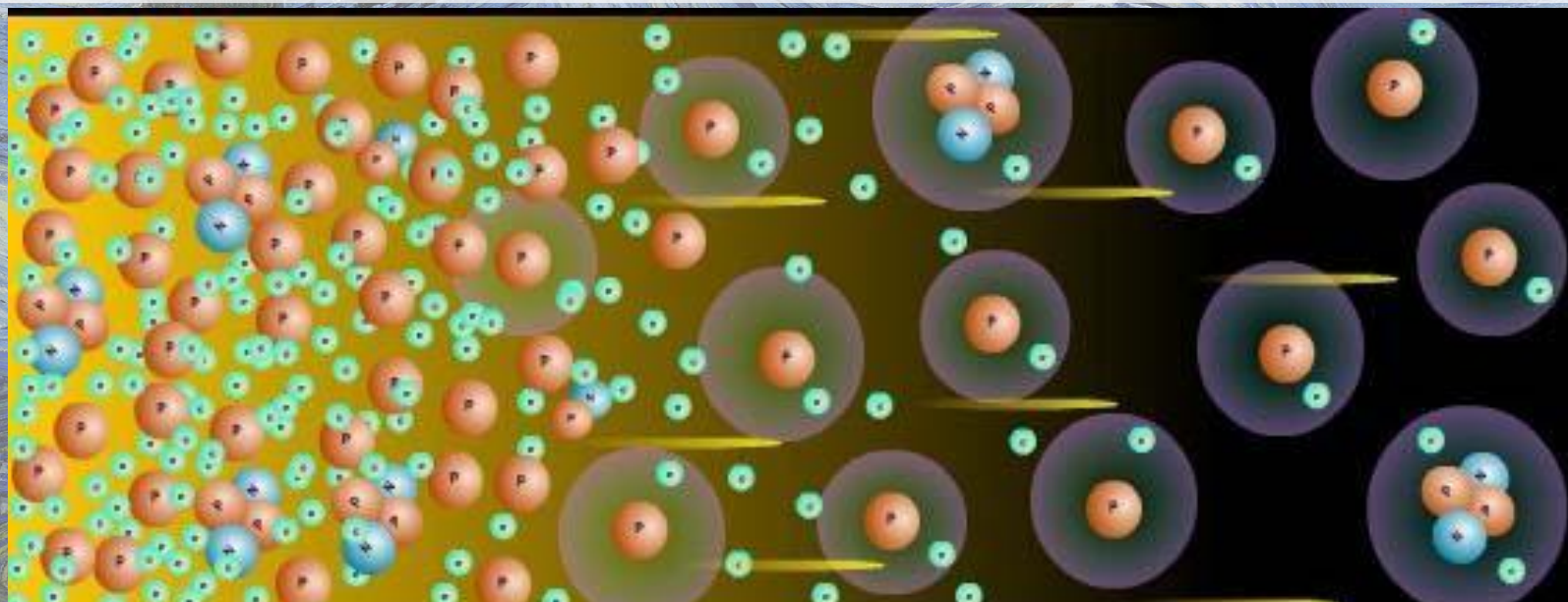
CMB restringe la densidad de bariones de forma independiente y en acuerdo con la Nucleosíntesis Primordial (BBN), proporcionando una confirmación sólida del modelo de concordancia.

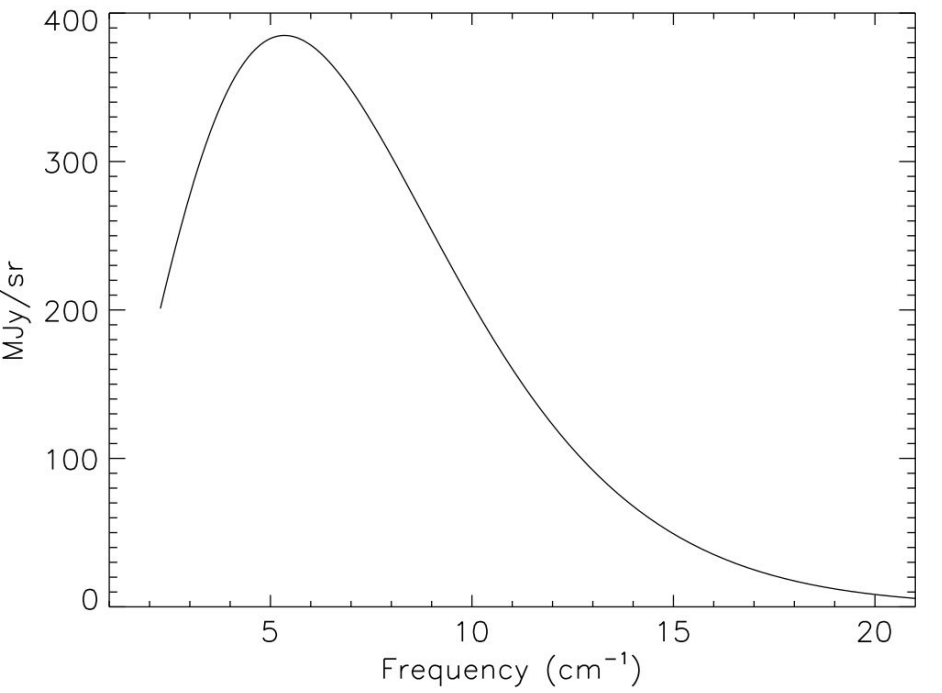
Las interacciones de los fotones con electrones antes de la última dispersión aseguraron que los fotones estuvieran en equilibrio, lo que implica que deben tener un espectro de cuerpo negro.

$$I_\nu = \frac{4\pi\hbar\nu^3/c^2}{\exp[2\pi\hbar\nu/k_B T] - 1}.$$

El Fondo Cósmico de Radiación (CMB) (cuantitativamente)

Esta imagen ilustra este período conocido como “recombinación”. Cuando se forman los átomos neutros, la densidad de electrones libre cae abruptamente, y la dispersión de Thomson se vuelve ineficiente. Esto sumado a la expansión del Universo con el consecuente corrimiento al rojo de los fotones, hace que la radiación se **desacople** del plasma y viaje libremente hasta hoy.





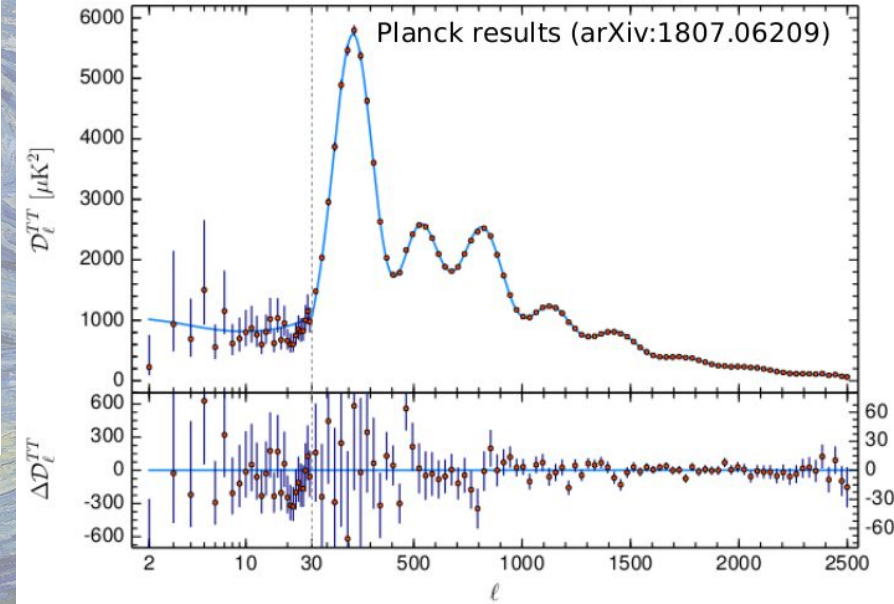
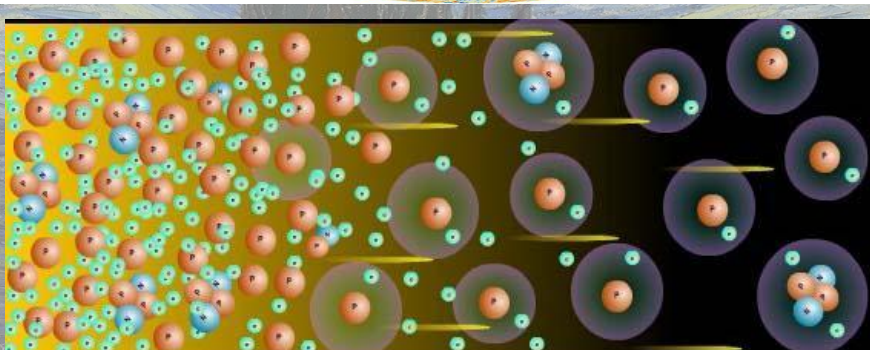
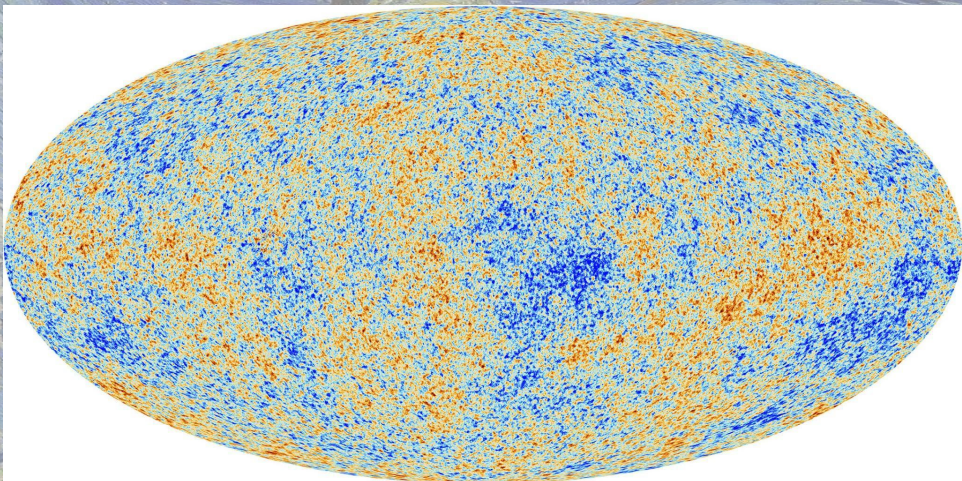
Intensidad del CMB como función de la frecuencia del instrumento FIRAS, sobre el satélite COBE.

La línea muestra un espectro de **cuerpo negro** a $T_0 = 2.728 \text{ K}$ (esta línea incluye las barras de error!)

Fixsen et al. (1996).

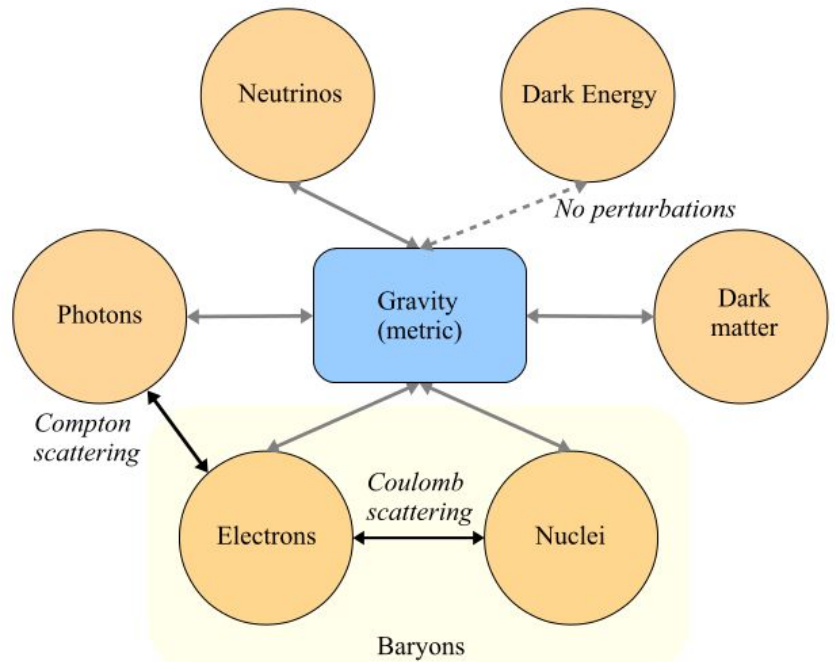
Diferencias relativas de temperatura $\sim 10^{-5}$ (anisotropías en la temperatura del CMB) medidas con gran precisión. Hoy buscamos efectos más sutiles, en la **polarización** y en el efecto de la distribución de materia interviniente a través del **lente gravitacional**.

CMB - radiación reliquia del Big Bang



$$\delta T(\theta, \phi) = \sum_{lm} a_{lm}^T Y_{lm}(\theta, \phi)$$

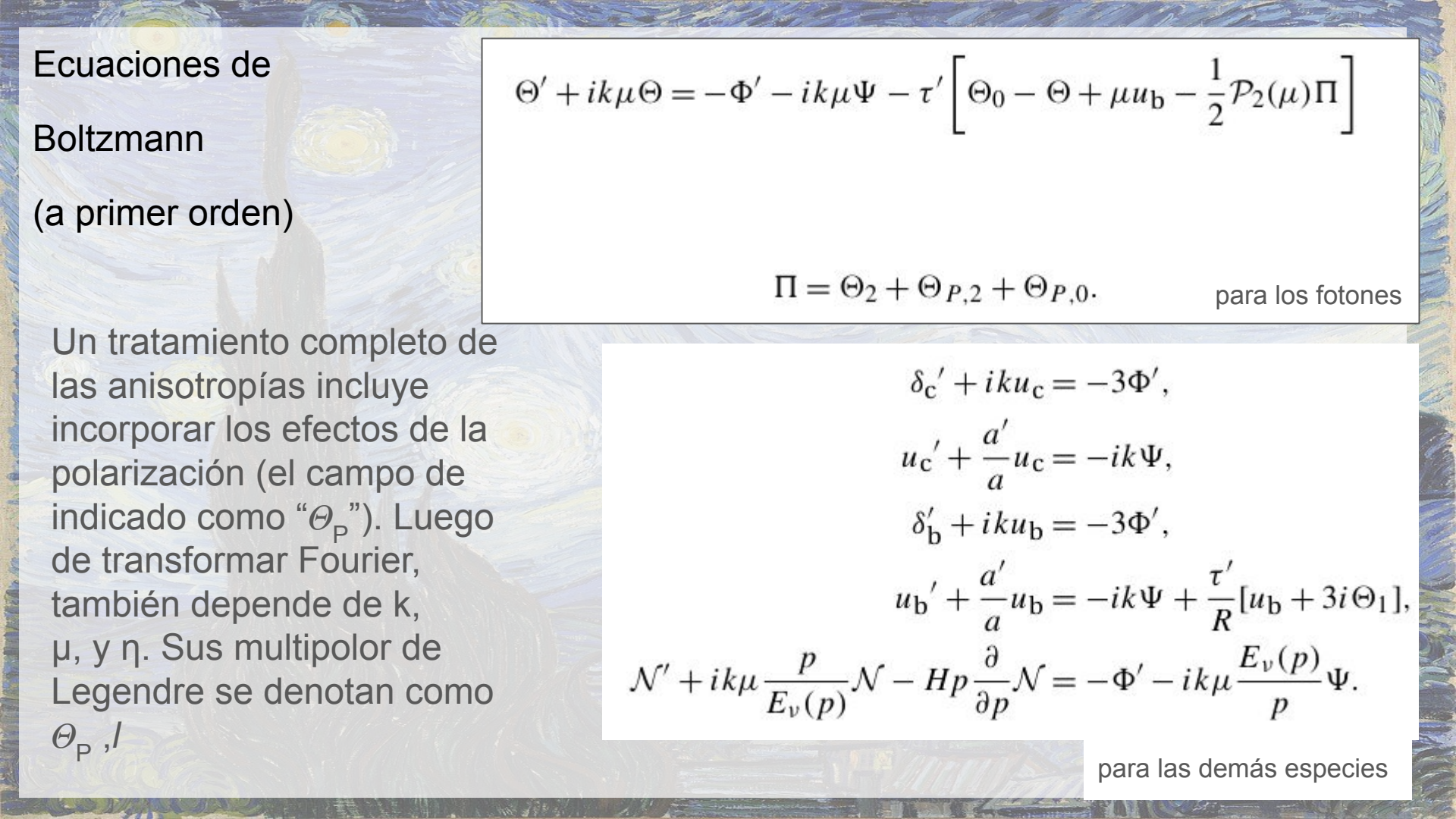
El Universo temprano es muy suave (homogéneo) pero presenta pequeñas **inhomogeneidades**, que dan lugar a la **estructura** que vemos hoy. Para describir la evolución de las perturbaciones, sobre todo a tiempos tempranos, se toma un enfoque perturbativo de las ecuaciones de Einstein, y de Boltzmann.



$$G_{\mu\nu} + \Lambda g_{\mu\nu} = 8\pi G T_{\mu\nu}$$

La evolución de gravedad y partículas están acopladas.

En la asignatura “*Cosmología*” se ve cómo tratar todas las interacciones no gravitacionales mediante las **ecuaciones de Boltzmann** e incluir luego los efectos de la gravedad en las distribuciones de partículas. También se estudia cómo las perturbaciones en las distribuciones de partículas afectan el campo gravitatorio.



Ecuaciones de Boltzmann (a primer orden)

$$\Theta' + ik\mu\Theta = -\Phi' - ik\mu\Psi - \tau'\left[\Theta_0 - \Theta + \mu u_b - \frac{1}{2}\mathcal{P}_2(\mu)\Pi\right]$$

$$\Pi = \Theta_2 + \Theta_{P,2} + \Theta_{P,0}. \quad \text{para los fotones}$$

Un tratamiento completo de las anisotropías incluye incorporar los efectos de la polarización (el campo de indicado como “ Θ_P ”). Luego de transformar Fourier, también depende de k , μ , y η . Sus multipolar de Legendre se denotan como Θ_P, I

$$\delta_c' + iku_c = -3\Phi',$$

$$u_c' + \frac{a'}{a}u_c = -ik\Psi,$$

$$\delta_b' + iku_b = -3\Phi',$$

$$u_b' + \frac{a'}{a}u_b = -ik\Psi + \frac{\tau'}{R}[u_b + 3i\Theta_1],$$

$$\mathcal{N}' + ik\mu \frac{p}{E_v(p)}\mathcal{N} - Hp \frac{\partial}{\partial p}\mathcal{N} = -\Phi' - ik\mu \frac{E_v(p)}{p}\Psi.$$

para las demás especies

Clase 2: Anisotropías en temperatura y polarización del CMB

- Fluctuaciones de temperatura: efecto Sachs-Wolfe, oscilaciones acústicas, amortiguación de Silk
- Polarización del CMB: E and B modes. Conexión con ondas gravitacionales primordiales.

El Universo perturbado: materia y radiación

Estamos interesados en las **anisotropías** en la distribución de fotones, y las **inhomogeneidades** en la materia.

Debemos resolver las ecs. de Einstein y de Boltzmann, con una ec. de Boltzmann para cada especie.

A partir de ahora, tendremos en cuenta la dependencia espacial y direccional de la función de distribución $f(\mathbf{x}, \mathbf{p}, t)$.

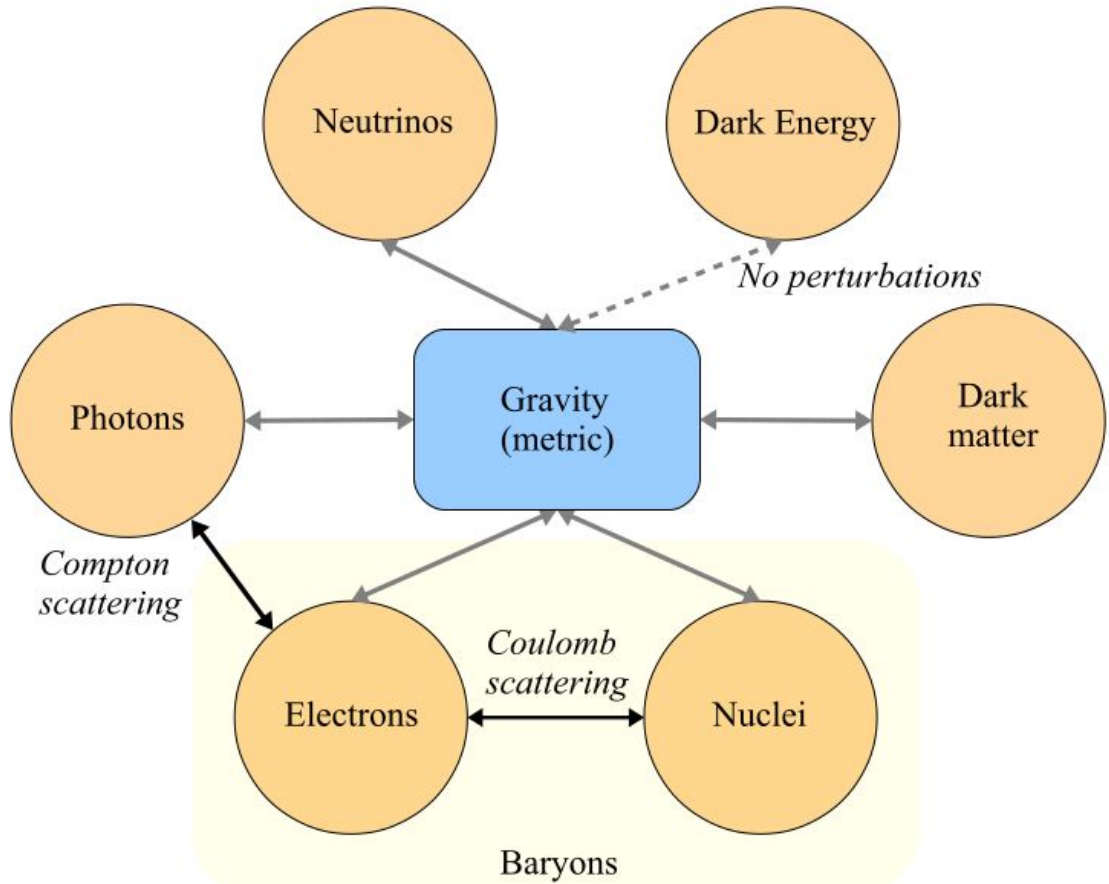
Los **fotones** están afectados por la gravedad y el scattering de Compton con electrones libres.

Los **e-** están acoplados a los protones. Ambos se ven afectados por la gravedad.

La métrica, que determina las fuerzas gravitacionales, está influenciada por todas estas especies, más los neutrinos y la materia oscura.

Las ecuaciones están acopladas.

El objetivo es tener la ecuación de evolución de las perturbaciones en todas las especies relevantes. Esto nos permitirá luego calcular cantidades observables.



Diferentes componentes interactúan entre sí.

Las conexiones son las que aparecen en las ecs. de Einstein-Boltzmann acopladas.

El acoplamiento fuertes entre electrones y núcleos a través del scattering de Coulomb, nos permite tratarlo como una única componente (bariones).

No consideramos perturbaciones de la energía oscura, por lo que sólo entra en la métrica de fondo.

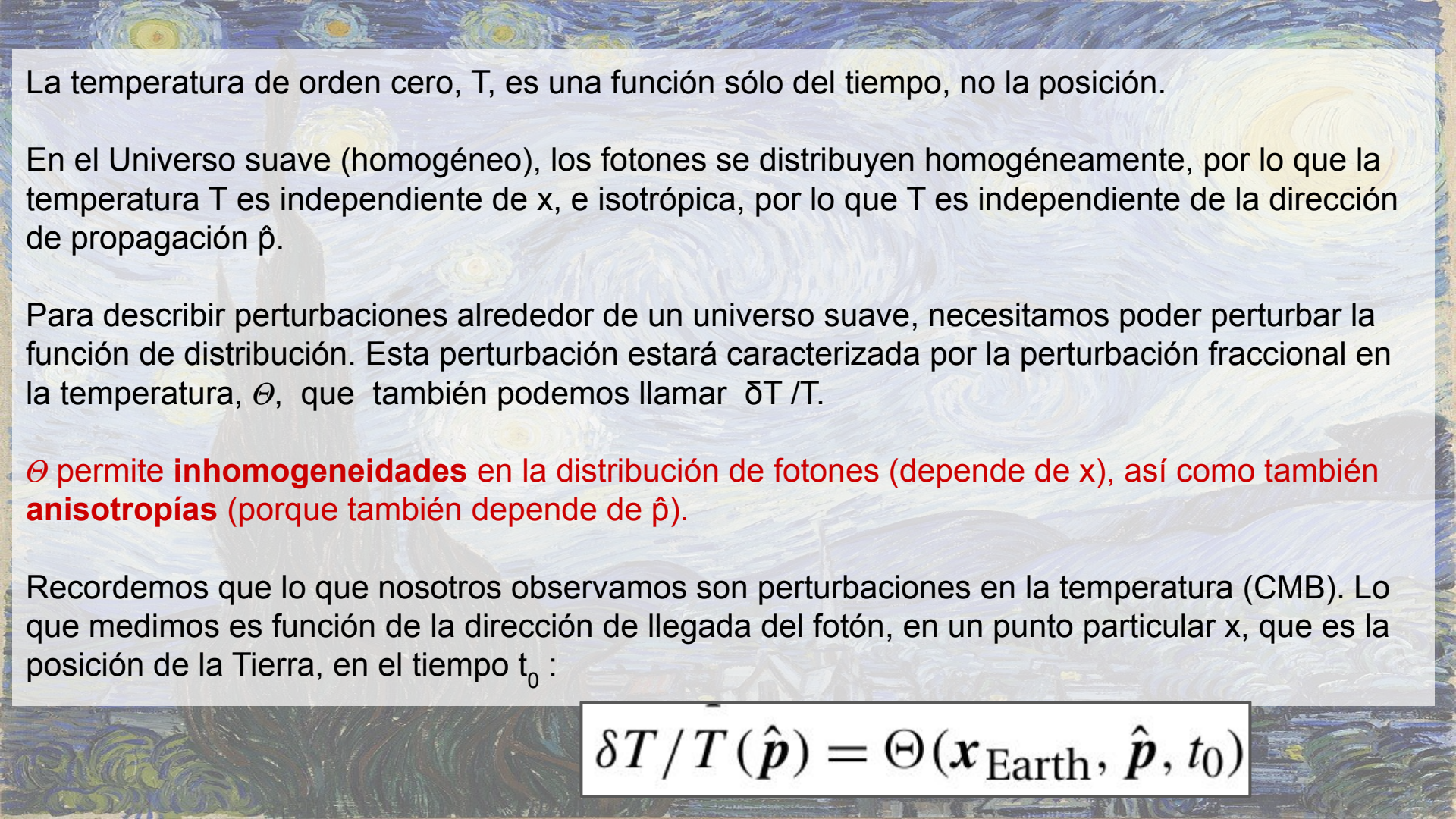
Ec. de Boltzmann para los fotones

Ya habíamos derivado el lado izquierdo de la ec., en un universo con perturbaciones lineales en la métrica:

$$\frac{df}{dt} = \frac{\partial f}{\partial t} + \frac{\hat{p}^i}{a} \frac{\partial f}{\partial x^i} - p \frac{\partial f}{\partial p} \left[H + \dot{\Phi} + \frac{\hat{p}^i}{a} \frac{\partial \Psi}{\partial x^i} \right]$$

Ahora desarrollamos la función de distribución de los fotones, f , alrededor de su distribución de equilibrio f_0 (que es la función de Bose-Einstein) de esta manera:

$$f(\mathbf{x}, p, \hat{\mathbf{p}}, t) = \left[\exp \left\{ \frac{p}{T(t)[1 + \Theta(\mathbf{x}, \hat{\mathbf{p}}, t)]} \right\} - 1 \right]^{-1}$$

A reproduction of Vincent van Gogh's painting "The Starry Night". The scene depicts a dark blue night sky filled with numerous small, white stars and a large, bright yellow crescent moon. Below the sky, a small town with houses and church spires is nestled among rolling green hills. The foreground consists of dark, swirling brushstrokes representing fields or trees.

La temperatura de orden cero, T , es una función sólo del tiempo, no la posición.

En el Universo suave (homogéneo), los fotones se distribuyen homogéneamente, por lo que la temperatura T es independiente de x , e isotrópica, por lo que T es independiente de la dirección de propagación \hat{p} .

Para describir perturbaciones alrededor de un universo suave, necesitamos poder perturbar la función de distribución. Esta perturbación estará caracterizada por la perturbación fraccional en la temperatura, Θ , que también podemos llamar $\delta T / T$.

Θ permite **inhomogeneidades** en la distribución de fotones (depende de x), así como también **anisotropías** (porque también depende de \hat{p}).

Recordemos que lo que nosotros observamos son perturbaciones en la temperatura (CMB). Lo que medimos es función de la dirección de llegada del fotón, en un punto particular x , que es la posición de la Tierra, en el tiempo t_0 :

$$\delta T / T(\hat{p}) = \Theta(x_{\text{Earth}}, \hat{p}, t_0)$$

Por ahora, consideraremos las colisiones entre electrones y fotones como choques elásticos, por lo que Θ no depende de la magnitud del momento p .

Este efecto se llama Thomson scattering. Sin embargo, seguiremos llamándolo “Compton scattering”.

Vamos a considerar que Θ es pequeño, y también los potenciales Φ, Ψ .

Desarrollamos f a primer orden en Θ :

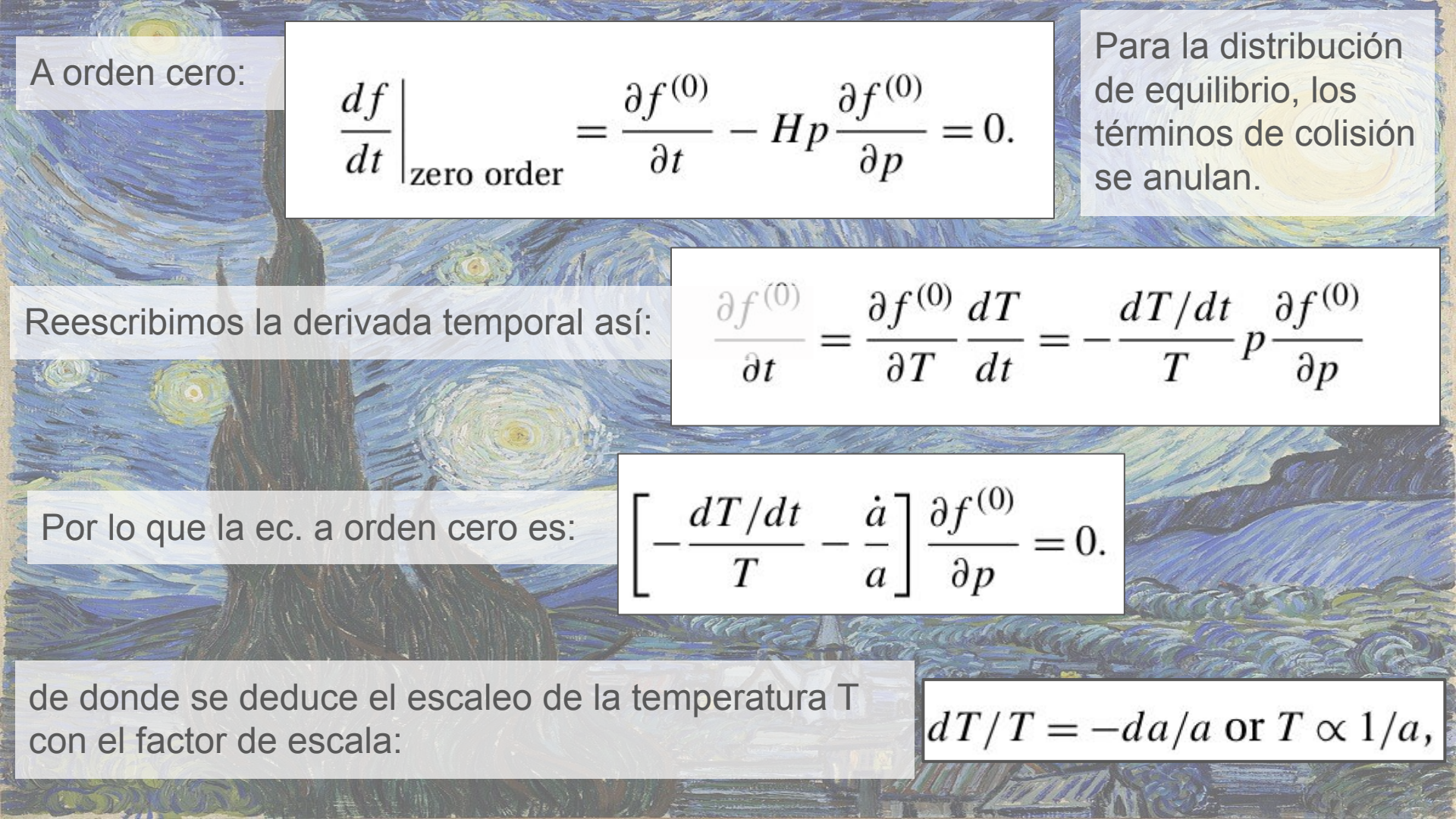
$$\begin{aligned} f(\mathbf{x}, \mathbf{p}, t) &\simeq \frac{1}{e^{p/T(t)} - 1} + \left(\frac{\partial}{\partial T} \left[\exp \left\{ \frac{p}{T(t)} \right\} - 1 \right]^{-1} \right) T(t) \Theta(\mathbf{x}, \hat{\mathbf{p}}, t) \\ &= f^{(0)}(p, t) - p \frac{\partial f^{(0)}(p, t)}{\partial p} \Theta(\mathbf{x}, \hat{\mathbf{p}}, t). \end{aligned}$$

donde $f^{(0)} \equiv \left[\exp \left\{ \frac{p}{T} \right\} - 1 \right]^{-1}$ es la función de distribución de B-E con potencial químico cero.

y hemos usado que para esta función:

$$T \partial f^{(0)} / \partial T = -p \partial f^{(0)} / \partial p.$$

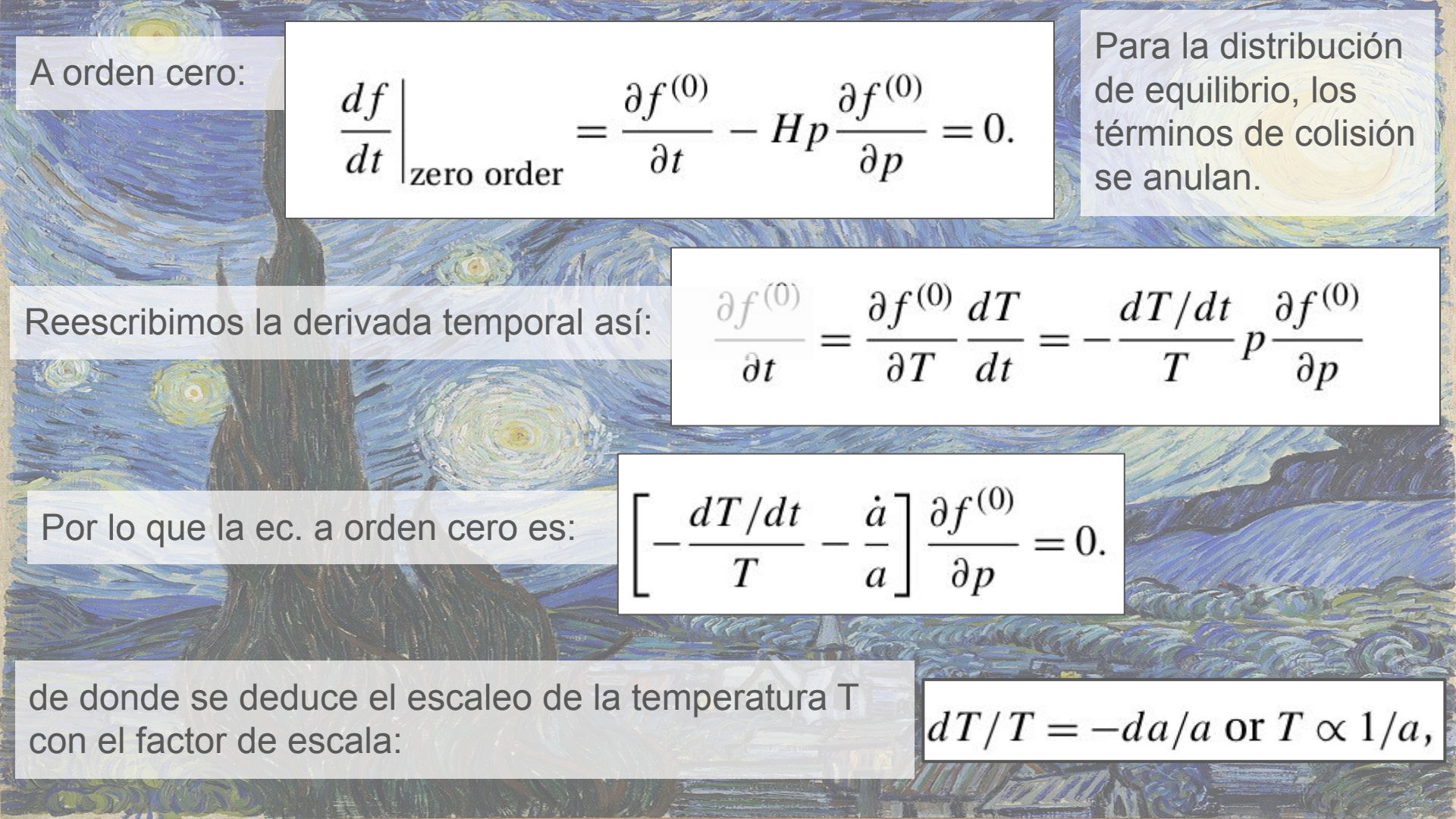
Ahora sepáramos la ec. de Boltzmann en una ec. de orden cero, y una a primer orden en θ



A orden cero:

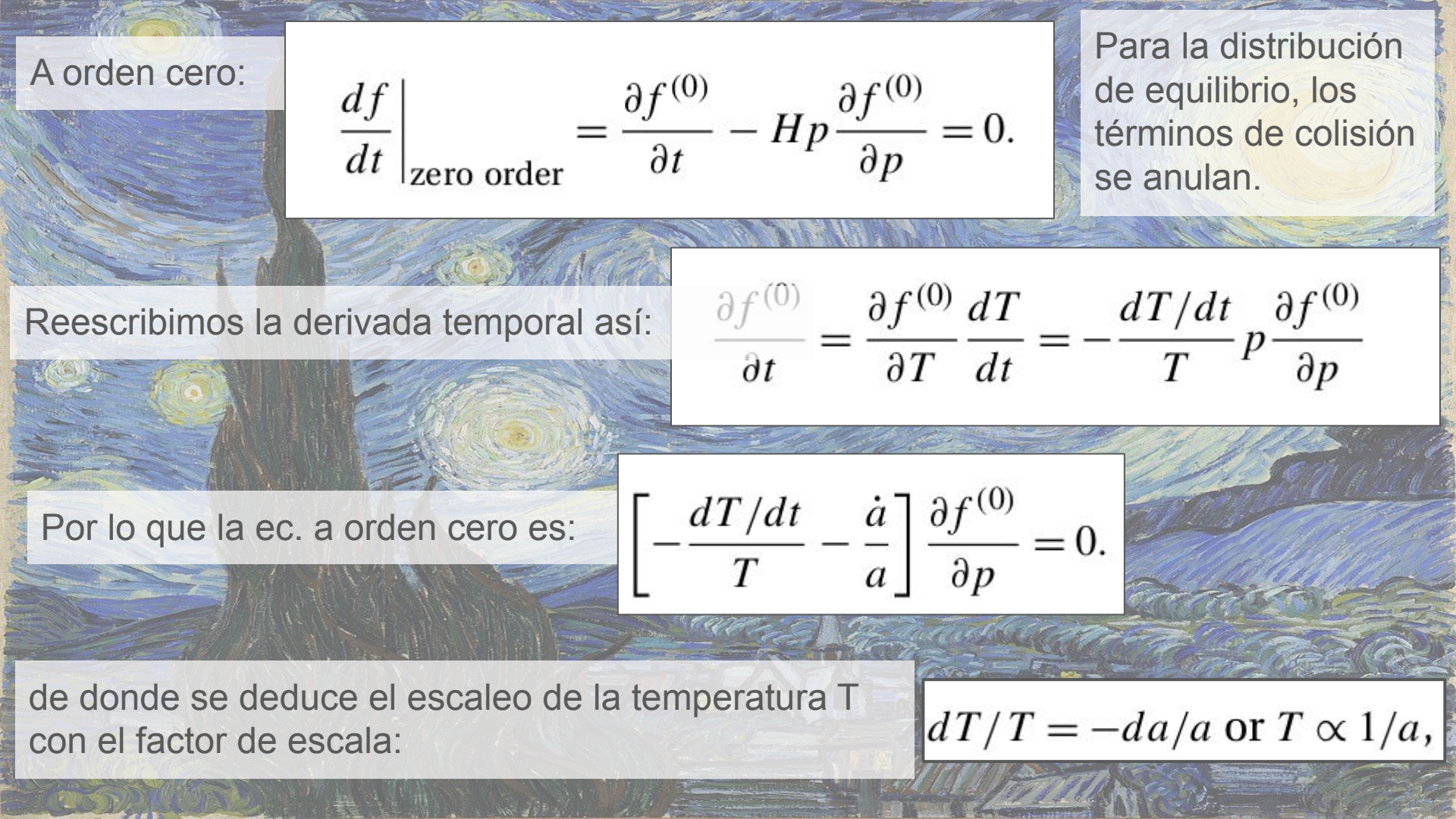
$$\left. \frac{df}{dt} \right|_{\text{zero order}} = \frac{\partial f^{(0)}}{\partial t} - H p \frac{\partial f^{(0)}}{\partial p} = 0.$$

Para la distribución de equilibrio, los términos de colisión se anulan.



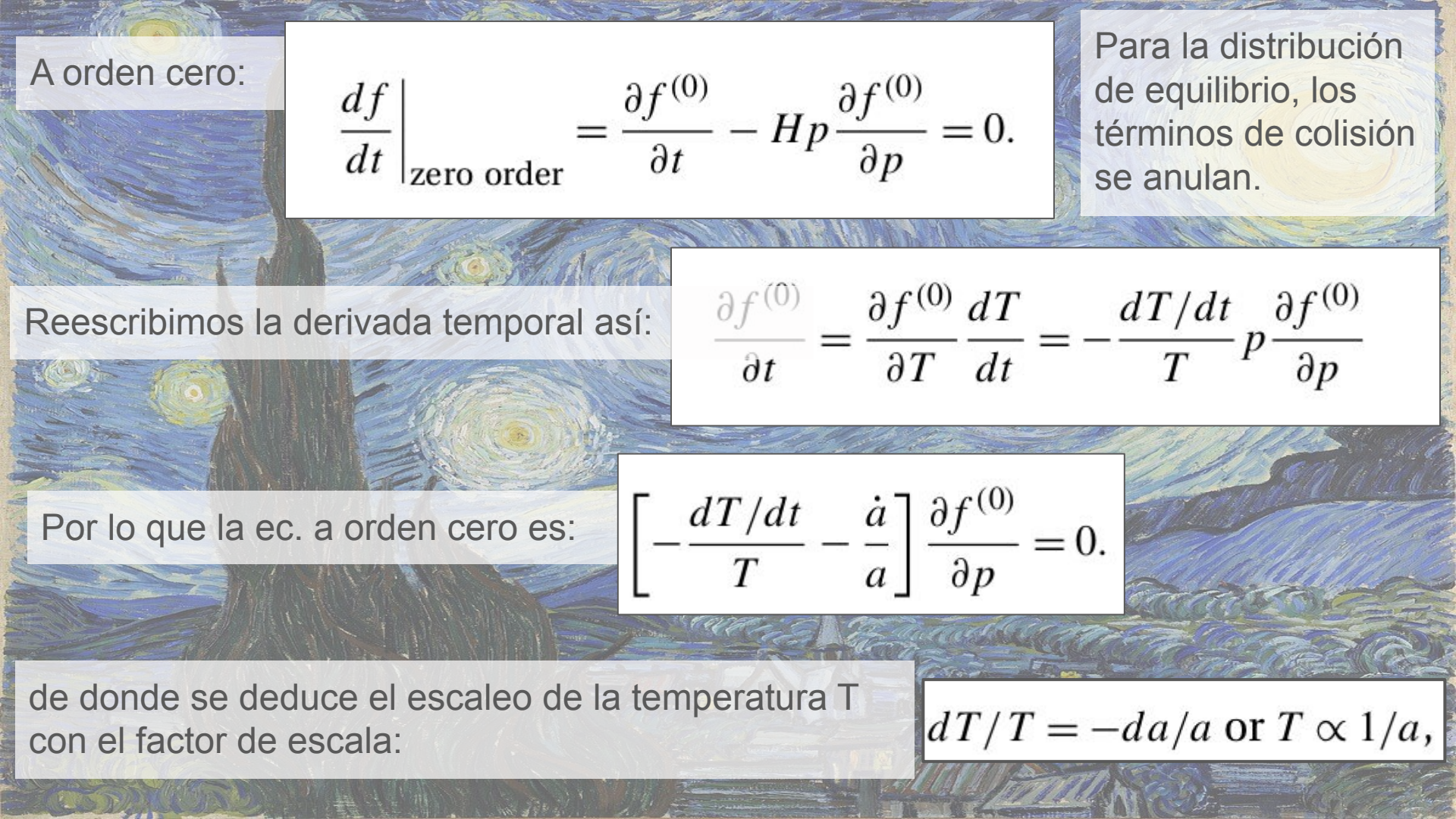
Reescribimos la derivada temporal así:

$$\frac{\partial f^{(0)}}{\partial t} = \frac{\partial f^{(0)}}{\partial T} \frac{dT}{dt} = -\frac{dT/dt}{T} p \frac{\partial f^{(0)}}{\partial p}$$



Por lo que la ec. a orden cero es:

$$\left[-\frac{dT/dt}{T} - \frac{\dot{a}}{a} \right] \frac{\partial f^{(0)}}{\partial p} = 0.$$



de donde se deduce el escaleo de la temperatura T con el factor de escala:

$$dT/T = -da/a \text{ or } T \propto 1/a,$$

La ec. a primer orden (sin colisiones) es:

$$\frac{df}{dt} \Big|_{\text{first order}} = -p \frac{\partial}{\partial t} \left[\frac{\partial f^{(0)}}{\partial p} \Theta \right] - p \frac{\hat{p}^i}{a} \frac{\partial \Theta}{\partial x^i} \frac{\partial f^{(0)}}{\partial p} + H \Theta p \frac{\partial}{\partial p} \left[p \frac{\partial f^{(0)}}{\partial p} \right] \\ - p \frac{\partial f^{(0)}}{\partial p} \left[\dot{\Phi} + \frac{\hat{p}^i}{a} \frac{\partial \Psi}{\partial x^i} \right].$$

que se puede escribir como:

$$\frac{df}{dt} \Big|_{\text{first order}} = -p \frac{\partial f^{(0)}}{\partial p} \left[\dot{\Theta} + \frac{\hat{p}^i}{a} \frac{\partial \Theta}{\partial x^i} + \dot{\Phi} + \frac{\hat{p}^i}{a} \frac{\partial \Psi}{\partial x^i} \right]$$

free-streaming

efecto de las perturbaciones

We now extract the equation for the deviation of the photon temperature from its zeroth-order value, i.e., an equation for Θ , from Eq. (5.1). To do this, we insert the expansion of Eq. (5.3) everywhere we encounter f :

$$\begin{aligned} \frac{df}{dt} \Big|_{\text{first order}} &= -p \frac{\partial}{\partial t} \left[\frac{\partial f^{(0)}}{\partial p} \Theta \right] - p \frac{\hat{p}^i}{a} \frac{\partial \Theta}{\partial x^i} \frac{\partial f^{(0)}}{\partial p} + H \Theta p \frac{\partial}{\partial p} \left[p \frac{\partial f^{(0)}}{\partial p} \right] \\ &\quad - p \frac{\partial f^{(0)}}{\partial p} \left[\dot{\Phi} + \frac{\hat{p}^i}{a} \frac{\partial \Psi}{\partial x^i} \right]. \end{aligned} \quad (5.7)$$

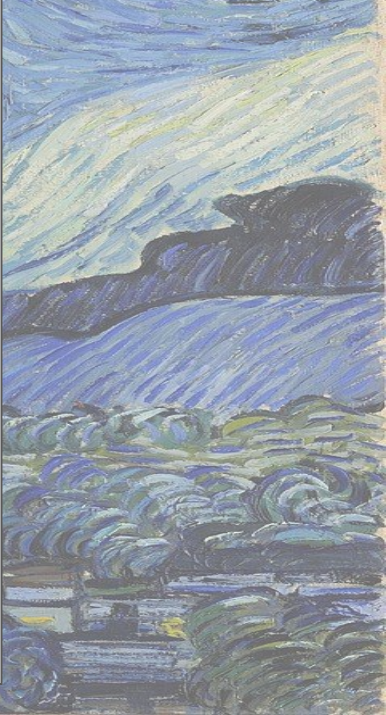
Consider the first term on the right-hand side here. The time derivative on $f^{(0)}$ can be rewritten as a temperature derivative so

$$\begin{aligned} -p \frac{\partial}{\partial t} \left[\frac{\partial f^{(0)}}{\partial p} \Theta \right] &= -p \frac{\partial f^{(0)}}{\partial p} \frac{\partial \Theta}{\partial t} - p \Theta \frac{dT}{dt} \frac{\partial^2 f^{(0)}}{\partial T \partial p} \\ &= -p \frac{\partial f^{(0)}}{\partial p} \frac{\partial \Theta}{\partial t} + p \Theta \frac{dT/dt}{T} \frac{\partial}{\partial p} \left[p \frac{\partial f^{(0)}}{\partial p} \right]. \end{aligned} \quad (5.8)$$

The second line follows here since $\partial f^{(0)} / \partial T = -(p/T) \partial f^{(0)} / \partial p$. The second term on this second line cancels the third term on the right in Eq. (5.7), so we can finally write down the left-hand side of the Boltzmann equation for Θ :

$$\frac{df}{dt} \Big|_{\text{first order}} = -p \frac{\partial f^{(0)}}{\partial p} \left[\dot{\Theta} + \frac{\hat{p}^i}{a} \frac{\partial \Theta}{\partial x^i} + \dot{\Phi} + \frac{\hat{p}^i}{a} \frac{\partial \Psi}{\partial x^i} \right]. \quad (5.9)$$

(pasos
detallados de
la filmina
anterior)



OBSERVACIONES: (para la ec. de Boltzmann de los fotones a primer orden)

Los primeros dos términos corresponden a derivadas a lo largo de geodésicas nulas, en el Universo homogéneo.

Describen como la función de distribución evoluciona en ausencia de colisiones, también conocido como “free streaming”.

Los últimos dos términos tienen en cuenta los efectos de las perturbaciones.

Notar que cada vez que aparece x , aparece multiplicado por a , el factor de escala.

Esto pasa porque las distancias físicas son: ax .

A esta ecuación le falta el término de colisiones.

Término de colisiones

Ahora, además de considerar el fenómeno fuera del equilibrio químico, también nos alejaremos del equilibrio cinético, para poder seguir la evolución de la distribución de los fotones en recombinação, y hasta hoy (CMB observable).

Este es el proceso de scattering que nos interesa:

$$e^-(\mathbf{q}) + \gamma(\mathbf{p}) \leftrightarrow e^-(\mathbf{q}') + \gamma(\mathbf{p}').$$

$$\begin{aligned} C[f(\mathbf{p})] = & \frac{1}{2E(p)} \int \frac{d^3 q}{(2\pi)^3 2E_e(q)} \int \frac{d^3 q'}{(2\pi)^3 2E_e(q')} \int \frac{d^3 p'}{(2\pi)^3 2E(p')} \sum_{\text{3 spins}} |\mathcal{M}|^2 \\ & \times (2\pi)^4 \delta_D^{(3)}[\mathbf{p} + \mathbf{q} - \mathbf{p}' - \mathbf{q}'] \delta_D^{(1)}[E(p) + E_e(q) - E(p') - E_e(q')] \\ & \times \{f_e(\mathbf{q}') f(\mathbf{p}') - f_e(\mathbf{q}) f(\mathbf{p})\}. \end{aligned}$$

La energía de los fotones es: $E(p) = p$ y $E(p') = p'$

Para los electrones, tomamos el límite no relativista. Esto es suficiente en la época de recombinação, cuando las energías cinéticas típicas de los electrones, del orden de T , son mucho menores que la masa del electrón.

$$E(p) = p \sim T,$$

$$E_e(q) - m_e = q^2/(2m_e) \sim T \quad \Rightarrow \quad q \sim T \sqrt{\frac{2m_e}{T}}.$$

Cerca del equilibrio, la energía típica de los fotones, y la energía cinética típica de los electrones es de orden T .

El **momento de los electrones (q)** es mucho mayor que el momento de los fotones, dado que $m_e/T \gg 1$.

El scattering de Compton es casi elástico, y usamos esa aprox. en lo que sigue.

$$C[f(\mathbf{p})] = \frac{\pi}{8m_e^2 p} \int \frac{d^3 q}{(2\pi)^3} f_e(\mathbf{q}) \int \frac{d^3 p'}{(2\pi)^3 p'} \sum_{3 \text{ spins}} |\mathcal{M}|^2$$

$$\times \left\{ \delta_D^{(1)}(p - p') + \frac{(\mathbf{p} - \mathbf{p}') \cdot \mathbf{q}}{m_e} \frac{\partial \delta_D^{(1)}(p - p')}{\partial p'} \right\} \{f(\mathbf{p}') - f(\mathbf{p})\}.$$

usando:

$$\sum_{3 \text{ spins}} |\mathcal{M}|^2 = 32\pi\sigma_T m_e^2 \quad (\text{spin- and angle-average}).$$

Al promediar en los estados de spin de los fotones, estamos ignorando el efecto de la polarización del campo de radiación. En realidad, la amplitud del scattering de Compton tiene una dependencia con la polarización, que lleva a que una pequeña polarización en el CMB. Más adelante la vamos a considerar.

El scattering teh Compton también acopla las perturbaciones en temperatura y polarización, por lo que es necesario considerarla.

Por ahora lo vamos a despreciar en el término de colisiones, pero lo vamos a retomar más adelante.

La integral de q da un factor $n_e/2$

y los términos con \mathbf{q}/m_e , dan $n_e \mathbf{u}_b/2$, donde \mathbf{u}_b es la velocidad de *bulk* de los electrones.

$$\begin{aligned} C[f(\mathbf{p})] &= \frac{2\pi^2 n_e \sigma_T}{p} \int \frac{d^3 p'}{(2\pi)^3 p'} \left\{ \delta_D^{(1)}(\mathbf{p} - \mathbf{p}') + (\mathbf{p} - \mathbf{p}') \cdot \mathbf{u}_b \frac{\partial \delta_D^{(1)}(\mathbf{p} - \mathbf{p}')}{\partial p'} \right\} \\ &\quad \times \left\{ f^{(0)}(\mathbf{p}') - f^{(0)}(\mathbf{p}) - p' \frac{\partial f^{(0)}}{\partial p'} \Theta(\hat{\mathbf{p}}') + p \frac{\partial f^{(0)}}{\partial p} \Theta(\hat{\mathbf{p}}) \right\} \\ &= \frac{n_e \sigma_T}{4\pi p} \int_0^\infty dp' p' \int d\Omega' \left[\delta_D^{(1)}(\mathbf{p} - \mathbf{p}') \left(-p' \frac{\partial f^{(0)}}{\partial p'} \Theta(\hat{\mathbf{p}}') + p \frac{\partial f^{(0)}}{\partial p} \Theta(\hat{\mathbf{p}}) \right) \right. \\ &\quad \left. + (\mathbf{p} - \mathbf{p}') \cdot \mathbf{u}_b \frac{\partial \delta_D^{(1)}(\mathbf{p} - \mathbf{p}')}{\partial p'} (f^{(0)}(\mathbf{p}') - f^{(0)}(\mathbf{p})) \right], \end{aligned}$$

ángulo sólido de \mathbf{p}'

colisiones
locales

En este $C[f]$, separamos f en parte de orden cero (que se cancela) y parte a primer orden.

$$\Theta_0(\mathbf{x}, t) \equiv \frac{1}{4\pi} \int d\Omega' \Theta(\hat{\mathbf{p}}', \mathbf{x}, t).$$

monopolio

El monopolio es una integral en la distribución de los fotones en cada punto, sobre todas las direcciones del fotón. Es la perturbación fraccional del flujo de fotones promediado en el ángulo, a una dada posición \mathbf{x} , y un dado tiempo t .

No se puede absorber el monopolio en la definición de la temperatura a orden cero, porque depende de la posición, mientras que la T es constante en el espacio.

$$C[f(\mathbf{p})] = \frac{n_e \sigma_T}{p} \int_0^\infty dp' p' \left[\delta_D^{(1)}(p - p') \left(-p' \frac{\partial f^{(0)}}{\partial p'} \Theta_0 + p \frac{\partial f^{(0)}}{\partial p} \Theta(\hat{\mathbf{p}}) \right) + \mathbf{p} \cdot \mathbf{u}_b \frac{\partial \delta_D^{(1)}(p - p')}{\partial p'} (f^{(0)}(p') - f^{(0)}(p)) \right].$$

Ahora hacemos la integral sobre p . La primera línea se integral trivialmente por la delta de Dirac, y la segunda se integra por partes:

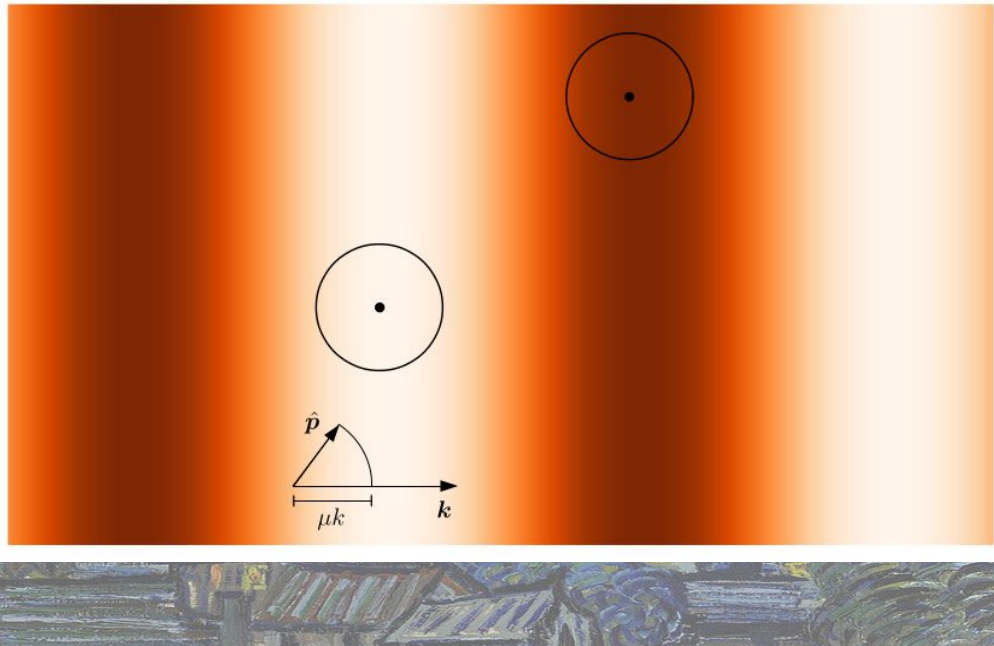
$$C[f(p)] = -p \frac{\partial f^{(0)}}{\partial p} n_e \sigma T [\Theta_0 - \Theta(\hat{p}) + \hat{p} \cdot \mathbf{u}_b]$$

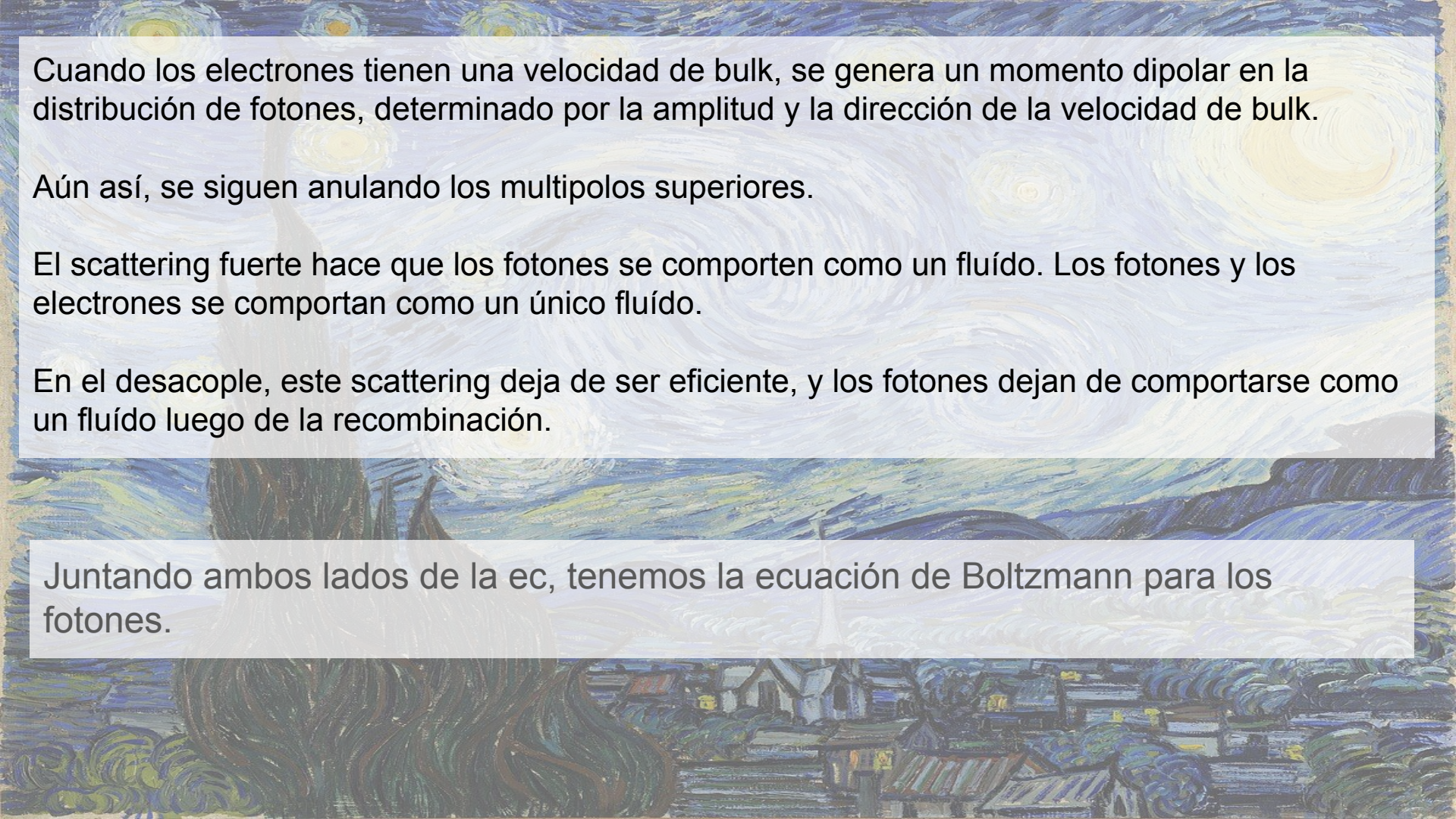
De acá se puede ver el efecto del scattering de Compton en la distribución de fotones.

En ausencia de velocidad de bulk de los electrones ($\mathbf{u}_b = 0$), el término de colisiones sirve para llevar Θ a Θ_0 .

Cuando el scattering es muy eficiente, sólo la perturbación del monopolo sobrevive.
Todas las demás anisotropías se borran.

Si el scattering es fuerte, el camino libre medio del fotón es muy corto. Entonces, los fotones que llegan a un punto x provienen de una región muy cercana, por lo que tienen una temperatura muy similar.



A background image of Vincent van Gogh's painting "The Starry Night". The sky is filled with swirling, star-filled clouds in shades of blue, white, and yellow. In the foreground, dark green trees are visible on the left, and a small town with houses and church spires is nestled in a valley below.

Cuando los electrones tienen una velocidad de bulk, se genera un momento dipolar en la distribución de fotones, determinado por la amplitud y la dirección de la velocidad de bulk.

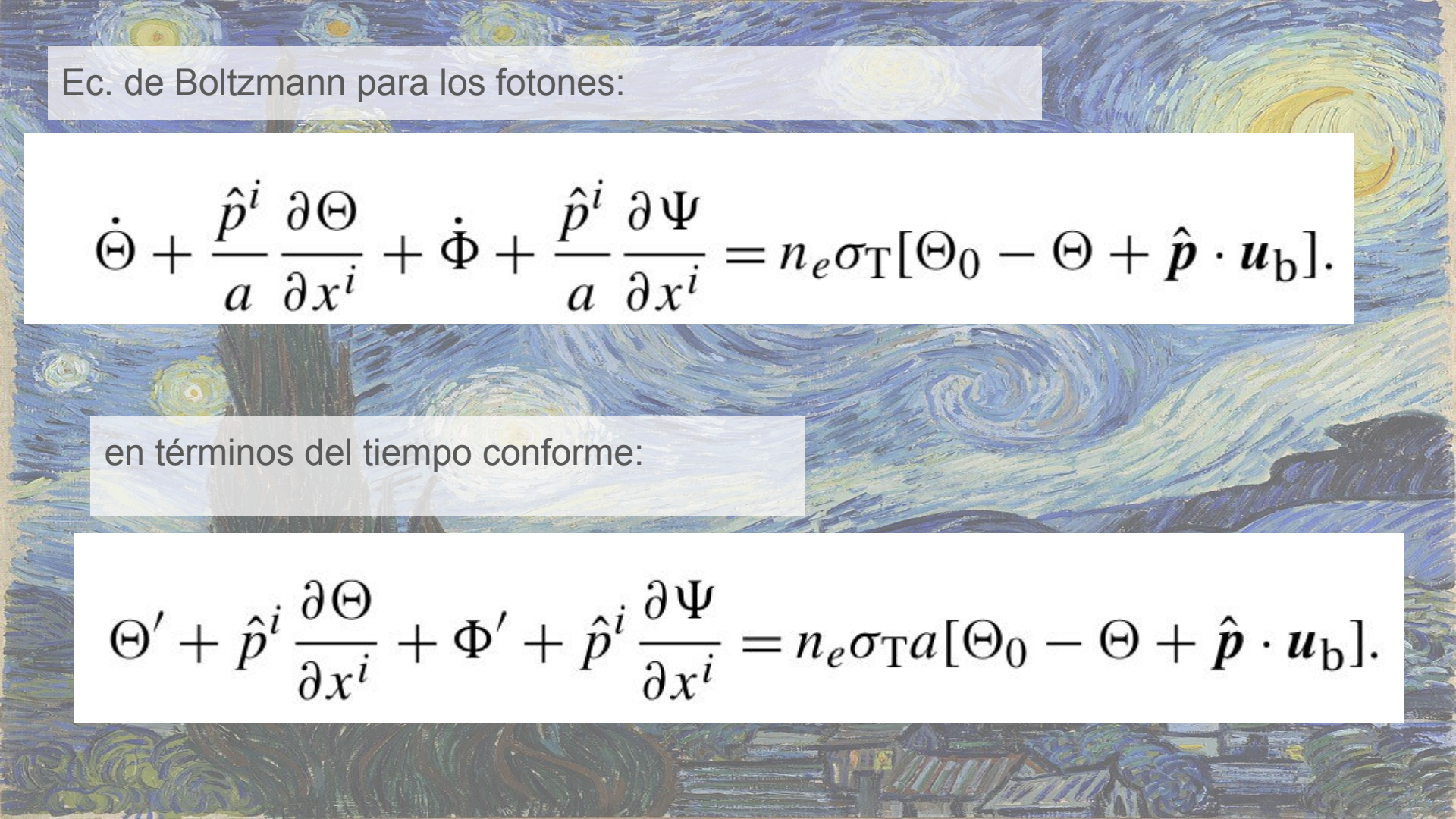
Aún así, se siguen anulando los multipolos superiores.

El scattering fuerte hace que los fotones se comporten como un fluído. Los fotones y los electrones se comportan como un único fluído.

En el desacople, este scattering deja de ser eficiente, y los fotones dejan de comportarse como un fluido luego de la recombinación.

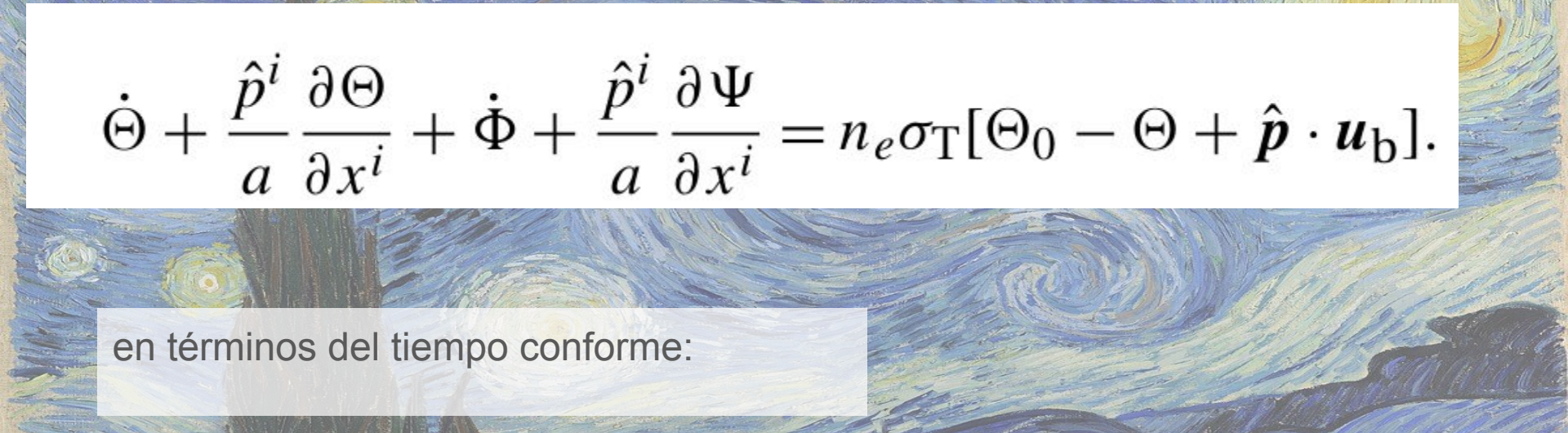
A continuation of the background image, showing the same scene of "The Starry Night" with its characteristic swirling brushwork and starry sky.

Juntando ambos lados de la ec, tenemos la ecuación de Boltzmann para los fotones.

A reproduction of Vincent van Gogh's painting "The Starry Night". The scene depicts a dark blue night sky filled with swirling, star-filled clouds. In the foreground, a small town with houses and church steeples is visible at the base of a hill. The brushwork is characterized by thick, expressive strokes.

Ec. de Boltzmann para los fotones:

$$\dot{\Theta} + \frac{\hat{p}^i}{a} \frac{\partial \Theta}{\partial x^i} + \dot{\Phi} + \frac{\hat{p}^i}{a} \frac{\partial \Psi}{\partial x^i} = n_e \sigma_T [\Theta_0 - \Theta + \hat{\mathbf{p}} \cdot \mathbf{u}_b].$$

A reproduction of Vincent van Gogh's painting "The Starry Night". The scene depicts a dark blue night sky filled with swirling, star-filled clouds. In the foreground, a small town with houses and church steeples is visible at the base of a hill. The brushwork is characterized by thick, expressive strokes.

en términos del tiempo conforme:

$$\Theta' + \hat{p}^i \frac{\partial \Theta}{\partial x^i} + \Phi' + \hat{p}^i \frac{\partial \Psi}{\partial x^i} = n_e \sigma_T a [\Theta_0 - \Theta + \hat{\mathbf{p}} \cdot \mathbf{u}_b].$$

5.1 The virtues of Fourier space

Consider a field $\delta(\mathbf{x}, t)$ that obeys a linear partial differential equation, for example

$$\frac{\partial^2}{\partial t^2} \delta + f(t) \frac{\partial}{\partial t} \delta + g(t) \nabla^2 \Psi = 0, \quad (5.25)$$

in terms of another field $\Psi(\mathbf{x}, t)$. What is noteworthy about this equation apart from its linearity is that the coefficients are functions of time t only. In fact, in cosmology this property follows directly when studying small perturbations around a smooth universe: the only \mathbf{x} dependence can be due to perturbations, and we work to linear order in them. A partial differential equation of the form Eq. (5.25) is particularly well-suited to working in Fourier space. Let us define spatial Fourier transforms through

$$\delta(\mathbf{x}) = \int \frac{d^3 k}{(2\pi)^3} e^{i \mathbf{k} \cdot \mathbf{x}} \tilde{\delta}(\mathbf{k}), \quad (5.26)$$

from which follows

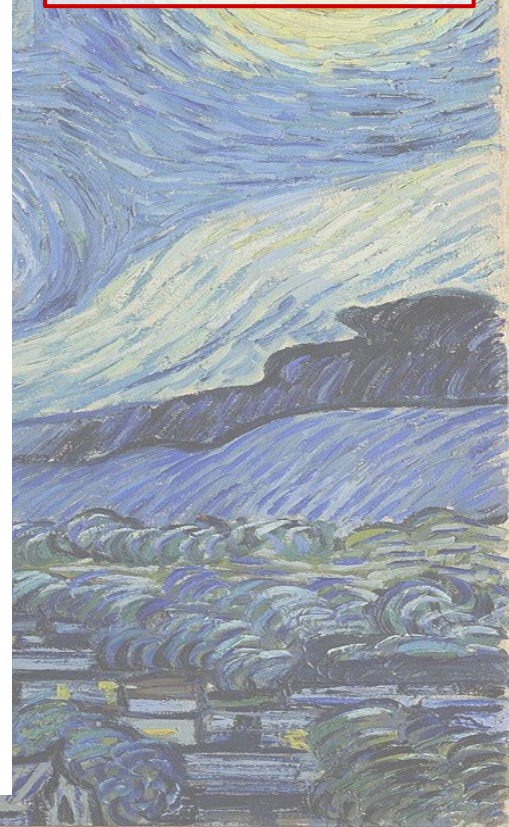
$$\tilde{\delta}(\mathbf{k}) = \int d^3 x e^{-i \mathbf{k} \cdot \mathbf{x}} \delta(\mathbf{x}). \quad (5.27)$$

Derivatives with respect to \mathbf{x} acting on $\delta(\mathbf{x})$ become algebraic relations in Fourier space:

$$\frac{\partial \delta(\mathbf{x}, t)}{\partial x^i} \rightarrow i k_i \tilde{\delta}(\mathbf{k}, t). \quad (5.28)$$

Note that k^i is a 3D vector in Euclidean space so that $k_i = k^i$; you do not need a factor of g_{ij} to go back and forth, just as is the case for the derivatives ∂_i . The same goes for the velocity u_b^i and other 3-vectors. We will often characterize a mode by the magnitude of its wavevector: $k = |\mathbf{k}|$.

Sobre la
Transformada de
Fourier



Convention: Throughout this book, with few exceptions, we will drop the tilde on Fourier-transformed quantities, so that, for example,

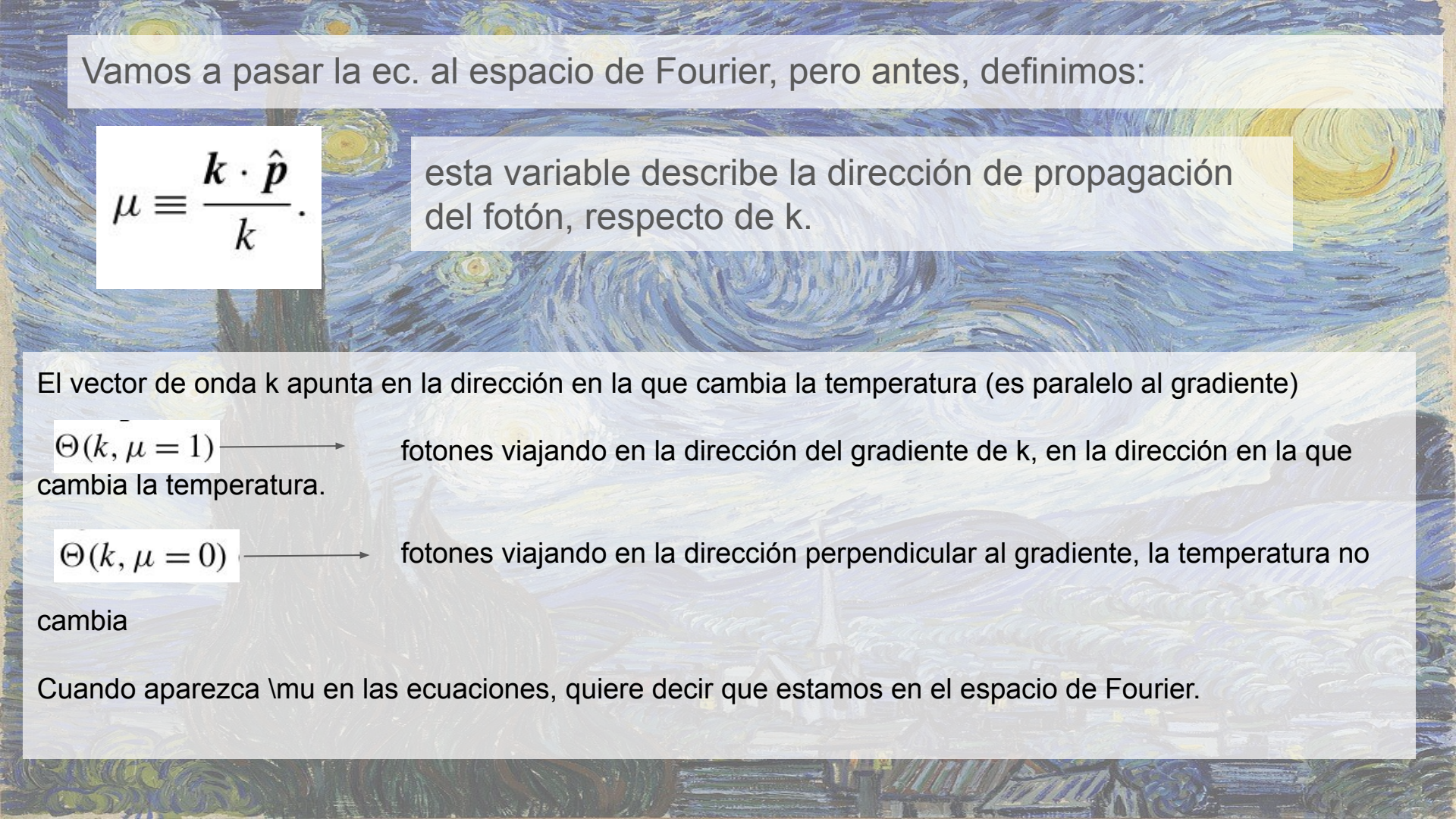
$$\tilde{\delta}(\mathbf{k}) \rightarrow \delta(\mathbf{k}). \quad (5.29)$$

This convention is used in much of the literature. Despite appearances, it is rarely confusing, because Fourier-space fields can be distinguished by their argument as in the above equation, and equations in Fourier space usually have factors of \mathbf{k} and no spatial derivatives.

With these relations, Eq. (5.25) becomes, in Fourier space,

$$\frac{\partial^2}{\partial t^2} \delta + f(t) \frac{\partial}{\partial t} \delta - g(t) k^2 \Psi = 0. \quad (5.30)$$

The partial differential equation magically turned into a set of ordinary differential equations which, moreover, are decoupled: we can solve the equation independently for each \mathbf{k} , without knowing the solution for other values of \mathbf{k}' . Another way of saying this is that every Fourier mode *evolves independently*. Instead of solving an infinite number of coupled equations, which is what Eq. (5.25) represents, we can solve for one \mathbf{k} -mode at a time. At linear order, this trick works every time in cosmology.



Vamos a pasar la ec. al espacio de Fourier, pero antes, definimos:

$$\mu \equiv \frac{\mathbf{k} \cdot \hat{\mathbf{p}}}{|\mathbf{k}|}.$$

esta variable describe la dirección de propagación del fotón, respecto de \mathbf{k} .

El vector de onda \mathbf{k} apunta en la dirección en la que cambia la temperatura (es paralelo al gradiente)

$\Theta(k, \mu = 1) \longrightarrow$ fotones viajando en la dirección del gradiente de \mathbf{k} , en la dirección en la que cambia la temperatura.

$\Theta(k, \mu = 0) \longrightarrow$ fotones viajando en la dirección perpendicular al gradiente, la temperatura no cambia

Cuando aparezca μ en las ecuaciones, quiere decir que estamos en el espacio de Fourier.

$$\mathbf{u}_b(k, \eta) = \frac{k}{\eta} u_b(k, \eta).$$

En cosmología, las velocidades suelen ser longitudinales (apuntan en la dirección de k)

Equivalent a decir que la velocidad es irrotacional.

$\mathbf{u}_b \cdot \hat{\mathbf{p}} = u_b \mu$. La profundidad óptica es:

(in real space, $\nabla \times \mathbf{u} = 0$). So,

$$\tau(\eta) \equiv \int_{\eta}^{\eta_0} d\eta' n_e \sigma_T a. \quad (5.33)$$

A tiempos tardíos, la densidad de electrones libre es muy baja, entonces: $\tau \ll 1$,
A tiempos tempranos, la prof óptica es muy grande.

$$\tau' \equiv \frac{d\tau}{d\eta} = -n_e \sigma_T a.$$

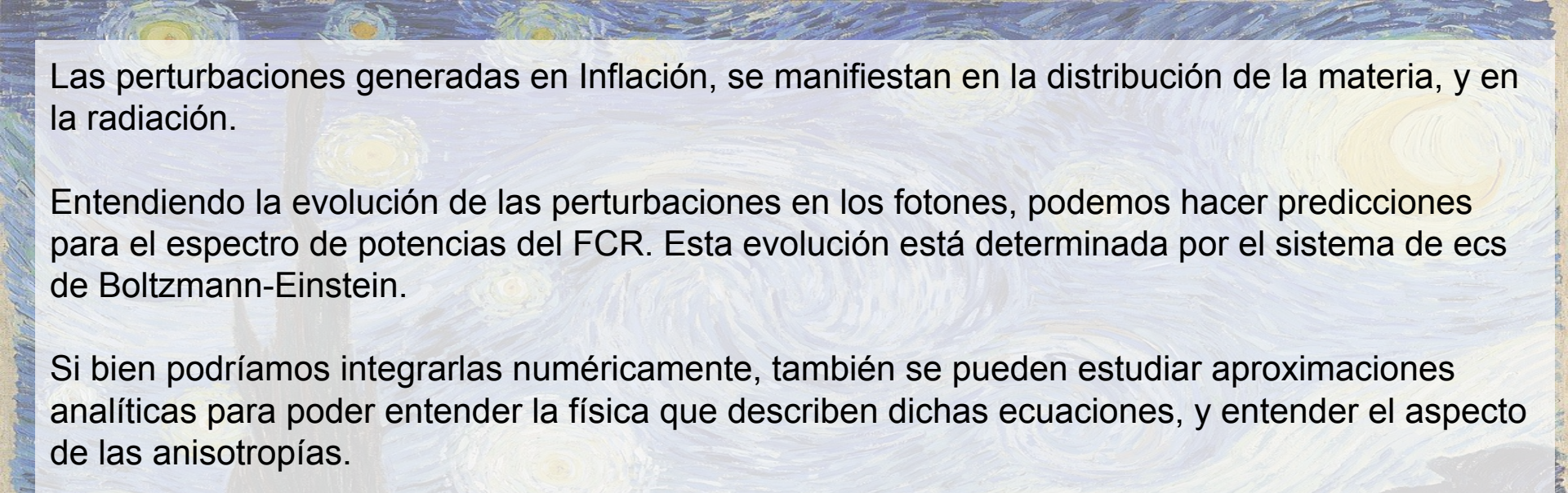
La ecuación de Boltzmann para los fotones, en el espacio de Fourier, es:

$$\Theta' + ik\mu\Theta + \Phi' + ik\mu\Psi = -\tau' [\Theta_0 - \Theta + \mu u_b].$$

Notar que todos los modos de Fourier están desacoplados. Se resuelve una ec. para cada modo k , y cada valor de μ , de manera independiente.

The background image is Vincent van Gogh's painting "Starry Night". It depicts a dark, swirling night sky filled with numerous small, yellow stars and a large, bright crescent moon on the right. In the foreground, a dark, gnarled cypress tree stands on the left. Below the tree, a small town with a church steeple is nestled among rolling hills under the starry sky.

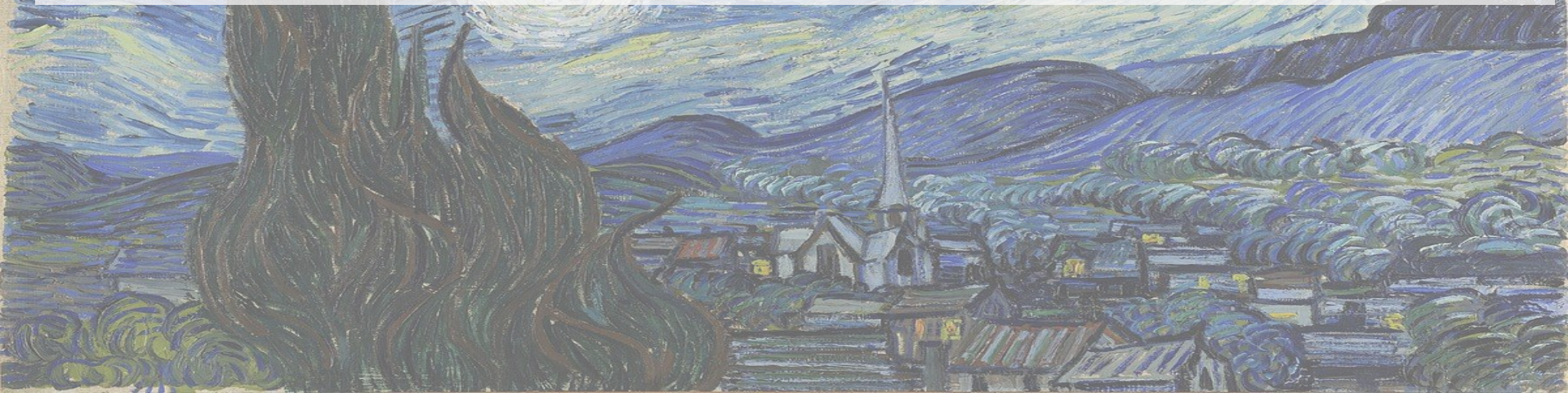
De inhomogeneidades a anisotropías

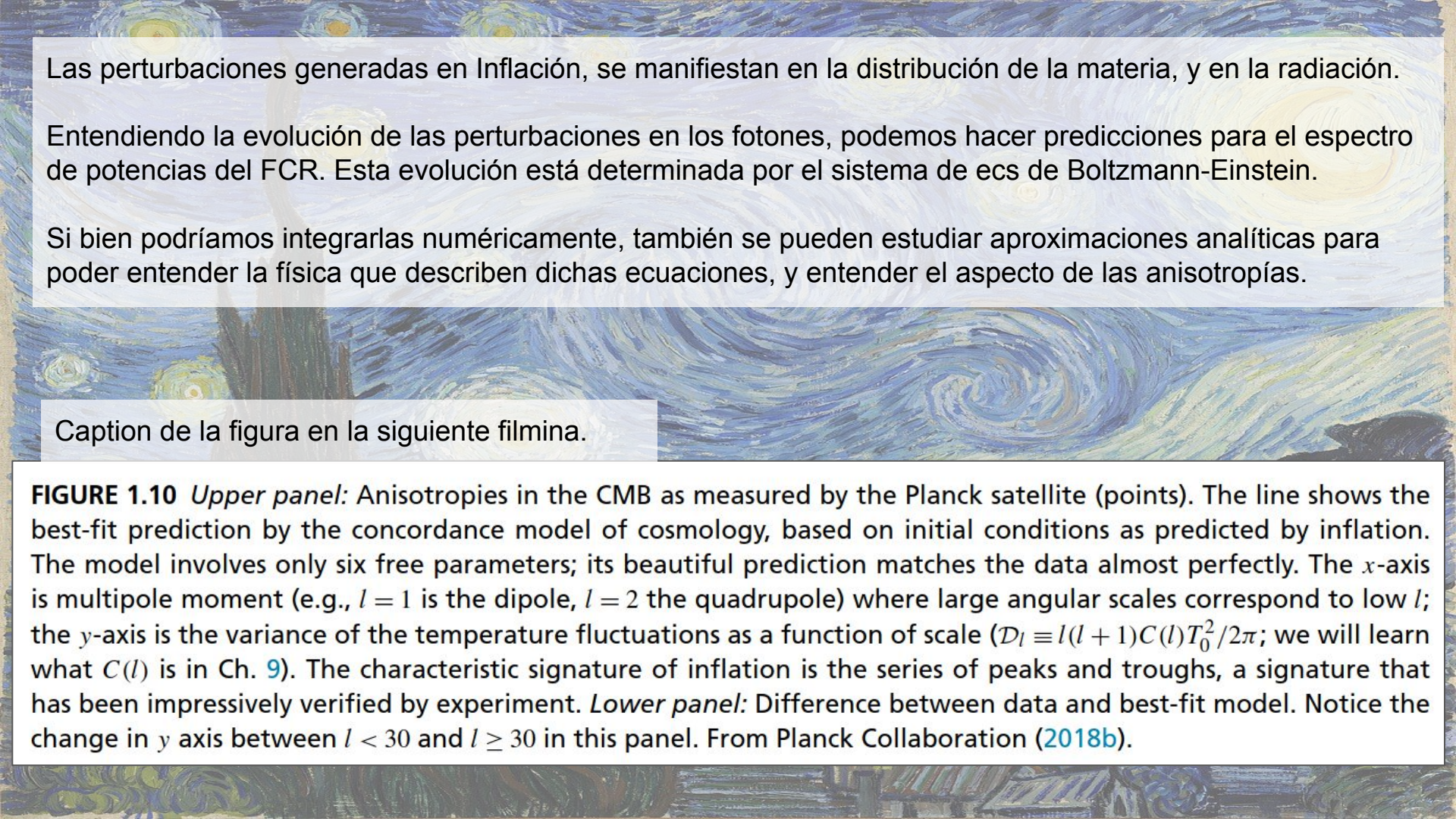


Las perturbaciones generadas en Inflación, se manifiestan en la distribución de la materia, y en la radiación.

Entendiendo la evolución de las perturbaciones en los fotones, podemos hacer predicciones para el espectro de potencias del FCR. Esta evolución está determinada por el sistema de ecs de Boltzmann-Einstein.

Si bien podríamos integrarlas numéricamente, también se pueden estudiar aproximaciones analíticas para poder entender la física que describen dichas ecuaciones, y entender el aspecto de las anisotropías.



A reproduction of Vincent van Gogh's painting "The Starry Night". It depicts a dark blue sky filled with swirling, luminous stars and a bright crescent moon. A small town with houses and church spires is nestled at the base of a hill, with a path leading up to it. The style is characterized by thick, expressive brushstrokes.

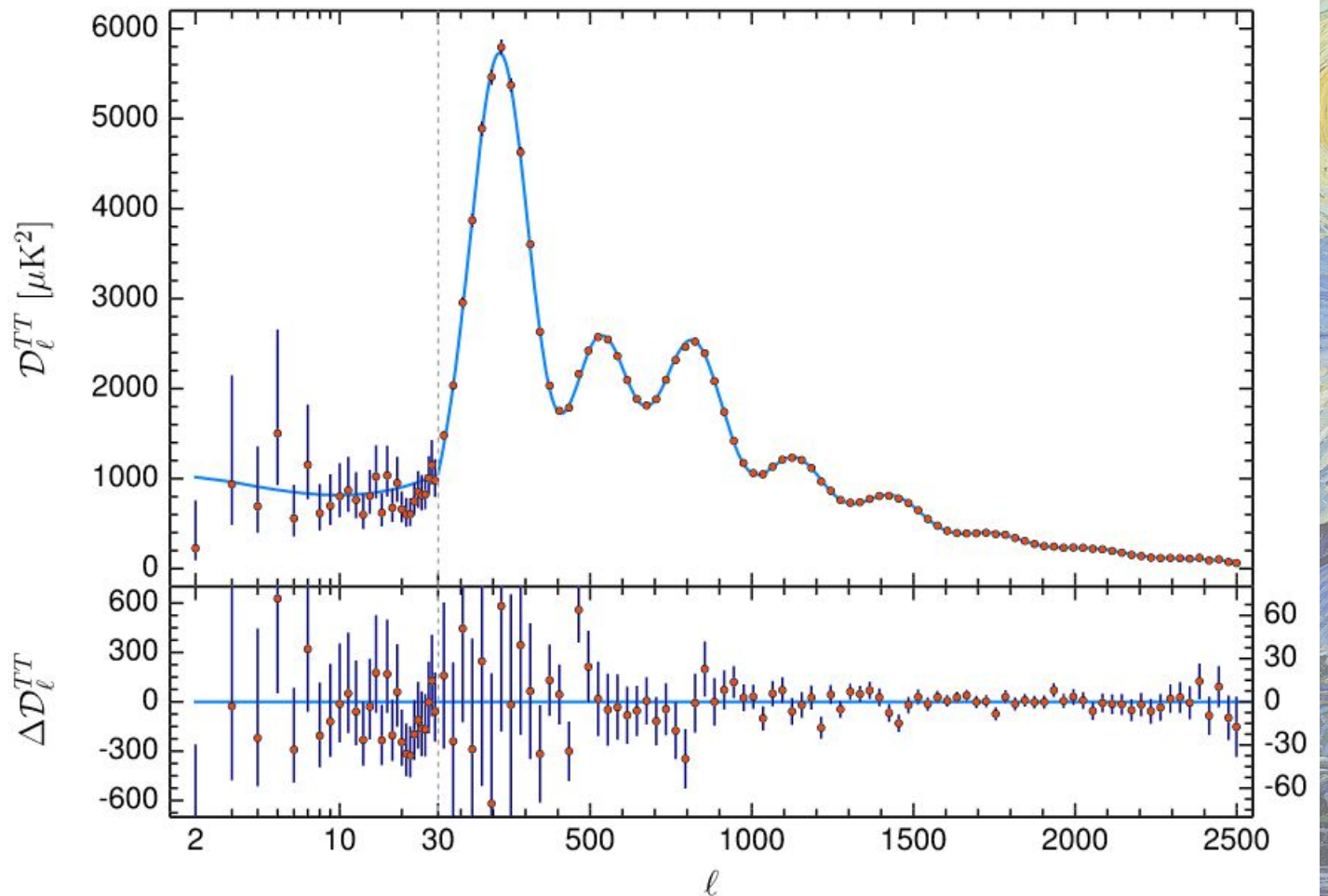
Las perturbaciones generadas en Inflación, se manifiestan en la distribución de la materia, y en la radiación.

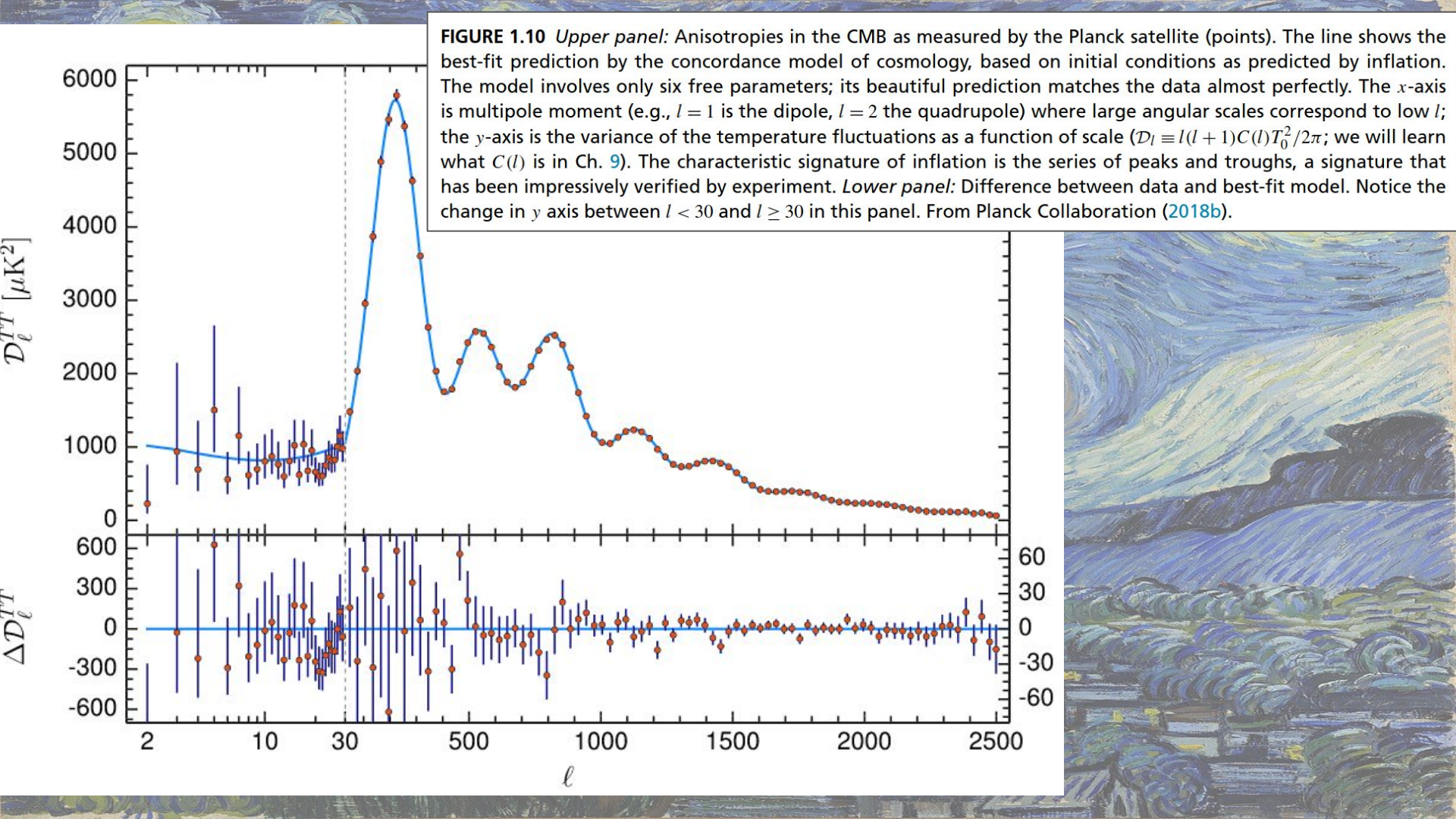
Entendiendo la evolución de las perturbaciones en los fotones, podemos hacer predicciones para el espectro de potencias del FCR. Esta evolución está determinada por el sistema de ecs de Boltzmann-Einstein.

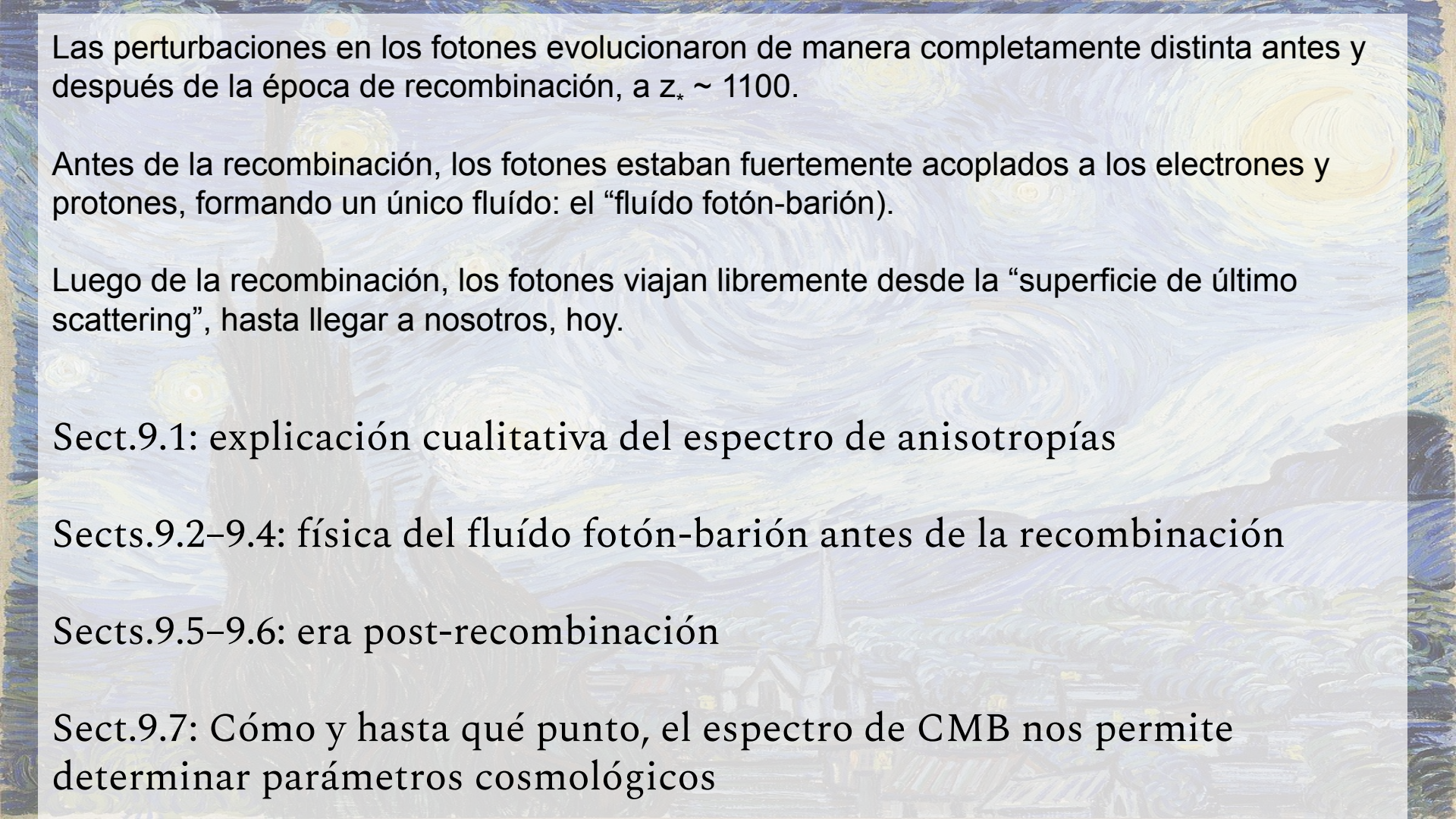
Si bien podríamos integrarlas numéricamente, también se pueden estudiar aproximaciones analíticas para poder entender la física que describen dichas ecuaciones, y entender el aspecto de las anisotropías.

Caption de la figura en la siguiente filmina.

FIGURE 1.10 *Upper panel:* Anisotropies in the CMB as measured by the Planck satellite (points). The line shows the best-fit prediction by the concordance model of cosmology, based on initial conditions as predicted by inflation. The model involves only six free parameters; its beautiful prediction matches the data almost perfectly. The x -axis is multipole moment (e.g., $l = 1$ is the dipole, $l = 2$ the quadrupole) where large angular scales correspond to low l ; the y -axis is the variance of the temperature fluctuations as a function of scale ($\mathcal{D}_l \equiv l(l+1)C(l)T_0^2/2\pi$; we will learn what $C(l)$ is in Ch. 9). The characteristic signature of inflation is the series of peaks and troughs, a signature that has been impressively verified by experiment. *Lower panel:* Difference between data and best-fit model. Notice the change in y axis between $l < 30$ and $l \geq 30$ in this panel. From Planck Collaboration (2018b).







Las perturbaciones en los fotones evolucionaron de manera completamente distinta antes y después de la época de recombinación, a $z_* \sim 1100$.

Antes de la recombinación, los fotones estaban fuertemente acoplados a los electrones y protones, formando un único fluído: el “fluído fotón-barión”).

Luego de la recombinación, los fotones viajan libremente desde la “superficie de último scattering”, hasta llegar a nosotros, hoy.

Sect.9.1: explicación cualitativa del espectro de anisotropías

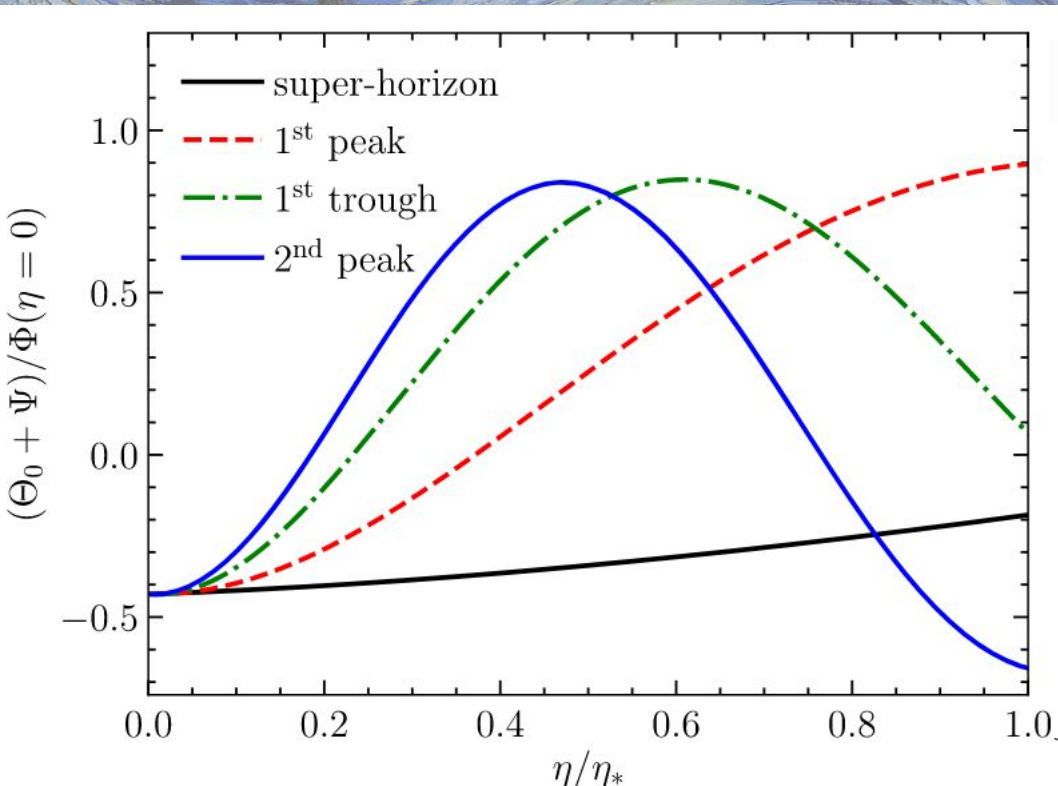
Sects.9.2–9.4: física del fluído fotón-barión antes de la recombinación

Sects.9.5–9.6: era post-recombinación

Sect.9.7: Cómo y hasta qué punto, el espectro de CMB nos permite determinar parámetros cosmológicos

Vamos a empezar mirando las soluciones:

FIGURE 9.1 Evolution of four different modes of photon perturbations before recombination at η_* , in the fiducial Λ CDM cosmology and normalized to the gravitational potential at the end of inflation. In the order of appearance in the legend (from top to bottom), the wavenumbers are $k [h \text{ Mpc}^{-1}] = 0.005, 0.020, 0.031, 0.039$.



Evolución de la perturbación en los fotones.

Las perturbaciones en los fotones **no crecen** después del desacople: como los potenciales gravitatorios en el Universo son muy débiles como para atrapar a los fotones, éstos viajan libremente después de desacoplarse de los bariones, y mantienen las perturbaciones en el nivel que tenían al momento del desacople. (en cambio, las perturbaciones en la materia, aumentan varios órdenes de magnitud entre desacople y hoy)

Época de desacople

Hemos normalizado $(\Theta_0 + \Psi)(k, \eta)$ al valor $\Phi(k, 0)$ al final de Inflación.

El gráfico muestra la suma del potencial gravitatorio y el monopolio, porque los fotones que vemos hoy han tenido que salir de los potenciales dentro de los que estaban al tiempo de recombinação. A medida que emergen de estos pozos de potencial, sus longitudes de onda se estiran (si la región es $\Psi < 0$ sobre-densa y) y decrece su energía (redshift gravitacional).

La temperatura que vemos hoy es en realidad Θ_0 plus Ψ en la época de recombinação.

Las anisotropías observadas hoy son la integral sobre k de la cantidad mostrada en el gráfico, elevada al cuadrado, y multiplicada por el espectro de potencias de $\Phi(k, 0)$, que es esencialmente $P_{\mathcal{R}}(k)$.

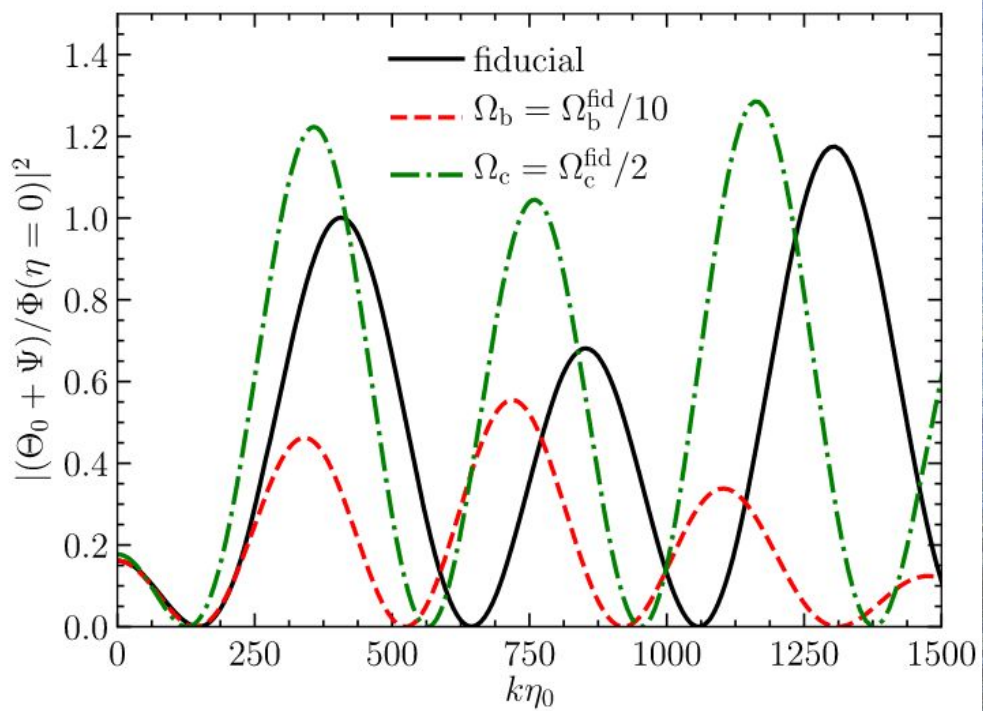
Para el espectro de anisotropías, solo importa la amplitud de la cantidad $(\Theta_0 + \Psi)(k, \eta)$ y no su signo.

- El modo de gran escala casi no evoluciona (escalas super-horizon, no afectadas por evolución causal). Estas perturbaciones quedan prácticamente igual a como salen de Inflación.

Las **perturbaciones** siguen una **ecuación de oscilador armónico**, entonces veremos **oscilaciones en el espectro**.

- Primer pico: Ese modo, desde que entra al horizonte empieza a crecer hasta que llega al máximo justo en el momento de recombinação. Se ve un pico en el espectro.
- Primer valle: Ese modo entró antes al horizonte, creció y decreció, y al momento de recombinação su amplitud vale casi cero.
- Segundo pico: Ese modo entró antes al horizonte, creció y luego decreció hasta llegar al mínimo en recombinação. En el espectro también se ve un máximo (segundo pico), porque estamos viendo la amplitud al cuadrado!

FIGURE 9.2 Perturbations to the observed photon temperature $\Theta_0 + \Psi$ squared, normalized to the potential at the end of inflation $\Phi(k, \eta = 0)$. All curves are evaluated at $\eta = \eta_*$, where η_* is the recombination time in the fiducial cosmology. The black solid line shows the fiducial cosmology, while the other two curves show results with a model with reduced baryons (leading to an increased oscillation frequency) and reduced CDM (leading to a suppressed asymmetry of even and odd peaks). The larger damping length λ_D of the low- Ω_b case is clearly evident in the suppression of perturbations with $k \gtrsim 1000/\eta_0$.



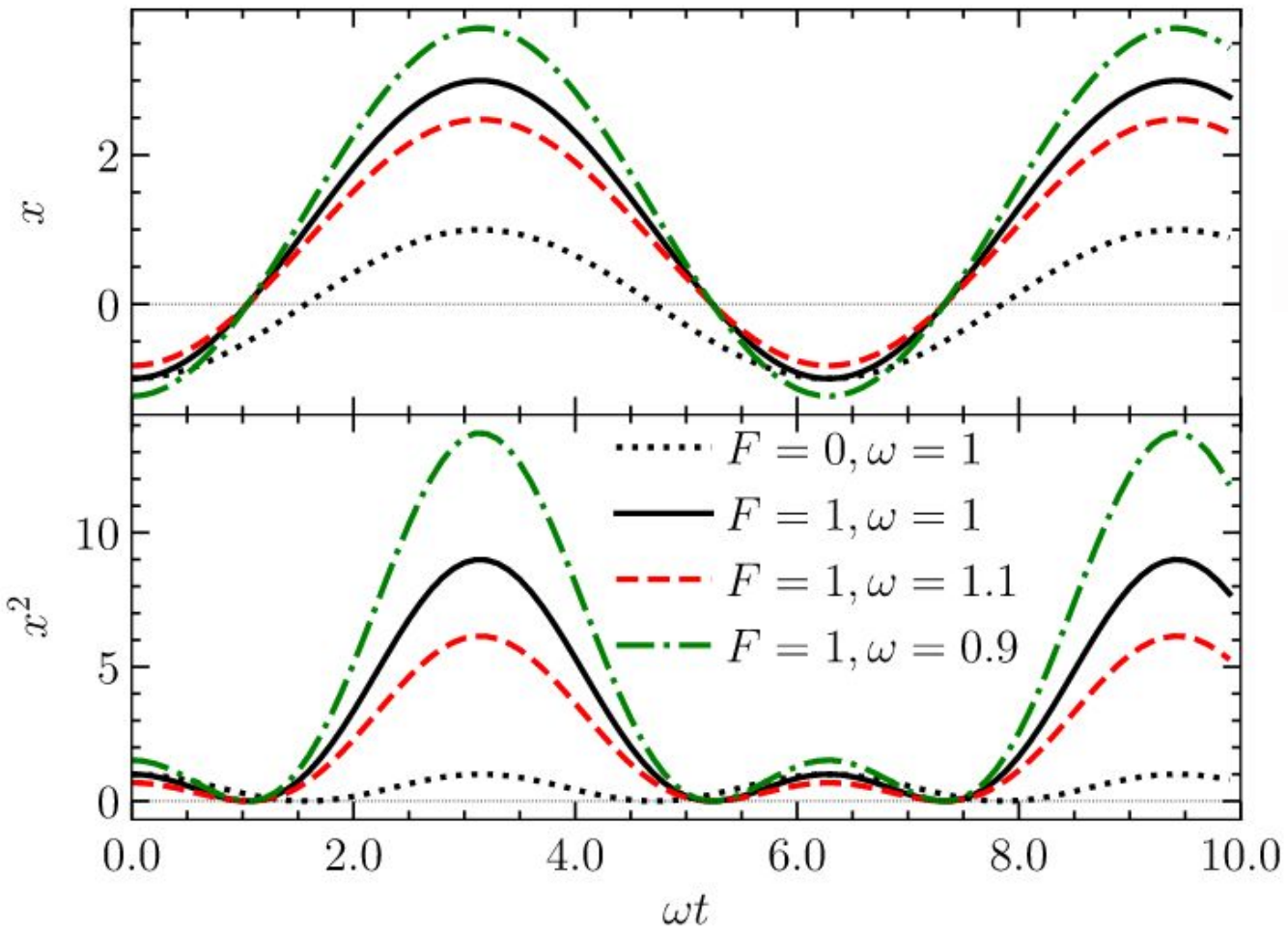
Espectro para un tiempo fijo (momento de la recombinação).

- Los picos pares son más altos que los picos impares

$$\Theta_0'' + k^2 c_s^2 \Theta_0 = F$$

Ec (simplificada) que gobierna las perturbaciones es la del oscilador armónico forzado (antes de recombinaión).

Oscilador armónico forzado



$$\ddot{x} + \frac{K}{m}x = F.$$

Frecuencia de oscilación

$$\omega \equiv \sqrt{K/m}.$$

Solución general:

$$x = A \cos(\omega t) + \frac{F}{\omega^2}.$$

Como está forzado oscila alrededor de un punto **por encima** de $x=0$.

F es la fuerza de gravedad

c_s es la velocidad de sonido del fluído fotón-barión

$$\Theta_0'' + k^2 c_s^2 \Theta_0 = F$$

En este caso, la velocidad de sonido (frecuencia del oscilador) aumenta si disminuye la materia Ω_b .

F dá la **asimetría de los picos pares/impares**. Cuanto mayor sea F , y menor sea la frecuencia, mayor es la asimetría entre los picos.

Consideremos una sobre-densidad inicial y que el signo de f es tal que tiende a aumentar la sobre-densidad. Cuando el fluido se empieza a contraer, su auto-gravedad y la fuerza externa (**dada por el potencial gravitatorio de la materia oscura**) actúan en consonancia, dando lugar a una contracción más fuerte que si F fuera nula.

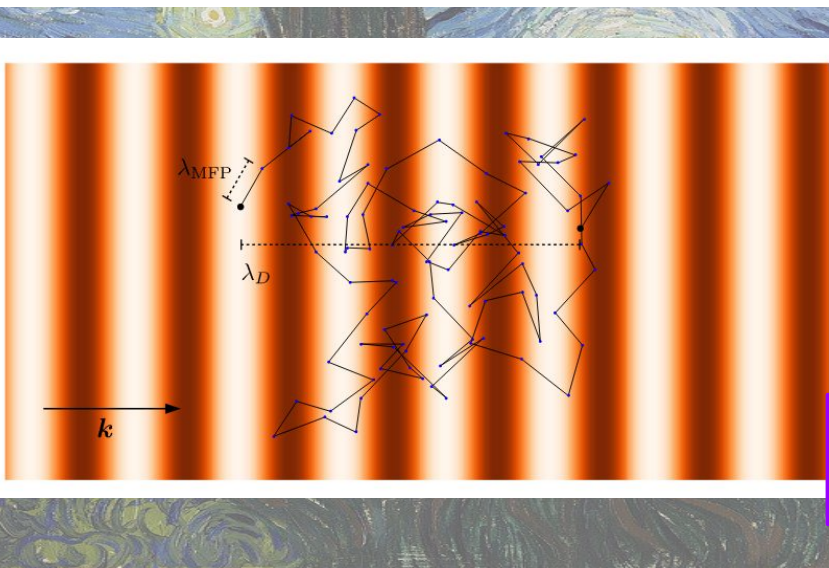
Cuando gana la presión, y el fluido se expande, la fuerza externa contraresta y la sub-densidad tiene una amplitud menor que la que tendría si F fuera cero.

La asimetría entre los picos pares e impares es una prueba directa de la cantidad de materia oscura Ω_c

Todavía faltan algunos detalles para entender bien el gráfico del espectro de potencias!

A pequeñas escalas se da un **atenuamiento (damping)** que tiene que ver con que el acoplamiento entre fotones y bariones no es perfecto. La tasa de scattering no es infinita, y existe un tiempo no nulo en el cual el fotón puede viajar libremente antes de dispersarse con un electrón libre.

FIGURE 9.4 Photon diffusion through the electron gas. The line illustrates the random walk of a photon. Scattering events are denoted as points, while the large dots denote the initial and final locations of the photon. Each scattering event is separated by a distance of order the mean free path λ_{MFP} , while the photon has overall moved a distance of order the damping length λ_D between its initial and final positions. Perturbations with $k \gtrsim 1/\lambda_D$, like the one sketched here, will be washed out by the diffusion.



Los fotones sufren **difusión** a través del gas de electrones.

$$\lambda_D \sim \lambda_{\text{MFP}} \sqrt{n_e \sigma_T H^{-1}} = \frac{1}{\sqrt{n_e \sigma_T H}} \frac{1}{a}$$

En el espectro, esto es un **damping** para k grandes!

En escalas más pequeñas que estas, los fotones viajando en distintas direcciones restauran la temperatura homogénea (borran las anisotropías).

Cómo se relacionan las perturbaciones al momento de la recombinación con las anisotropías que vemos hoy?

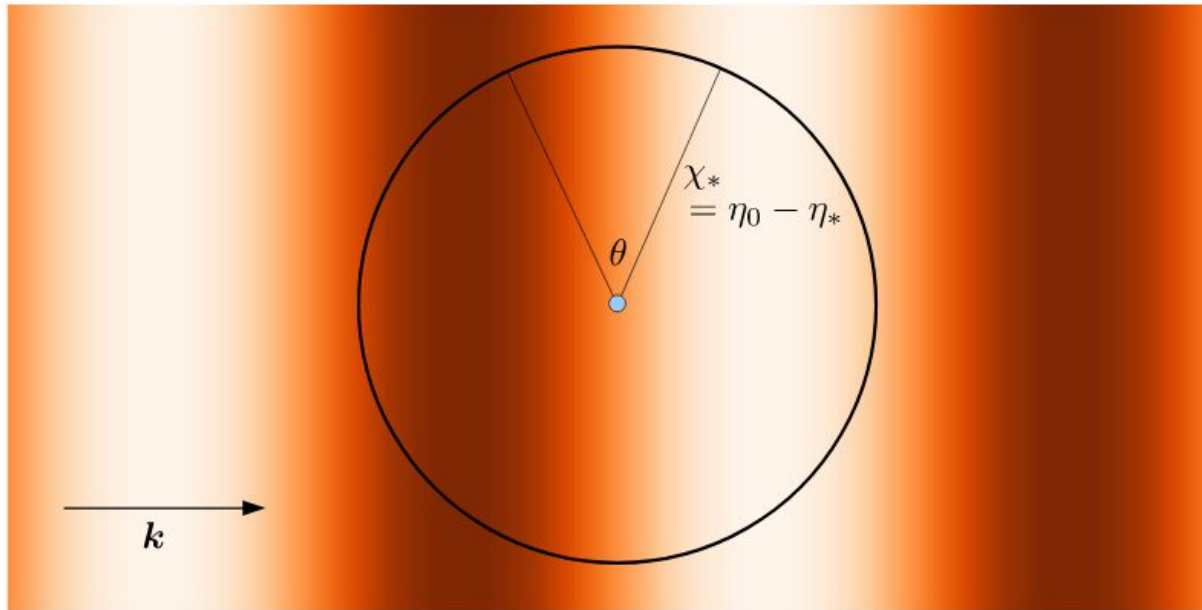


FIGURE 9.5 Perturbations in the temperature due to a plane wave with wavenumber k . Hot and cold regions are shaded light and dark. After recombination, photons from the hot and cold spots travel freely to us, denoted by the blue dot at the center. This k -mode contributes anisotropy on a scale $\theta \sim k^{-1}/\chi_*$, where $\chi_* = \eta_0 - \eta_*$ is the comoving distance to the last-scattering surface.

The final step is to relate the perturbations at recombination, as depicted in Fig. 9.2, to the anisotropies we observe today. The math of this is a little complicated, but the physics is perfectly straightforward. Consider one Fourier mode, i.e. a plane-wave perturbation. Fig. 9.5 shows the temperature variations for one mode at recombination. Photons from hot and cold spots separated by a typical comoving distance k^{-1} travel to us coming from an angular separation $\theta \simeq k^{-1}/\chi_*$ where $\chi_* = \eta_0 - \eta_*$ is the comoving distance between us and the surface of last scattering.¹ If we decompose the temperature field into multipole moments, then an angular scale θ roughly corresponds to $1/l$. So, using the fact that $\eta_* \ll \eta_0$, we project inhomogeneities on scales k onto anisotropies on angular scales $l \simeq k\eta_0$.

There is one final caveat to this picture of free-streaming. We have been implicitly assuming that nothing happens to the photons on their journey from the last-scattering surface to Earth. This is not completely true. While gravitational potentials are constant deep in matter domination, they do evolve right after recombination (due to the presence of radiation) and at late times (due to dark energy). Evolving potentials produce additional perturbations to the photons via the *integrated Sachs–Wolfe (ISW) effect*. Finally, the universe is no longer completely neutral at redshifts $z \lesssim 10$, and the presence of free electrons leads to scattering of CMB photons which in turn slightly dampens the anisotropies. This is, in a nutshell, how primordial perturbations are processed to form the present-day anisotropy spectrum.² Now let us work through each step again quantitatively.

Anisotropías a escalas grandes

Usamos la ec en el régimen super horizon. Inmediatamente, se llega a esto:

$$(\Theta_0 + \Psi)(\mathbf{k}, \eta_*) = -\frac{1}{3}\Phi(\mathbf{k}, \eta_*) = -\frac{1}{5}\mathcal{R}(\mathbf{k}).$$

Haciendo las
aproximaciones
en este régimen

Combinándola con la expresión para la c.i. para la perturbación de la materia oscura, tenemos:

$$(\Theta_0 + \Psi)(\mathbf{k}, \eta_*) = -\frac{1}{6}\delta_c(\mathbf{k}, \eta_*).$$

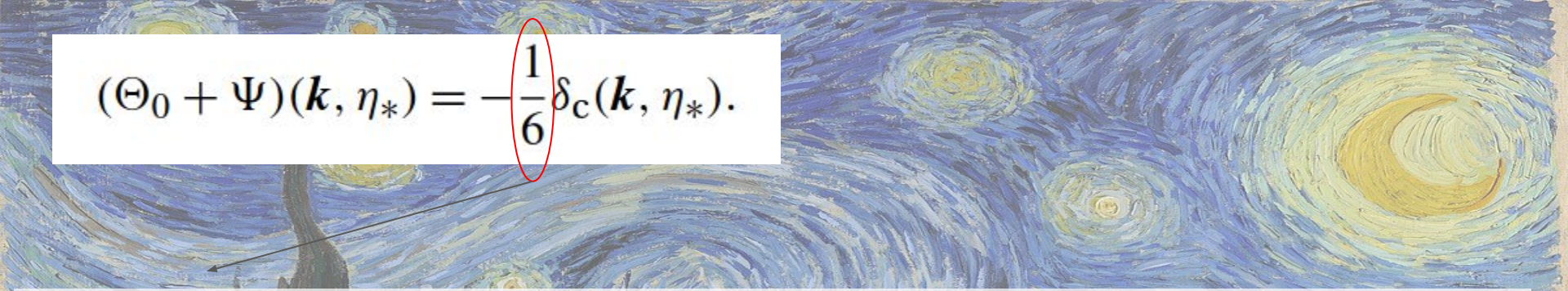
La perturbación de temperatura de una
región sobre-densa es negativa!

Las sobre-densidades a gran escala contienen fotones más calientes (en recombinação) que las regiones sub-densas i.e., $\Theta_0 > 0$ when $\Psi < 0$.

Sin embargo, para llegar hasta nosotros, los fotones deben salir de los pozos de potencial. Al hacerlo pierden energía, más de la que originalmente los hacía ser más calientes. Es decir $\Theta_0 + \Psi$ es negativo cuando $\Psi < 0$.

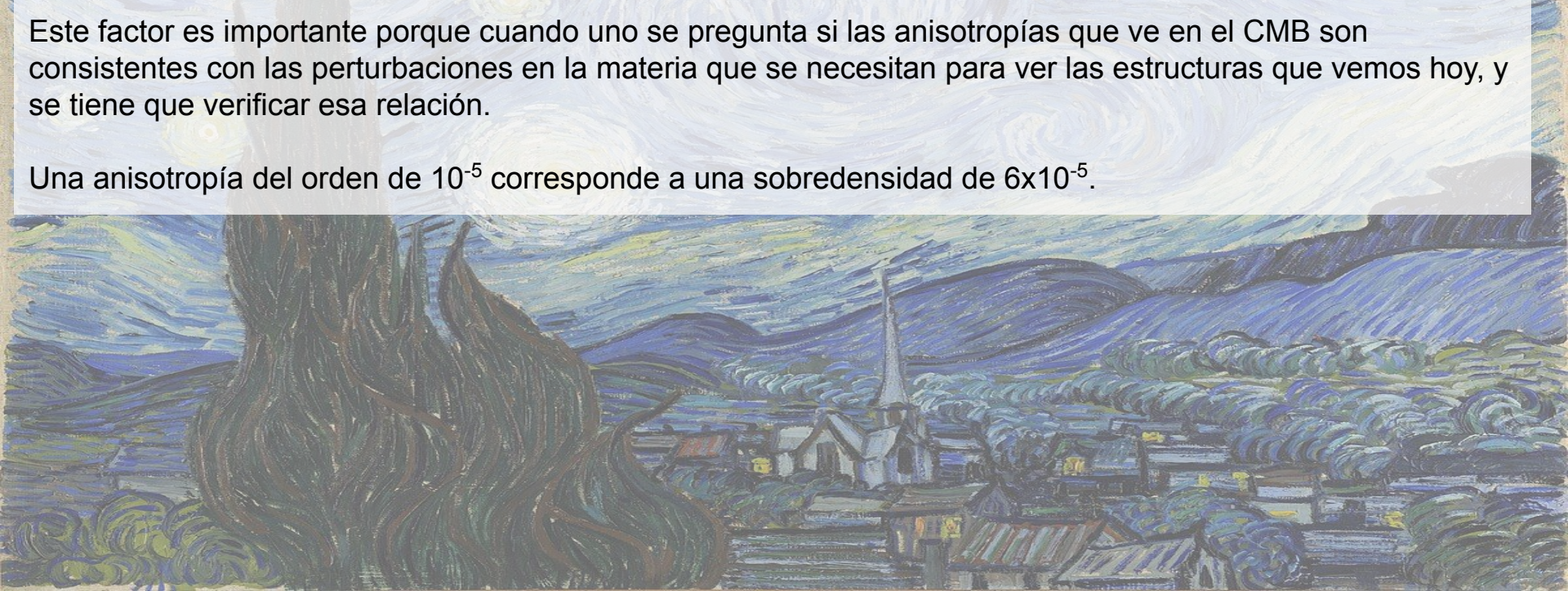
Cuando observamos “hot spots” (regiones calientes) a gran escala en el CMB hoy, estamos observando regiones sub-densas en la época de recombinação!

$$(\Theta_0 + \Psi)(\mathbf{k}, \eta_*) = -\frac{1}{6} \delta_c(\mathbf{k}, \eta_*).$$



Este factor es importante porque cuando uno se pregunta si las anisotropías que ve en el CMB son consistentes con las perturbaciones en la materia que se necesitan para ver las estructuras que vemos hoy, y se tiene que verificar esa relación.

Una anisotropía del orden de 10^{-5} corresponde a una sobredensidad de 6×10^{-5} .



Oscilaciones acústicas

Antes de que los electrones y los núcleos comenzaran a formar átomos (recombinación), el camino libre medio para un fotón era mucho más pequeño que el horizonte. La dispersión de Compton hizo que el fluido electrón-protón se acoplara fuertemente con los fotones. Ahora exploramos este régimen cuantitativamente utilizando las ecuaciones de Boltzmann.

Límite de tight-coupling de las ecuaciones de Boltzmann

Este límite se aplica cuando el camino libre medio del fotón es mucho menor que las escalas de interés.

$$\tau \gg 1.$$

Se muestra que los únicos momentos que se mantienen de Θ_l son el monopolo ($l = 0$) y el dipolo ($l = 1$).

La estrategia es pasar de una ecuación para Θ a una ecuación para los momentos: θ_l ,

$$\Theta'_l + \frac{k}{(-i)^{l+1}} \int_{-1}^1 \frac{d\mu}{2} \mu \mathcal{P}_l(\mu) \Theta(\mu) = \tau' \Theta_l \quad (l > 2).$$

Ecuación de Boltzmann
(ec. (5.66) queda así)

Note that all other terms in the Boltzmann equation (e.g., $-\Phi'$) scale either as μ^0 , μ^1 , or μ^2 , so they disappear after the integral over μ against \mathcal{P}_l with $l > 2$. To do the integral in the second term here, we make use of the recurrence relation for Legendre polynomials, Eq. (C.3), to get

$$\Theta'_l - \frac{kl}{2l+1} \Theta_{l-1} + \frac{k(l+1)}{2l+1} \Theta_{l+1} = \tau' \Theta_l. \quad (9.11)$$

Let us consider the order of magnitude of the terms in Eq. (9.11). The first term on the left is of order Θ_l/η which is much smaller than the term on the right which is enhanced by the factor τ' . Neglecting the Θ_{l+1} term for the moment, this tells us that in the tightly-coupled regime

$$\Theta_l \sim -\frac{k}{\tau'} \frac{l}{2l+1} \Theta_{l-1}. \quad (9.12)$$

$\lambda_{\text{MFP}} = -1/\tau'$, the prefactor is $k\lambda_{\text{MFP}}$.

For modes with wavelengths much larger than the mean free path, we have $\Theta_l \ll \Theta_{l-1}$.

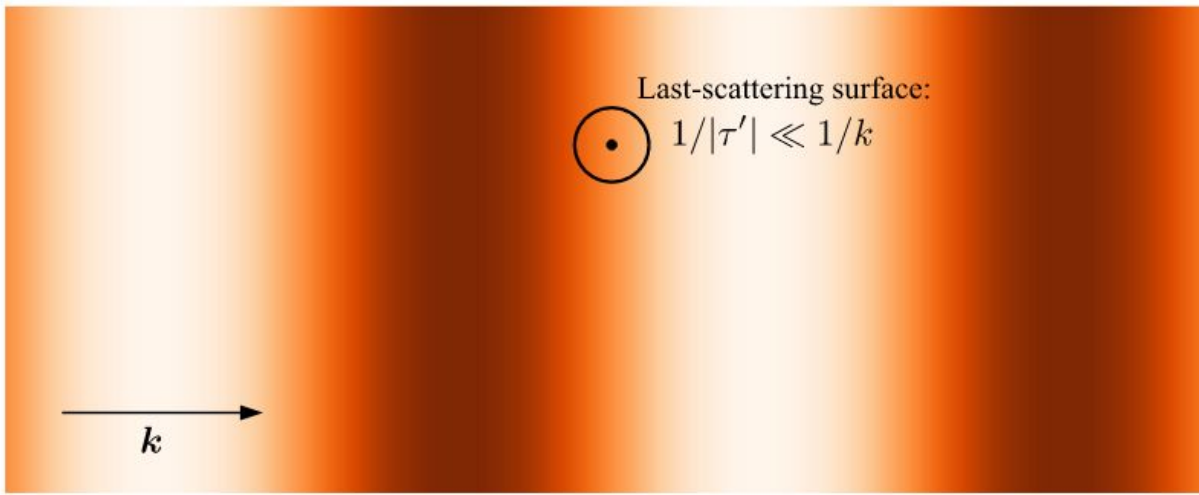


FIGURE 9.6 Anisotropies in the tightly-coupled era, for a perturbation that is of much larger scale than the mean free path of the photons $1/|\tau'|$. The photons measured by an observer (denoted by the dot) come from within a distance $1/|\tau'|$ away that is much smaller than the wavelength of the mode. Hence, an observer sees photons arriving from all angles with virtually identical temperatures; more precisely, she will measure a monopole and a small dipole, with all higher moments being negligible.

$$\Theta_0'' + \frac{a'}{a} \frac{R}{1+R} \Theta_0' + k^2 c_s^2 \Theta_0 = F(k, \eta),$$

$$F(k, \eta) \equiv -\frac{k^2}{3} \Psi - \frac{a'}{a} \frac{R}{1+R} \Phi' - \Phi'',$$

Ecuación válida para el régimen de tight-coupling

donde

$$c_s(\eta) \equiv \sqrt{\frac{1}{3(1+R[\eta])}}.$$

$$\Theta_0(\mathbf{k}, \eta) + \Phi(\mathbf{k}, \eta) = [\Theta_0(\mathbf{k}, 0) + \Phi(\mathbf{k}, 0)] \cos(kr_s)$$

$$+ \frac{k}{\sqrt{3}} \int_0^\eta d\tilde{\eta} [\Phi(\mathbf{k}, \tilde{\eta}) - \Psi(\mathbf{k}, \tilde{\eta})] \sin[k(r_s(\eta) - r_s(\tilde{\eta}))].$$

$$\Theta_1(\mathbf{k}, \eta) = \frac{1}{\sqrt{3}} [\Theta_0(\mathbf{k}, 0) + \Phi(\mathbf{k}, 0)] \sin(kr_s)$$

Fuera de fase respecto al monopolio

$$- \frac{k}{3} \int_0^\eta d\tilde{\eta} [\Phi(\mathbf{k}, \tilde{\eta}) - \Psi(\mathbf{k}, \tilde{\eta})] \cos[k(r_s(\eta) - r_s(\tilde{\eta}))].$$

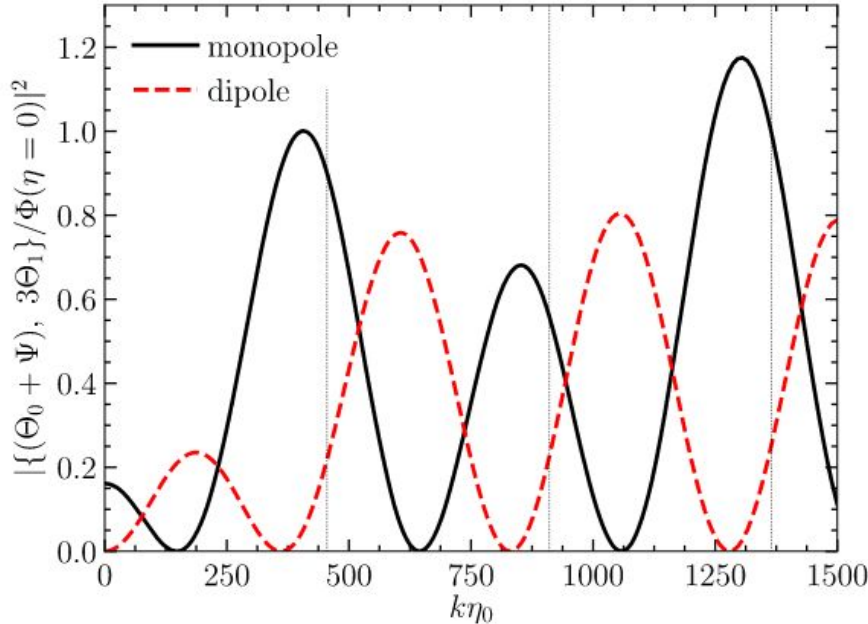


FIGURE 9.7 The monopole $\Theta_0 + \Psi$ and dipole $3\Theta_1$ at recombination in the fiducial concordance cosmology. The dashed vertical lines indicate the rough analytic peak locations of Eq. (9.27). The dipole is completely out of phase with the monopole, and vanishes for the longest-wavelength modes that have not entered the horizon by recombination.

Posición de los picos:

$$k_{\text{pk}} = n\pi/r_s \quad n = 1, 2, \dots$$

- **Efecto Sachs-Wolfe:** Es la variación en la temperatura del CMB causada por pozos de potencial gravitatorio. Los fotones pierden energía al salir de regiones densas del universo temprano, generando anisotropías a grandes escalas.
- **Oscilaciones acústicas:** Son las fluctuaciones en la densidad del plasma primordial debido a la competencia entre la gravedad (que atrae la materia) y la presión de radiación (que la empuja), generando patrones característicos en el CMB.
- **Amortiguación de Silk:** Es la disipación de fluctuaciones pequeñas en el CMB debido a la difusión de fotones antes del desacople, lo que suaviza las anisotropías en escalas pequeñas.

Atenuamiento por difusión

Para poder describir el atenuamiento por difusión (*diffusion damping*) es necesario relajar la hipótesis de que todos los multipolos superiores al dipolo se anulan.

El atenuamiento por difusión aparece cuando hay un valor no nulo de cuadrupolo (aunque sea pequeño)

A lo que tenía de acoplamiento fuerte (*tight coupling*) le tenemos que agregar una ecuación para el cuadrupolo.

Nos interesan las escalas pequeñas. En estas escalas, los potenciales gravitatorios son más chicos que las perturbaciones en los fotones.

En la jerarquía de Boltzmann sigue pasando que los multipolos superiores se pueden despreciar, así que las ecuaciones que quedan son:

$$\begin{aligned}\Theta'_0 + k\Theta_1 &= 0, \\ \Theta'_1 + k \left(\frac{2}{3}\Theta_2 - \frac{1}{3}\Theta_0 \right) &= \tau' \left(\Theta_1 - \frac{iu_b}{3} \right), \\ \Theta'_2 - \frac{2k}{5}\Theta_1 &= \frac{9}{10}\tau'\Theta_2.\end{aligned}$$

Aquí hemos
despreciado la
polarización

Complementamos con una ecuación para la velocidad:

$$3i\Theta_1 + u_b = \frac{R}{\tau'} \left[u_b' + \frac{a'}{a} u_b \right],$$

Escribimos la dependencia temporal para la velocidad como:
(y lo mismo para las otras variables)

$$u_b \propto e^{i \int \omega d\tilde{\eta}}$$

Sabemos que en el límite de tight-coupling: $\omega \simeq kc_s$

Ahora buscamos el atenuamiento, es decir la parte imaginaria de ω

Dado que el atenuamiento ocurre a pequeñas escalas, tenemos que $k \gg 1/\eta \sim a'/a$,

lo que implica que la parte real de la frecuencia satisface también: $\omega \gg a'/a$.

Entonces: $|u_b'| = |i\omega u_b| \gg \frac{a'}{a} |u_b|$.

Por lo que llegamos a la expresión aproximada:

$$u_b = -3i\Theta_1 \left[1 - \frac{i\omega R}{\tau'} \right]^{-1}$$

$$\simeq -3i\Theta_1 \left[1 + \frac{i\omega R}{\tau'} - \left(\frac{\omega R}{\tau'} \right)^2 \right]$$

Donde hemos
expandido
hasta τ'^{-2} .
Porque $u_b + 3i\Theta_1$
Está
multiplicado por τ'

La ecuación para el cuadrupolo se puede simplificar también analizando los órdenes de magnitud.

Reemplazando todo en la segunda ecuación que aparece en la filmina 3, tenemos la **relación de dispersión**:

$$\omega^2(1+R) - \frac{k^2}{3} + \frac{i\omega}{\tau'} \left[\omega^2 R^2 + \frac{8k^2}{27} \right] = 0.$$

Definimos la perturbación en la frecuencia:

$$\delta\omega = -\frac{ik^2}{2(1+R)\tau'} \left[c_s^2 R^2 + \frac{8}{27} \right].$$

La dependencia temporal de las perturbaciones es:

$$\Theta_0, \Theta_1 \sim \exp \left\{ ik \int d\tilde{\eta} c_s(\tilde{\eta}) \right\} \exp \left\{ -\frac{k^2}{k_D^2} \right\}$$

El número de onda del damping es:

$$\frac{1}{k_D^2(\eta)} \equiv \int_0^\eta \frac{d\tilde{\eta}}{6(1+R)n_e\sigma_{\text{Ta}}(\tilde{\eta})} \left[\frac{R^2}{1+R} + \frac{8}{9} \right].$$

Ignorando factores de orden 1, esto nos dice que: $\lambda_D \sim 1/k_D \sim [\eta/n_e\sigma_{\text{Ta}}]^{1/2}$

Teniendo en cuenta la densidad que hay antes del desacople (donde todos los átomos son libres menos los del Helio), tenemos

$$k_D^{-2} = 3.1 \times 10^6 \text{ Mpc}^2 a^{5/2} f_D(a/a_{\text{eq}}) \left(\Omega_b h^2\right)^{-1} \left(1 - \frac{Y_P}{2}\right)^{-1} \left(\Omega_m h^2\right)^{-1/2}$$

Evolución de la escala de difusión antes de la recombinação. Despreciar la recombinação es útil a tiempos tempranos, pero da errores grandes a medida que nos acercamos a η^*

Este escaleo con la densidad bariónica se ve afectado cuando consideramos la recombinação, y que la densidad de electrones libres va cayendo.

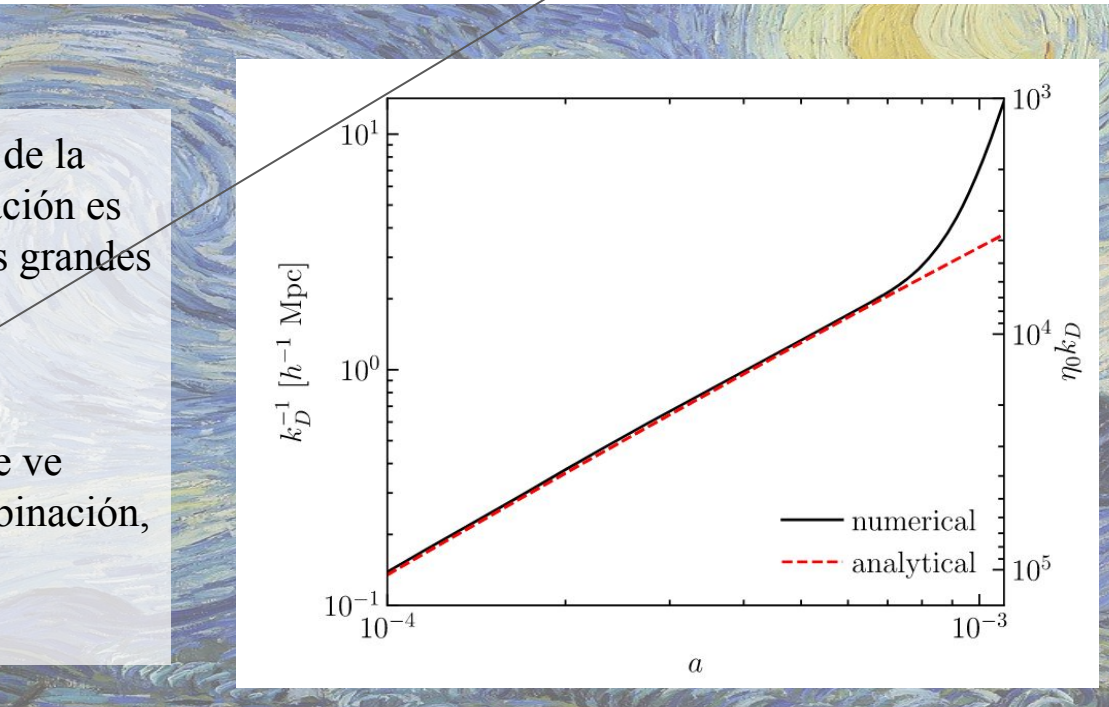


FIGURE 9.8 Damping scale as a function of the scale factor. The solid line is obtained from numerically integrating over the standard recombination history, while the dashed curve uses the approximation of Eq. (9.44) which assumes electrons remain ionized. The right axis shows the equivalent $k_D \eta_0$; damping occurs on angular scales $l > k_D \eta_0$.

Para pasar de las inhomogeneidades a las anisotropías:

$$\begin{aligned}\Theta_l(k, \eta_0) \simeq & \left[\Theta_0(k, \eta_*) + \Psi(k, \eta_*) \right] j_l [k(\eta_0 - \eta_*)] \\ & + 3\Theta_1(k, \eta_*) \left(j_{l-1} [k(\eta_0 - \eta_*)] - (l+1) \frac{j_l [k(\eta_0 - \eta_*)]}{k(\eta_0 - \eta_*)} \right) \\ & + \int_0^{\eta_0} d\eta e^{-\tau} [\Psi'(k, \eta) - \Phi'(k, \eta)] j_l [k(\eta_0 - \eta)].\end{aligned}\quad (9.59)$$

A esta expresión queremos llegar, que relaciona los multipolos hoy, con el monopolo y dipolo en recombinação.

Y luego al espectro de potencias, que relaciona los C , con dichos momentos:

$$C(l) = \frac{2}{\pi} \int_0^\infty dk k^2 P_{\mathcal{R}}(k) |\mathcal{T}_l(k)|^2. \quad (9.74)$$

9.5.2 The angular power spectrum

How is the observed anisotropy pattern today related to the rather abstract $\Theta_l(k, \eta_0)$, which refer to a plane-wave perturbation k ? To answer this question, we must first describe the way in which the temperature field is characterized today and then relate this characterization to Θ_l .

Recall that in Eq. (5.2), we wrote the temperature of the CMB radiation field in the universe as

$$T(x, \hat{p}, \eta) = T(\eta) [1 + \Theta(x, \hat{p}, \eta)]. \quad (9.62)$$

Although this field is defined at every point in space and time, we can observe it only here (at x_0) and now (at η_0).³ Our only handle on the anisotropies is their dependence on the direction of the incoming photons, \hat{p} . So all the richness we observe comes from the changes in the temperature as the direction vector \hat{p} changes. Observers typically make maps, wherein the temperature is reported at a number of incoming directions, or “locations on the sky.” These locations are usually labeled not by the $\hat{p}_x, \hat{p}_y, \hat{p}_z$ components of \hat{p} , but rather by polar coordinates θ, ϕ . However, it is a simple matter to move back and forth between the unit vector \hat{p} and polar coordinates. We will continue to use the by-now familiar \hat{p} in the derivation.

We now expand the temperature perturbation in terms of spherical harmonics. That is, we write

$$\Theta(\mathbf{x}, \hat{\mathbf{p}}, \eta) = \sum_{l=1}^{\infty} \sum_{m=-l}^l a_{lm}(\mathbf{x}, \eta) Y_{lm}(\hat{\mathbf{p}}). \quad (9.63)$$

The subscripts l, m are conjugate to the real-space unit vector $\hat{\mathbf{p}}$, just as the variable \mathbf{k} is conjugate to the three-dimensional position \mathbf{x} . We are by now familiar with Fourier transforms, so it is useful to think of the expansion in terms of spherical harmonics as a kind of 2D Fourier transform. Whereas the complete set of eigenfunctions for the 3D Fourier transform are $e^{i\mathbf{k}\cdot\mathbf{x}}$, here the complete set of eigenfunctions for expansion on the surface of a sphere are $Y_{lm}(\hat{\mathbf{p}})$ (see Appendix C.2). All of the information contained in the temperature field T is also contained in the (\mathbf{x}, η) -dependent amplitudes a_{lm} . As an example of this, consider an experiment that maps the full sky with an angular resolution of 7° . The full sky has 4π radians $^2 \simeq 41,000$ degrees 2 , so there are 840 pixels with area of $(7^\circ)^2$. Thus, such an experiment would have 840 independent pieces of information.

Were we to characterize

information with a_{lm} instead of temperatures in pixels, there would be some l_{\max} above which there is no information. One way to determine this l_{\max} is to set the total number of recoverable a_{lm} as $\sum_{l=0}^{l_{\max}} (2l + 1) = (l_{\max} + 1)^2 = 840$. So the information could be equally well characterized by specifying all the a_{lm} up to $l_{\max} = 28$. Incidentally, this is a fairly good caricature of the COBE experiment (Smoot et al., 1992; Bennett et al., 1996), the discoverer of CMB anisotropies. They presented temperature data over many more pixels, but these pixels were overlapping. So, the independent information was contained in multipoles up to $l \sim 30$. The current generation of experiments is capable of measuring the moments all the way up to l of several thousands, at which point the primary CMB anisotropies are sufficiently damped by photon diffusion that the observed radiation is dominated by astrophysical foreground sources (as well as gravitational lensing, Sect. 13.3).

Este texto explica cómo se relaciona la resolución angular de un experimento con el l máximo hasta el cual tiene sentido hacer el desarrollo multipolar.

We want to relate the observables, the a_{lm} , to the moments of the temperature distribution we have been dealing with. To do this, we can use the orthogonality property of the spherical harmonics. The Y_{lm} are normalized via Eq. (C.11),

$$\int d\Omega Y_{lm}(\hat{\mathbf{p}}) Y_{l'm'}^*(\hat{\mathbf{p}}) = \delta_{ll'} \delta_{mm'}. \quad (9.64)$$

Therefore the expansion of Θ in terms of spherical harmonics, Eq. (9.63), can be inverted by multiplying both sides by $Y_{lm}^*(\hat{\mathbf{p}})$ and integrating:

$$a_{lm}(\mathbf{x}, \eta) = \int \frac{d^3k}{(2\pi)^3} e^{i\mathbf{k}\cdot\mathbf{x}} \int d\Omega Y_{lm}^*(\hat{\mathbf{p}}) \Theta(\mathbf{k}, \hat{\mathbf{p}}, \eta). \quad (9.65)$$

Here we have written the right-hand side in terms of the Fourier transform ($\Theta(\mathbf{k})$ instead of $\Theta(\mathbf{x})$), since that is the quantity for which we obtained solutions.

As with the density perturbations, we cannot make predictions about any particular a_{lm} , just about the distribution from which they are drawn, a Gaussian distribution that traces its origin to the quantum fluctuations laid down during inflation. Fig. 9.10 illustrates this Gaussian distribution. The mean value of the a_{lm} is zero, but they have a nonzero variance. The variance of the a_{lm} is called $C(l)$. Thus,

$$\langle a_{lm} \rangle = 0; \quad \langle a_{lm} a_{l'm'}^* \rangle = \delta_{ll'} \delta_{mm'} C(l), \quad (9.66)$$

where $\langle \cdot \rangle$ now denotes an ensemble average, i.e. the result obtained in the limit of measuring over an infinite volume. It is very important to note that, for a given l , each a_{lm} has the same variance. For $l = 100$, say, all 201 $a_{100,m}$ are drawn from the same distribution. When we measure these 201 coefficients, we are sampling the distribution. These 201 samples give us a good handle on the underlying variance of the distribution (this will be made more rigorous in Sect. 14.1). On the other hand, if we measure the five components of the quadrupole ($l = 2$), we have much less statistical precision on the underlying variance, $C(2)$. Thus, *there is a fundamental uncertainty in the knowledge we may get about the $C(l)$.*

Este concepto es muy importante!!

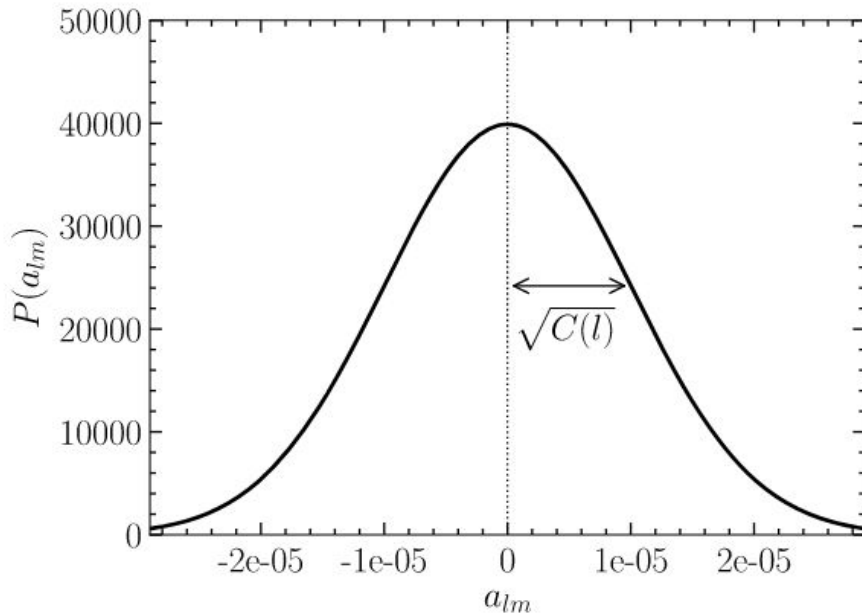


FIGURE 9.10 The distribution from which the a_{lm} are drawn. The Gaussian distribution has expectation value equal to zero and an RMS width of $[C(l)]^{1/2}$.

This uncertainty, which is most pronounced at low l , is called *cosmic variance*. Quantitatively, the uncertainty scales as the inverse of the square root of the number of samples. More precisely, it is the uncertainty on the estimate of $C(l)$ after using the $2l + 1$ samples to infer it (again, more on this in Ch. 14):

$$\left(\frac{\Delta C(l)}{C(l)} \right)_{\text{cosmic variance}} = \sqrt{\frac{2}{2l + 1}}. \quad (9.67)$$

In practice, this limit is never quite achieved, because even if an instrument observes the full sky (such as the satellite experiments COBE, WMAP, and Planck), the large foreground emission in the Milky Way plane means that some parts of the sky need to be masked. For a measurement based on a fraction f_{sky} of the full sky, the error bar is increased by roughly a factor $1/\sqrt{f_{\text{sky}}}$.

We can now obtain an expression for $C(l)$ in terms of $\Theta_l(k)$. You might rightfully worry about a notation collision here, but we will see that the index l in $C(l)$ and Θ_l is indeed the same. First we square a_{lm} in Eq. (9.65) and take the expectation value of the distribution. For this we need $\langle \Theta(\mathbf{k}, \hat{\mathbf{p}}) \Theta^*(\mathbf{k}', \hat{\mathbf{p}}') \rangle$, where from now on we will keep the $\eta = \eta_0$ dependence implicit. This expectation value is complicated because it depends on two separate phenomena: (i) the initial amplitude and phase of the perturbation, randomly chosen during inflation from a Gaussian distribution, and (ii) the evolution we have studied in this chapter that turns this initial perturbation into anisotropies. The former is a random variable, the latter is deterministic: given an initial value for the amplitude and phase of the perturbation, the equations uniquely determine its evolution. To simplify then, it makes sense to separate these two phenomena and write the photon distribution as $\mathcal{R} \times (\Theta/\mathcal{R}) = \mathcal{R} \times \mathcal{T}$, where the primordial curvature perturbation \mathcal{R} depends on \mathbf{k} , but not on the direction vector $\hat{\mathbf{p}}$. The ratio

$$\mathcal{T}(\mathbf{k}, \hat{\mathbf{p}}) \equiv \frac{\Theta(\mathbf{k}, \hat{\mathbf{p}}, \eta_0)}{\mathcal{R}(\mathbf{k})} \quad (9.68)$$

is precisely what we have solved for in this chapter: given the initial amplitude of a mode, we have learned how to evolve forward in time. $\mathcal{T}(\mathbf{k}, \hat{\mathbf{p}})$ does *not* depend on the initial

we have learned how to evolve forward in time. $\mathcal{T}(k, \hat{p})$ does *not* depend on the initial amplitude of each mode and is not random, so it can be removed from the averaging over the distribution. Therefore,

$$\begin{aligned}\langle \Theta(\mathbf{k}, \hat{\mathbf{p}}) \Theta(\mathbf{k}', \hat{\mathbf{p}}') \rangle &= \langle \mathcal{R}(\mathbf{k}) \mathcal{R}^*(\mathbf{k}') \rangle \mathcal{T}(\mathbf{k}, \hat{\mathbf{p}}) \mathcal{T}^*(\mathbf{k}', \hat{\mathbf{p}}') \\ &= (2\pi)^3 \delta_D^{(3)}(\mathbf{k} - \mathbf{k}') P_{\mathcal{R}}(k) \mathcal{T}(\mathbf{k}, \hat{\mathbf{p}}) \mathcal{T}^*(\mathbf{k}', \hat{\mathbf{p}}'),\end{aligned}\quad (9.69)$$

where the second equality uses the definition of the power spectrum of curvature perturbations $P_{\mathcal{R}}(k)$. Now we make use of one more simplification, which holds specifically for the scalar perturbations we have focused on: the ratio (or transfer function) \mathcal{T} only depends on $\hat{\mathbf{p}}$ through its angle with $\hat{\mathbf{k}}$, $\mu = \hat{\mathbf{k}} \cdot \hat{\mathbf{p}}$:

$$\mathcal{T}(\mathbf{k}, \hat{\mathbf{p}}) = \mathcal{T}(k, \hat{\mathbf{k}} \cdot \hat{\mathbf{p}}). \quad (9.70)$$

This will help us do the angular integrals in the following. After squaring Eq. (9.65), the anisotropy spectrum becomes

$$C(l) = \int \frac{d^3 k}{(2\pi)^3} P_{\mathcal{R}}(k) \int d\Omega Y_{lm}^*(\hat{\mathbf{p}}) \mathcal{T}(k, \hat{\mathbf{k}} \cdot \hat{\mathbf{p}}) \int d\Omega' Y_{lm}(\hat{\mathbf{p}}') \mathcal{T}^*(k, \hat{\mathbf{k}} \cdot \hat{\mathbf{p}}'). \quad (9.71)$$

Now we can expand $\mathcal{T}(k, \hat{\mathbf{k}} \cdot \hat{\mathbf{p}})$ and $\mathcal{T}(k, \hat{\mathbf{k}} \cdot \hat{\mathbf{p}}')$ in Legendre polynomials using the inverse of Eq. (5.66):

$$\mathcal{T}(k, \hat{\mathbf{k}} \cdot \hat{\mathbf{p}}) = \sum_l (-i)^l (2l + 1) \mathcal{P}_l(\hat{\mathbf{k}} \cdot \hat{\mathbf{p}}) \mathcal{T}_l(k). \quad (9.72)$$

So, $\mathcal{T}_l(k) = \Theta_l(k, \eta_0)/\mathcal{R}(k)$. This leaves

$$C(l) = \int \frac{d^3 k}{(2\pi)^3} P_{\mathcal{R}}(k) \sum_{l' l''} (-i)^{l'} (i)^{l''} (2l' + 1) (2l'' + 1) \mathcal{T}_{l'}(k) \mathcal{T}_{l''}^*(k) \\ \times \int d\Omega \mathcal{P}_{l'}(\hat{\mathbf{k}} \cdot \hat{\mathbf{p}}) Y_{lm}^*(\hat{\mathbf{p}}) \int d\Omega' \mathcal{P}_{l''}(\hat{\mathbf{k}} \cdot \hat{\mathbf{p}}') Y_{lm}(\hat{\mathbf{p}}'). \quad (9.73)$$

The two angular integrals here (Exercise 9.9) are identical. They are nonzero only if $l' = l$ and $l'' = l$, in which case they are equal to $4\pi Y_{lm}(\hat{\mathbf{k}})/(2l + 1)$ and its complex conjugate, respectively. The angular part $d\Omega$ of the integral over \mathbf{k} then becomes an integral over $|Y_{lm}|^2$, which is just equal to 1, leaving

$$C(l) = \frac{2}{\pi} \int_0^\infty dk k^2 P_{\mathcal{R}}(k) |\mathcal{T}_l(k)|^2. \quad (9.74)$$

For a given l , then, the variance $C(l)$ is an integral over all Fourier modes of the variance of $\Theta_l(\mathbf{k})$, which is given by $|\mathcal{T}_l(k)|^2$ times the variance of curvature perturbations. We can then use Eq. (9.59) and Eq. (9.74) to compute the anisotropy spectrum today.

As an example, we can rewrite the tight-coupling solution of Eq. (9.26) as

$$\Theta_0(\mathbf{k}, \eta) = \mathcal{R}(\mathbf{k}) \left[-\frac{2}{3} \frac{\Phi(\mathbf{k}, \eta)}{\Phi(\mathbf{k}, 0)} + \cos(kr_s) + \frac{4}{3} \frac{k}{\sqrt{3}} \int_0^\eta d\tilde{\eta} \frac{\Phi(\mathbf{k}, \tilde{\eta})}{\Phi(\mathbf{k}, 0)} \sin[k(r_s(\eta) - r_s(\tilde{\eta}))] \right] e^{-k^2/k_D^2(\eta)}. \quad (9.75)$$

The exponential factor at the end accounts for damping. This works similarly for the dipole in Eq. (9.28). Then, we insert these expressions into Eq. (9.59), which evolves the anisotropies forward using free-streaming, to obtain $\mathcal{T}_l(k) = \Theta_l(k, \eta_0)/\mathcal{R}(k)$.

9.6 The CMB power spectrum

9.6.1 Large angular scales

The large-angle CMB anisotropies are determined by extremely large-scale modes that have entered our horizon only recently. As such, they offer a particularly direct way of measuring the initial conditions. On these largest of scales, we can neglect the dipole in Eq. (9.59). So the large-angle anisotropy is determined by $\Theta_0 + \Psi$ evaluated at recombination, in addition to the last term in Eq. (9.59) which we will turn to below. The large-scale solution we found in Eq. (9.6) was that the combination $\Theta_0 + \Psi$ is equal to $-\mathcal{R}/5$. This gives us what we need: an expression for $\Theta_0 + \Psi$ at recombination that we can plug into the monopole term in Eq. (9.59). To get the anisotropy spectrum today, we then integrate as in Eq. (9.74), leaving

$$C(l)^{\text{SW}} \simeq \frac{2}{25\pi} \int_0^\infty dk k^2 P_{\mathcal{R}}(k) |j_l [k(\eta_0 - \eta_*)]|^2 \quad (9.76)$$

where the superscript denotes *Sachs–Wolfe*, in honor of the authors of the first paper to compute the large-angle anisotropy (Sachs and Wolfe, 1967). The power spectrum of curvature perturbations is given by Eq. (7.99). Therefore,

$$C(l)^{\text{SW}} \simeq \frac{4\pi}{25} \mathcal{A}_s k_p^{1-n_s} \int_0^\infty dk k^{n_s-2} j_l^2 [k(\eta_0 - \eta_*)]. \quad (9.77)$$

The integral here can be computed analytically. First, we will use the fact that $\eta_* \ll \eta_0$ and define the integration variable $x \equiv k\eta_0$. Then, Eq. (9.77) can be rewritten as

$$C(l)^{\text{SW}} \simeq \frac{4\pi}{25} \mathcal{A}_s (\eta_0 k_p)^{1-n_s} \int_0^\infty dx x^{n_s-2} j_l^2(x). \quad (9.78)$$

The integral over the spherical Bessel functions can be analytically expressed in terms of gamma functions (Eq. (C.18)), leaving

$$C(l)^{\text{SW}} \simeq 2^{n_s-2} \frac{\pi^2}{25} \mathcal{A}_s (\eta_0 k_p)^{1-n_s} \frac{\Gamma\left(l + \frac{n_s}{2} - \frac{1}{2}\right)}{\Gamma\left(l + \frac{5}{2} - \frac{n_s}{2}\right)} \frac{\Gamma(3 - n_s)}{\Gamma^2(2 - \frac{n_s}{2})}. \quad (9.79)$$

If the spectrum is scale-invariant, $n_s = 1$, then the first ratio of the gamma functions $\Gamma(l)/\Gamma(l+2)$ is equal to $[l(l+1)]^{-1}$ using Eq. (C.27). The remaining ratio of gamma functions $\Gamma(2)/\Gamma^2(3/2) = 4/\pi$ using Eq. (C.28), so

$$l(l+1)C(l)^{\text{SW}} = \frac{8}{25} \mathcal{A}_s \quad (9.80)$$

is a constant. Indeed, $l(l+1)C(l)$ is the variance of the temperature anisotropies per logarithmic interval in l , analogously to $k^3 P_{\mathcal{R}}(k)$ for the three-dimensional power spectrum. Since the latter is a constant if $n_s = 1$, it is perhaps not surprising that $l(l+1)C(l)$ becomes a constant in this case. It has become customary to plot $l(l+1)C(l)$ vs l on a logarithmic scale, which then becomes approximately constant at low l .

Fig. 9.11 shows the Planck measurements of the large-angular-scale anisotropies along with the Boltzmann solutions of the fiducial Euclidean Λ CDM model. The deviation from a constant is due to the ISW effect and the contribution from the dipole (neglected in Eq. (9.79)) becoming nonnegligible at higher l . Nevertheless, Eq. (9.80) provides a reasonable approximation. Since the y -axis gives the variance contributed by a given scale l , we can read off the amplitude of the large-angular-scale fluctuations: roughly, $\langle (\Delta T / T_0)^2 \rangle \sim 10^{-10}$, so the RMS fluctuations are the square root of this, of order $10^{-5} T_0 = 27 \mu\text{K}$.

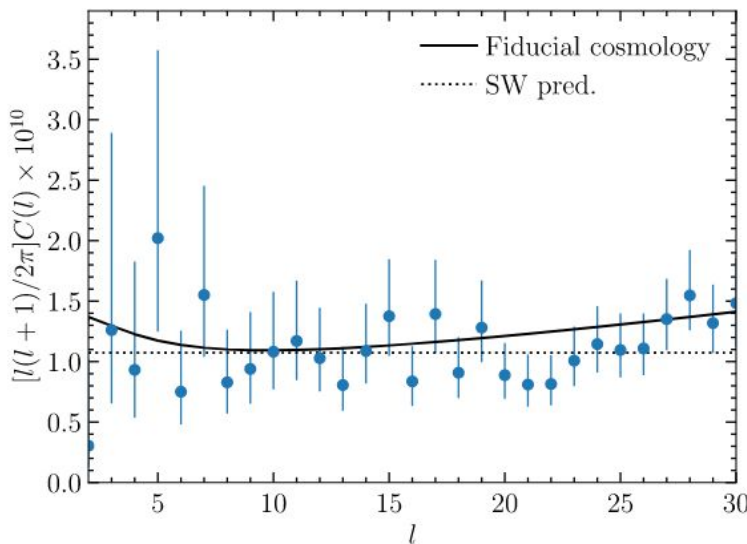


FIGURE 9.11 Large-scale CMB power spectrum as measured by Planck (Planck Collaboration, 2018b), and fiducial Λ CDM prediction (solid). The dotted line shows the scale-invariant Sachs–Wolfe plateau predicted by Eq. (9.80).

Going beyond the scale-invariant case, following our analytic result, the power spectrum multiplied by $l(l + 1)$ should scale as $(l/l_p)^{n_s - 1}$, where l_p is the angular wavenumber roughly corresponding to the pivot scale k_p . You can see this scaling from Eq. (9.79) or more directly from the integral in Eq. (9.78). The integrand peaks at $x \sim l$, so roughly every appearance of x there can be replaced by l . The generalization of the integrand from x^{-1} to $x^{n_s - 2}$ therefore leads to a change in the spectrum that scales as $l^{n_s - 1}$. Given the smallness of $n_s - 1$, this scaling is, however, masked by the other contributions mentioned above. To get constraints on the spectral index as well as the amplitude, the data have to span a larger range in l . That is, we have to include anisotropies on smaller scales.

9.6.2 Acoustic peaks

On smaller scales, i.e. those that are inside the horizon at recombination, the anisotropy spectrum depends on all terms in Eq. (9.59): the monopole Θ_0 , the dipole Θ_1 , and the integrated Sachs–Wolfe effect, $\propto \int d\eta (\Psi - \Phi)'$. Fig. 9.12 shows all these contributions to the angular power spectrum. Let us consider each in turn.

The monopole at recombination $(\Theta_0 + \Psi)(k, \eta_*)$ free-streams to us today, creating anisotropies on angular scales $l \sim k\eta_0$. This is what we expected back in Fig. 9.5, showed to be true in Eq. (9.59), and what we can now see directly in Fig. 9.12. There are two interesting features of the quantitative aspect of the free-streaming process. First, note that the “zeros” in the monopole spectrum, here at $l \sim 70, 400, 650$, and 1000 , are smoothed out because many Fourier modes contribute to anisotropy on a given angular scale. If only the $k = 400/\eta_0$ modes contributed to the anisotropy at $l = 400$, then $C(400)$ would really be zero. But many nonzero modes, with wavenumbers different from $400/\eta_0$, contribute. These change the zero to a trough in the $C(l)$ spectrum.

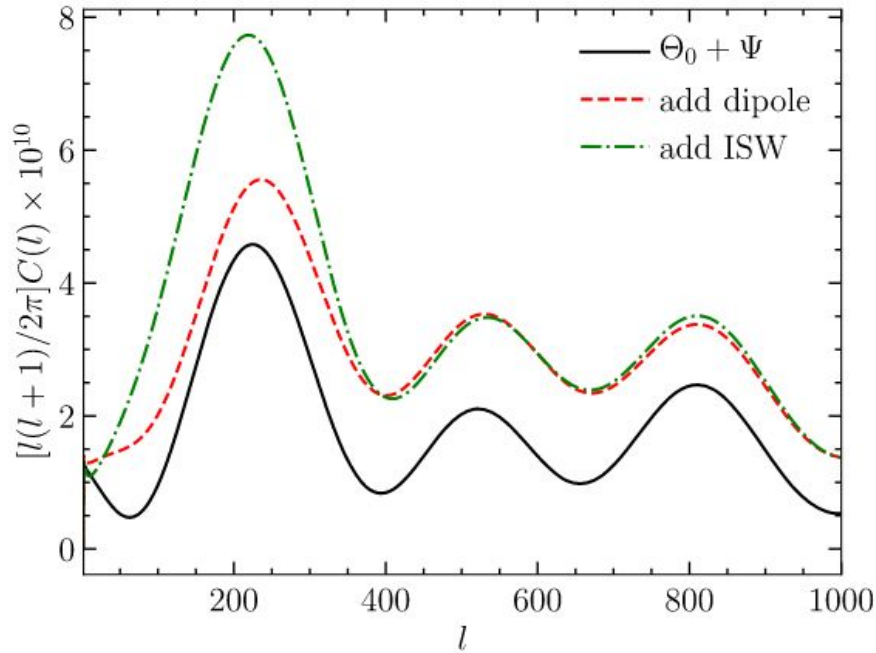


FIGURE 9.12 Intermediate- to small-scale CMB power spectrum. The solid black line shows the result obtained if only the monopole at recombination ($\Theta_0 + \Psi$) ($k = l/\eta_0, \eta_*$) were present, and contains most of the structure of the final anisotropy spectrum. Including the dipole (red dashed) raises the anisotropy spectrum. Since the dipole is out of phase with the monopole, the troughs become less pronounced. Adding the integrated Sachs–Wolfe effect (green dash-dotted) enhances the anisotropy mostly on scales comparable to or larger than the horizon at recombination. Thus the first peak gets most of the additional power.

The second feature of free-streaming worth noticing is that our initial estimate of the peak positions is not exactly right. Inhomogeneity on scale k does *not* show up as anisotropy precisely on angular scale $l = k\eta_0$. Rather, there is a noticeable shift, suggesting that a given k -mode contributes to slightly smaller l than we anticipated. This shift partially arises from the spherical Bessel function in Eq. (9.59). As shown in Fig. 9.13, the peak in the Bessel function comes not when $l = k\eta_0$, but rather at slightly smaller values of l . A better approximation for the first peak position is $l_{\text{pk}} \simeq 0.75\pi\eta_0/r_s$.

The dipole at recombination is smaller than the monopole and out of phase with it. The dashed line in Fig. 9.12 shows that the effect of adding it is to raise the overall anisotropy level, but in particular in the region of the troughs, lowering the prominence of the peaks.

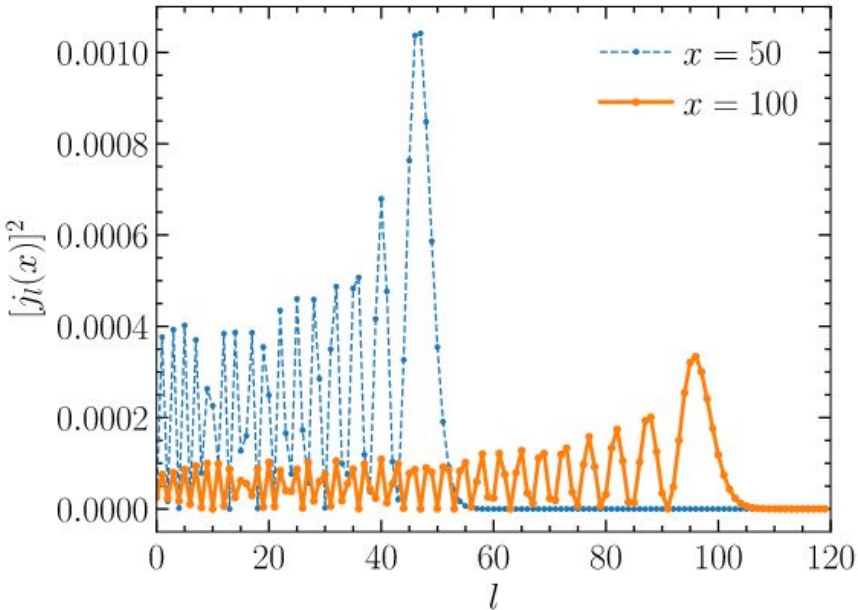


FIGURE 9.13 The spherical Bessel function squared at $x = 50$ and $x = 100$ as a function of l . Note that the peak occurs when l is slightly smaller than x .

This is a direct manifestation of the dipole and monopole being out of phase with one another. That is, at the places where the monopole contributes least to the anisotropies, at its troughs, the dipole contributes the most. Another feature of the monopole and dipole contributions is that they add incoherently. By incoherently, we mean that the cross-term of Θ_l from the monopole multiplied by Θ_l from the dipole vanishes when integrating over all k -modes to get the $C(l)$. This can be seen mathematically from the properties of the spherical Bessel function (Exercise 9.11). Incoherence implies that the dipole is not as important in the power spectrum as one might naively think. If the amplitude of the dipole is 30% of that of the monopole at recombination, the dipole's contribution to the $C(l)$ is only 10%.

The third contribution is from the integrated Sachs–Wolfe effect due to the time evolution of the potentials after recombination, which is mostly due to the fact that the energy density in radiation is not entirely negligible at recombination. If the universe were purely matter dominated, there would be no such effect. But, the transition to pure matter domination is not abrupt, and even for $a_{\text{eq}} \sim 10^{-4}$, an ISW effect occurs right after recombination. To see which scales are affected by the ISW effect, consider the integral in Eq. (9.59). Suppose the potential evolves at time η_c , with all sub-horizon scales ($k\eta_c > 1$) being affected. The Bessel function peaks at $l \sim k(\eta_0 - \eta_c)$; so all angular scales $l > (\eta_0 - \eta_c)/\eta_c$ are affected. The largest effect is typically on scales of the horizon at the time η_c .

This early ISW effect is particularly important because it adds coherently with the monopole. To see this, integrate the last term in Eq. (9.59) by parts. Then, the dominant contribution comes from $\eta \simeq \eta_*$, so the Bessel function can be evaluated there, leaving the trivial integral which gives

$$\Theta_l(k, \eta_0)^{\text{early ISW}} = [\Psi(k, \eta_0) - \Psi(k, \eta_*) - \Phi(k, \eta_0) + \Phi(k, \eta_*)] j_l [k(\eta_0 - \eta_*)]. \quad (9.81)$$

This adds exactly in phase with the monopole (which is proportional to the same Bessel function) so even though the magnitude of the effect on Θ_l is much smaller than is the dipole, the effect on the anisotropy spectrum is comparable. A 30% dipole leads to a 10% shift in the $C(l)$, while a 5% ISW effect leads to the same 10% shift in the $C(l)$. The dash-dotted line in Fig. 9.12 shows that the anisotropies on large scales, those with $l \lesssim \eta_0/\eta_*$, get a big boost from this early ISW effect.

The late-time ISW effect occurs when potentials decay during the dark energy epoch at $z \lesssim 1$ (Sect. 8.5). This late-time effect therefore is restricted to extremely large scales, $l \lesssim 30$, and is just barely visible when plotting $C(l)$ on a linear scale in l ; it is much more obvious as the upturn at the lowest l in Fig. 9.11. The most direct way to detect this effect is to cross-correlate the large-angle CMB anisotropies with large-scale structure at low redshifts, such as angular galaxy correlations (Sect. 11.2).

9.7 Cosmological parameters

The power spectrum of CMB anisotropies has rich structure, and its shape depends on cosmological parameters. By measuring it precisely, we can constrain the various parameters that describe the ingredients that enter the calculation. The price of this multidimensional parameter space is that there are partial degeneracies: the effect of varying one parameter can be mimicked by varying, in general, several other parameters in specific ways. In this section, we will try to get a feel for which parameters can be constrained directly, and which important degeneracies exist and how they work.

One very important decision that must be made is which parameters will be allowed to vary. We will consider the following seven Λ CDM parameters:

- Curvature parameter, $\Omega_K \equiv 1 - \Omega_m - \Omega_\Lambda$, often set to zero in the concordance model
- Cosmological constant, parametrized by Ω_Λ
- Normalization of the primordial spectrum, A_s
- Scalar spectral index, n_s
- Reionization, parametrized by the optical depth τ_{rei} to a redshift after recombination is completed
- Baryon density, $\Omega_b h^2$
- CDM density, $\Omega_c h^2$.

There are two aspects of this list worth stressing. The first is that obviously it does not include all possible cosmological parameters. Some favorites missing are neutrino masses (we will set the sum of neutrino masses to its minimum experimentally allowed value, $\sum m_\nu = 0.06$ eV), the equation of state for dark energy w (fixed here at -1 corresponding to a cosmological constant), and tensor modes (amplitude r fixed to zero). The main reason for these omissions is that these parameters are not directly constrained by the CMB temperature power spectrum. The effect of neutrino masses is simply too small at early times, and the same holds for the details of dark energy (which mostly affects the CMB through the distance to the last-scattering surface). Dark energy and neutrino masses are best constrained by combining the CMB with large-scale structure probes, which are the topic of Ch. 11. On the other hand, tensor modes are now most constrained by CMB *polarization*, so we defer their discussion to Ch. 10.

The second important point is that we have deliberately chosen specific combinations of some of these parameters, e.g., $\Omega_b h^2$, not Ω_b and h separately. Notice that, by allowing for Ω_K and Ω_Λ in addition to $\Omega_m h^2 = (\Omega_b + \Omega_c)h^2$, we have effectively accounted for the Hubble parameter, since Ω_m is fixed by the constraint $\Omega_m = 1 - \Omega_\Lambda - \Omega_K$. There is a good reason for considering this combination of parameters. $\Omega_m h^2$, for example, parametrizes the proper physical matter density in the universe today, written in some odd units involving $8\pi G$ and 100 km/s/Mpc . The physics determining the CMB anisotropies cares much more about the physical matter density than the density parameter Ω_m . The same holds for the baryons. Finally, the physical energy density in photons, $\Omega_\gamma h^2$, is extremely well determined through the CMB temperature. Thus, the equality epoch a_{eq} is essentially a function of $\Omega_m h^2$ only.

Let us now consider the effect of each parameter in turn.

9.7.1 Curvature and Λ

If the universe is not Euclidean, then the simple picture of Fig. 9.5 is no longer accurate, since the photon geodesics which start out parallel to each other converge or diverge. Consider the implication of this effect for anisotropies. Suppose the identical pattern of inhomogeneities was in place at recombination in both a Euclidean and an open universe (a very good approximation if Ω_K is small). As shown in Fig. 9.14, a fixed physical scale such as that of the first peak, say, gets projected onto a much smaller angular scale in an open universe. The peaks therefore shift to higher l . The opposite happens in a closed universe. As shown in Fig. 9.15, this is precisely what happens in the numerical calculation.

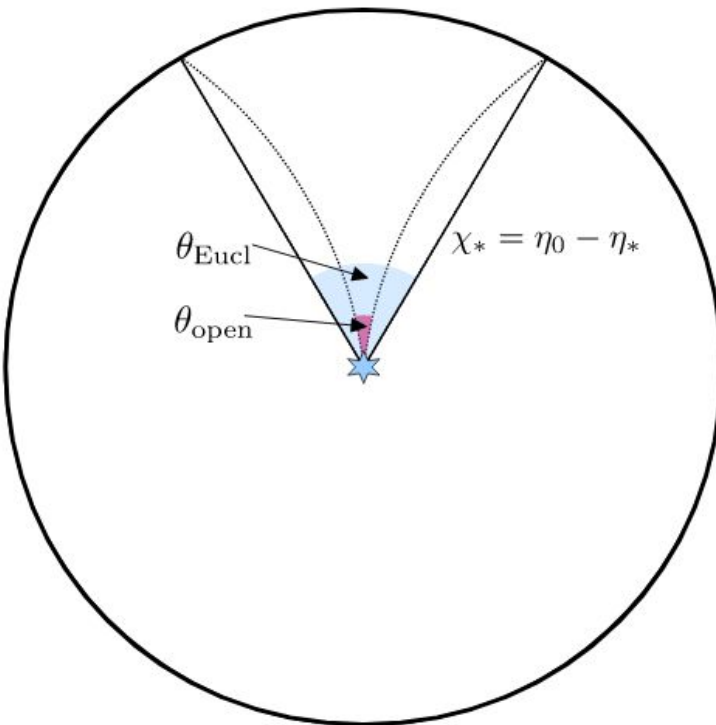


FIGURE 9.14 In comoving coordinates (η, x) , photon trajectories in a Euclidean universe are straight lines (solid), while those in an open universe diverge (dashed). Perturbations at last scattering appear on smaller scales in an open universe (θ_{open}) than they do in a Euclidean universe (θ_{Eucl}).

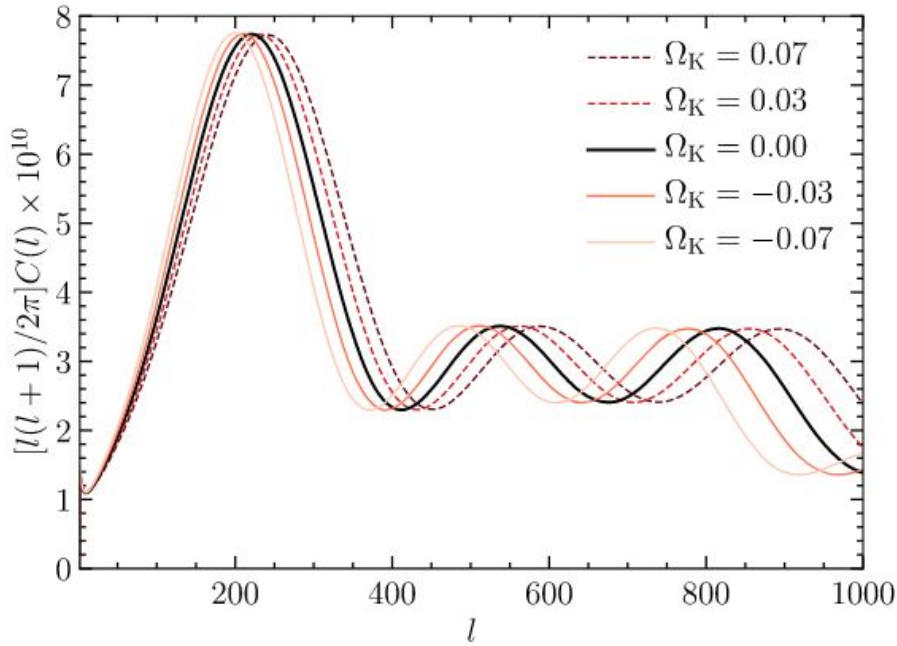


FIGURE 9.15 The anisotropy spectrum in Euclidean versus open and closed universes. The pattern of peaks and troughs persists in curved universes but is shifted to smaller scales for open universes ($\Omega_K > 0$), while the opposite happens for closed universes ($\Omega_K < 0$). Only Ω_K and Ω_Λ are varied in this figure, while all other parameters are fixed at their values for the fiducial cosmology.

The magnitude of this effect is determined by the angular diameter distance to the last-scattering surface, given in a Euclidean universe simply by $\eta_0 - \eta_*$, and in a universe with curvature by Eq. (2.39). Because of the large distance to last scattering, the CMB peaks respond very sensitively to curvature, resulting in a correspondingly tight constraint. Current best constraints on Ω_K , obtained by combining CMB and large-scale structure probes, are at the level of $|\Omega_K| < 0.002$ (Planck Collaboration, 2018b). We have come a long way since the time when the open CDM model with $\Omega_K = 1 - \Omega_m \simeq 0.7$ was a viable scenario!

Now, an exactly Euclidean universe is only one point in parameter space, the point at which the sum of the energy densities exactly equals the critical density, and no data will ever rule out all values except for this one point. In fact, we expect to observe very small but nonzero curvature even in the inflationary paradigm. Inflation produces perturbations on all scales, including those just at our current horizon. The isotropic part of such a horizon-scale perturbation appears to us precisely as curvature, with $\Omega_K \sim (k/a_0 H_0)^2 \mathcal{R}(k) \Big|_{k=H_0}$ (this provides yet another justification for the name “curvature perturbation;” see the discussion at the end of Sect. 7.4.3). Given the approximate scale-invariant spectrum for $\mathcal{R}(k)$, inflation thus predicts that Ω_K should be a random number with RMS value of order $\sqrt{A_s} \sim 10^{-4}$. Evidence for a value much larger than that would be problematic for the inflationary scenario, however.

Changing the cosmological constant has a similar effect to curvature, in that it shifts the peak locations due to the change in the angular diameter distance to last scattering (recall that we are also modifying H_0 when varying Ω_Λ while keeping $\Omega_m h^2$ fixed). After all, both are late-time phenomena that do not play a role at recombination. You will show in Exercise 9.12 that the effect of changing Λ can be readily explained in this way. This also explains why the CMB constraint on Ω_K is partially degenerate with that on Ω_Λ , if no large-scale structure probes are included to break the degeneracy. In addition, changing Λ also affects the late-time ISW contribution at $l \lesssim 30$, with an increase in Λ boosting the $C(l)$ on these scales (see Fig. 9.11), although the constraining power of this effect is unfortunately limited due to the large cosmic variance errors.

9.7.2 Amplitude, spectral index, and optical depth

The effect of changing the amplitude \mathcal{A}_s and spectral index n_s of primordial perturbations is quite simple to understand: changing \mathcal{A}_s by a factor means multiplying all $C(l)$ by the same factor. Shifting $n_s \rightarrow n_s + \alpha$ changes the small-scale $C(l)$ by a factor $(l/l_p)^\alpha$, where l_p is the angular wavenumber corresponding to the pivot scale k_p . This is not quite correct on large scales due to the wide support of j_l for low l .

However, we also need to consider the optical depth due to *reionization*. After recombination, the gas in the universe was neutral. On the other hand, most of the gas we observe in the late universe is ionized; for example, we see no evidence for neutral gas in the absorption spectra of high-redshift quasars until we go back as far as $z \sim 6$ (Bouwens et al., 2015). So at some point the gas had to be *reionized*.⁴ We currently believe that this happened between redshifts 15 and 6. After reionization, the CMB photons could scatter off the now-free electrons again. If enough scattering takes place, that is, if the optical depth $\tau_{\text{rei}} \equiv \tau(\eta_{\text{late}})$ back to some time η_{late} after the end of the recombination epoch is high enough, isotropy is restored; equivalently, primordial anisotropies are washed out.

To study this quantitatively, imagine a photon traveling in our direction with temperature $T(1 + \Theta)$, where T is the background temperature and Θ is the perturbation. If these photons hit a region with optical depth τ_{rei} , only a fraction $e^{-\tau_{\text{rei}}}$ will escape and continue on their way to us. In addition to these, we will observe a fraction $1 - e^{-\tau_{\text{rei}}}$ scattered into the beam while traveling through the ionized region (since scattering conserves the total number of photons). These scattered-in photons come from all directions, so we can assume them to have the mean temperature T . So the temperature we see today is

$$T(1 + \Theta)e^{-\tau_{\text{rei}}} + T(1 - e^{-\tau_{\text{rei}}}) = T(1 + \Theta e^{-\tau_{\text{rei}}}). \quad (9.82)$$

Subtracting from this the mean temperature T tells us that the fractional anisotropy will be the primordial one set up at $z \simeq 1100$ multiplied by $e^{-\tau_{\text{rei}}}$. This scattering, however, affects only those perturbations within the horizon at the time of reionization, so only multipoles l larger than η_0/η_{rei} will be suppressed by $e^{-\tau_{\text{rei}}}$; small l will be unaffected. This is seen in Fig. 9.16, which shows the effect of changing τ_{rei} . Clearly, increasing τ_{rei} suppresses the anisotropies on small scales, but leaves them unchanged for $l \lesssim 100$.

This explains why we considered reionization together with the amplitude and spectral index: a change in \mathcal{A}_s , together with n_s , can largely mimic the effect of τ_{rei} , especially considering the fact that the cosmic variance error on the $C(l)$ is largest at low l . Conversely, the uncertain value of τ_{rei} is by far the leading source of uncertainty on \mathcal{A}_s .

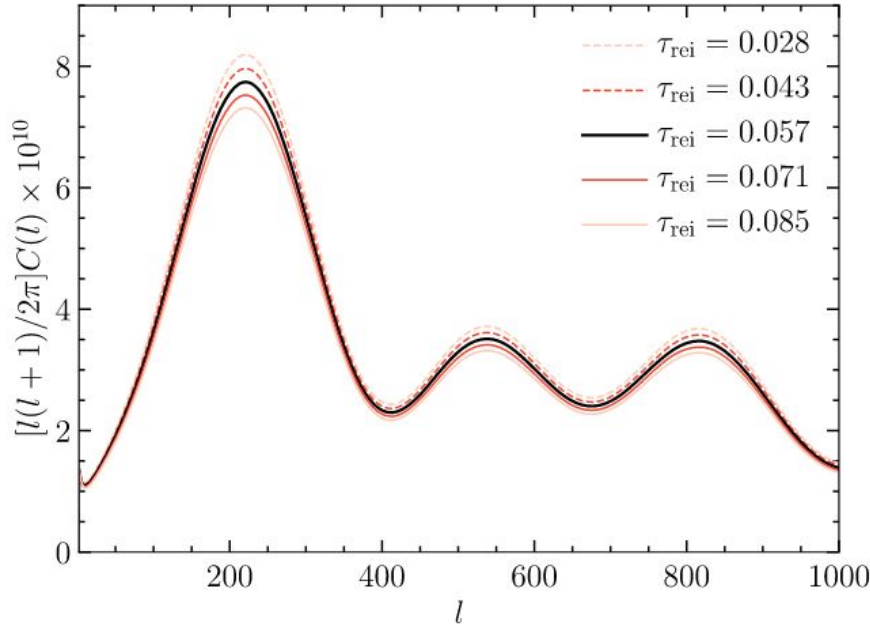


FIGURE 9.16 Effect on the CMB power spectrum of varying the optical depth to reionization. On scales $l \gtrsim 150$, the effect is essentially an overall multiplicative factor, while the CMB is insensitive to τ_{rei} on very large scales.

9.7.3 Baryon and CDM densities

The final variations we will consider are changes in the baryon density $\Omega_b h^2$ and the CDM density $\Omega_c h^2$. In each case, we keep a Euclidean universe and compensate the change in the density parameters through Ω_Λ . As expected from our considerations at the beginning of this chapter, these changes lead to richer variations in the anisotropy spectrum than a mere shift and tilt; instead, they induce a small relative shift in the locations of the peaks and troughs in the spectrum, as well as changing their amplitudes. To understand these effects, it is important to recall that, since inhomogeneities on scales k show up at $l = k\eta_0$ in a Euclidean universe, the peaks in a Euclidean universe will show up at $l_{\text{pk}} \simeq k_{\text{pk}}\eta_0 \simeq n\pi\eta_0/r_s(\eta_*)$ (Eq. (9.27), but see the discussion in Sect. 9.6.2 that argues that the actual value of l_{pk} is $\sim 25\%$ lower).

The effects of changing the *baryon density* (Fig. 9.17) are a shift in the peak locations, due to the change in the sound horizon $r_s(\eta_*)$, as well as modifications in the heights of the peaks. We have already touched on the ways in which the anisotropy spectrum depends on the baryon density. The foremost, clearly visible in Fig. 9.17, is that the ratio of the heights of the odd to even peaks is higher when the baryon density is large. The second change due to $\Omega_b h^2$ is that an increased baryon density reduces the diffusion length (increases k_D). Therefore, a larger baryon density means damping moves to smaller angular scales, so the anisotropy spectrum on scales $l > 1000$ is larger in a high- $\Omega_b h^2$ model. This characteristic combination of effects allows for very tight constraints on $\Omega_b h^2$; the parameter variations around the fiducial values shown in Fig. 9.17 are ruled out by the data at high significance.

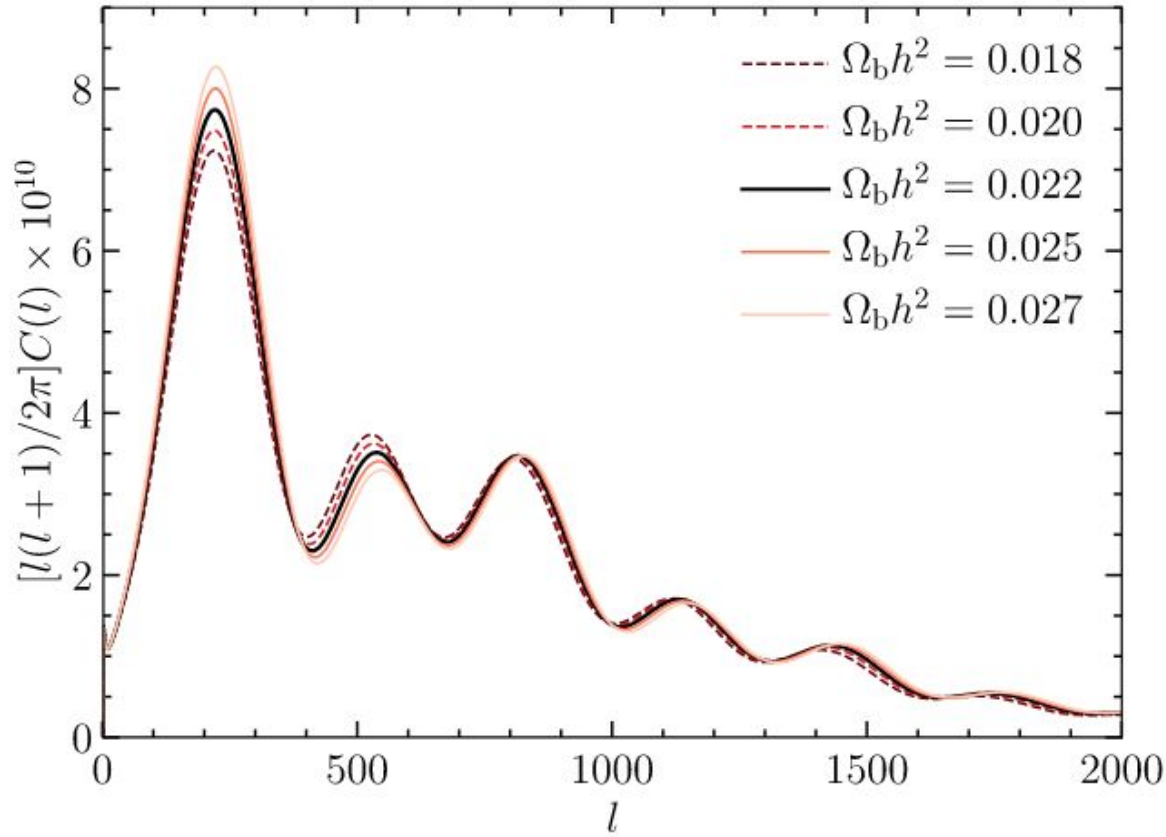
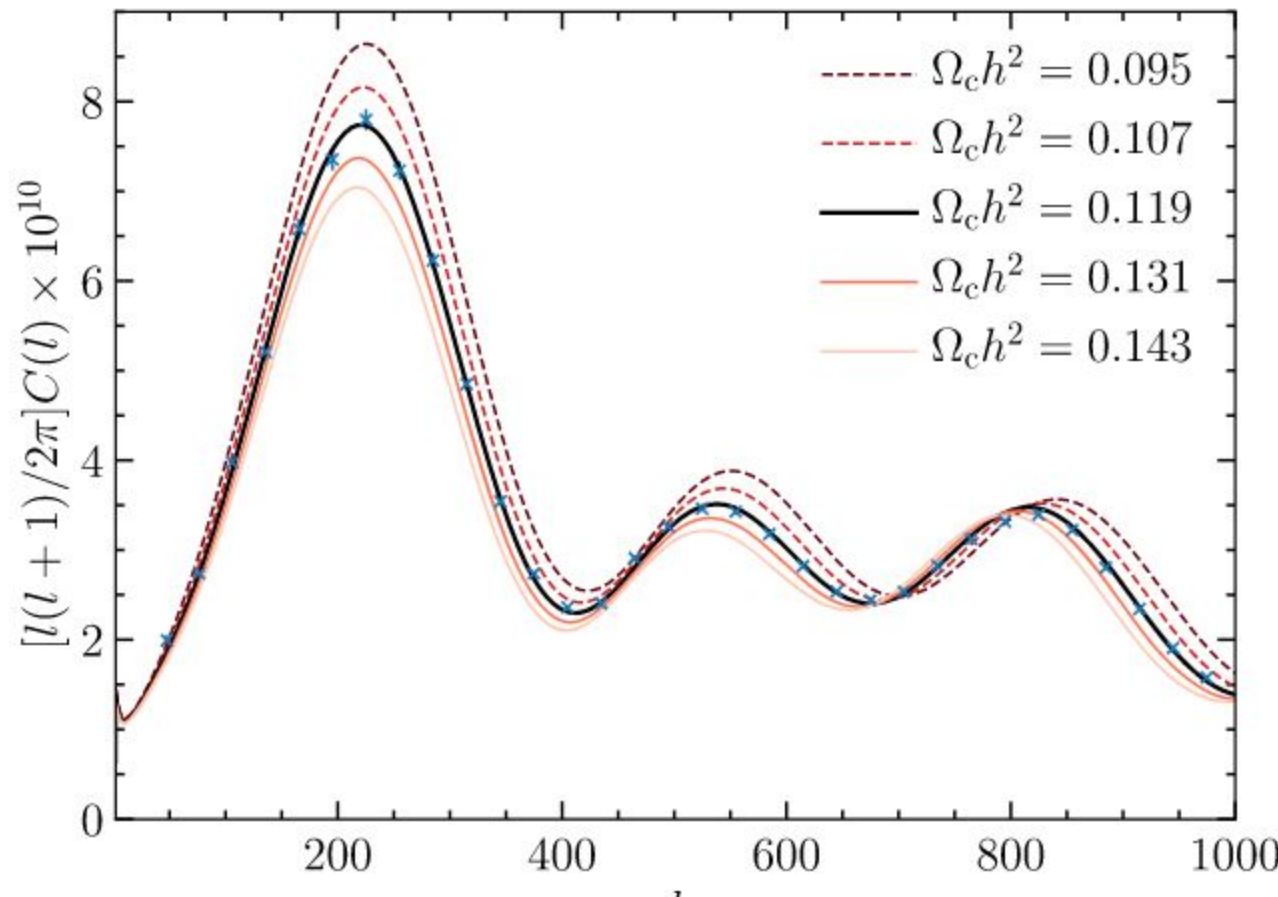


FIGURE 9.17 Changes in the anisotropy spectrum as the baryon density $\Omega_b h^2$ is varied.

Next, we consider the effect of changing the *cold dark matter density* $\Omega_{\text{c}}h^2$ (Fig. 9.18). Part of the effect is changing the driving term for the acoustic oscillations (since the gravitational potential is dominated by CDM), which is similar to what a modification to the baryon density does. In addition, CDM determines to a large extent the epoch of equality, affecting both the evolution of perturbations (more growth for increased $\Omega_{\text{c}}h^2$) and the early ISW effect (less ISW for increased $\Omega_{\text{c}}h^2$, since the potentials decay less after recombination). The $C(l)$ are similarly sensitive to a given fractional change in $\Omega_{\text{c}}h^2$ as one in $\Omega_{\text{b}}h^2$. We also show binned power spectrum measurements—measurements for a range of l combined into a single data point for presentation purposes—of the Planck team. They lie right on top of the fiducial Euclidean Λ CDM prediction. Given the barely visible error bars, the data precisely constrain $\Omega_{\text{c}}h^2$, ruling out at high significance the alternative parameter values we have shown for illustration.

FIGURE 9.18 Changes in the anisotropy spectrum as the CDM density $\Omega_c h^2$ is varied. Also shown are binned Planck measurements (Planck Collaboration, 2018b); the error bars are so small that they are only discernible for l around and below the first peak. Clearly, $\Omega_c h^2$ and $\Omega_b h^2$ can be determined very precisely.



9.8 Summary

The observed CMB anisotropies are a combination of three contributions (Eq. (9.59)):

- $\Theta_0 + \Psi$, which includes intrinsic photon temperature perturbation and gravitational redshift, and which we loosely refer to as “monopole.” This contribution shows acoustic oscillations, whose behavior is to first order described by the semi-analytic tight-coupling solution.
- The Doppler-shift contribution $3\Theta_1$, which shows the same acoustic oscillations but is out of phase (as generally the case for velocities and positions of oscillators).
- The ISW contribution due to the time evolution of gravitational potentials around recombination and at late times. Unlike the first two, this is an integrated contribution along the line of sight, and has a smooth scale dependence.

The sum of these three contributions (and the associated cross-correlations) leads to the characteristic angular power spectrum of the CMB. The $C(l)$ contain rich information in particular on $\Omega_c h^2$ and $\Omega_b h^2$, but also on curvature and the amplitude of primordial perturbations \mathcal{A}_s and the spectral index n_s (although the constraint on \mathcal{A}_s is limited by the degeneracy with the optical depth τ_{rei}). The CMB becomes even more powerful in combination with the large-scale structure probes discussed in Ch. 11. This combination has already led to percent-level constraints on the curvature and cosmological-constant parameters Ω_K , Ω_Λ .

Our semi-analytic approach to the CMB anisotropies follows Hu and Sugiyama (1995), whose extremely clear presentation is recommended as further reading. The benchmark for measurements of CMB temperature anisotropies is now set by the Planck satellite, at least for $l \lesssim 2000$, for which Planck's error bars have reached the fundamental cosmic variance limit. The latest data release is described in Planck Collaboration (2018a), while the parameter constraints, along with excellent concise descriptions of other data sets, are presented in Planck Collaboration (2018b).

Conclusión

Hoy recorrimos la deducción completa del espectro del CMB, desde las **ecuaciones de Boltzmann** hasta la **formación de anisotropías**. Vimos cómo la física del universo temprano deja su huella en las fluctuaciones observadas, con contribuciones clave del **efecto Sachs-Wolfe**, las **oscilaciones acústicas** y la **amortiguación de Silk**. Este marco teórico es fundamental para interpretar las observaciones actuales y extraer información cosmológica precisa.

